Electrochemical Planarization of Copper for Microelectronic Applications

Jinshan Huo

M.S., Materials Science and Engineering,
Oregon Graduate Institute of Science and Technology, USA, 1999

M.S., Metallurgy and Materials Engineering,
Chongqing University, P. R. China, 1989

B.S., Metallurgy and Materials Engineering,
Chongqing University, P. R. China, 1983

A dissertation presented to the faculty of the

OGI School of Science & Engineering

at Oregon Health & Science University

in partial fulfillment of the requirements for the degree

Doctor of Philosophy

in

Electrical Engineering

February, 2004

The dissertation "Electrochemical Planarization of Copper for Microelectronic Applications" by Jinshan Huo has been examined and approved by the following Examination Committee:

Dr. Raj Solanki, Thesis Advisor
Professor, Department of Electrical and Computer Engineering

Dr. Jack McCarthy
Assistant Professor, Department of Electrical and Computer Engineering

Dr. John L. Freeouf
Professor, Department of Electrical and Computer Engineering

Dr. Robert J. Contolini
Technologist, Novellus Inc., Tualatin, Oregon

Dr. James McAndrew
Manager, Electronics R&D Group,
Air Liquide, Countryside, Illinois

Dr. Kenneth C. Cadien
Intel Fellow, Director of Innovative Technology
Intel Corporation, Hillsboro, Oregon

ACKNOWLEDGEMENTS

I would like to express my deep appreciation to Dr. Raj Solanki, my thesis adviser, for his academic guidance and financial aid through my PhD study. It is a great pleasure to work under him.

I am grateful to Dr. Robert J. Contolini for his academic guidance, literature, and precious time in participating in this study.

Special thanks are due to Dr. Jack McCarthy, Dr. Kenneth C. Cadien, Dr. John L. Freeouf, and Dr. James McAndrew for their information, guidance, and effort in reviewing the dissertation.

I would like to express my gratitude to OGI librarians, to all the stuff and faculty in the Department of Electrical and Computer engineering for their help and assistance. I also appreciate my fellow and students friends William Meyer, Hidayat Kisdarjono, Behrooz Tahmasebi, and Weiming He, as well as Dr. Jinhong Yang and Dr. Charlie Zhi, former PhD students at OGI for their help during this research work.

Thanks also go to Dr. Michael McKeag and Ms. Nancy Zelick at Intel Corporation, as well as Mr. Jay Jordan at FEI Company for their assistance in preparing wafer samples and SEM images.

I appreciate Technic, Inc. for donating the EG&G 273A Potentiostat/Galvanostat apparatus to Oregon Graduate Institute so that I could complete this research work.

This research was funded by Air Liquide. I appreciate Dr. James McAndrew for his precious time and effort in discussing technical issues, providing literature, reviewing manuscript for publication and filing patent.

Last, I heartedly thank my parents, my wife and son for their patience, encouragement and support through my PhD study.

TABLE OF CONTENTS

LIST OF FIGURES

LIST OF TABLES

ABSTRACT

Electrochemical Planarization of Copper for Microelectronic Applications

Jinshan Huo, B.S., M.S.

Ph.D., OGI School of Science & Engineering
at Oregon Health & Science University

December 2003
Thesis Advisor: Dr. Raj Solanki

Copper damascene is the most common technique used in ULSI device fabrication. To meet the challenges of continuing increase of device speed and shrinkage of device dimensions, one of the strategies is to use ultra low dielectric constant (k) materials with porosity as the interlayer dielectric (ILD) between the layers of copper interconnects. Unfortunately, these ultra low-k ILDs are too fragile to be integrated with conventional chemical mechanical polishing (CMP) technique. To explore the possibility of using electrochemical polishing/planarization (ECP) as an alternate polishing technique for replacement of CMP, this work studied: (1) copper anodic polarization behavior in various electrolyte solutions, (2) copper anodic layers in different solutions, (3) ECP effects of copper bulk material and films electroplated on trenched silicon substrates, (4) ECP mechanisms, and (5) correlation between anode surface profiles and ECP effects.

Copper anodic polarization curves in phosphoric acid, sulphuric acid, sodium chloride, ethylene glycol, and hydroxyethylidenediphosphonic acid (HEDP), with or without organic and inorganic additives were measured with a computer-controlled potentiostat. The data indicated that a limiting current plateau existed in certain concentration ranges of the above electrolyte solutions. Steady-state data were collected to validate that the limiting current conditions were mass transport controlled, which is a prerequisite for ECP.

Electrochemical impedance spectroscopy (EIS) and SEM observations of anodic layers suggested that an electrically resistive salt film formed on a copper anode in

solutions of hydroxyethylidenediphosphonic acid (HEDP). Whereas, in solutions of phosphoric acid or phosphoric acid with copper oxide, ethylene glycol and sodium tripolyphosphate as additives, no salt film was detected. Analysis of EIS data further suggested that H_2O molecules are the mass transport controlling species in solutions of phosphoric acid and of phosphoric acid with copper oxide, whereas Cu^{++} ions are the mass transport controlling species in solutions of HEDP and of phosphoric acid with additives ethylene glycol or sodium tripolyphosphate.

ECP effects of copper bulk material and film electroplated on trenched silicon substrate in various electrolyte solutions were evaluated with computer-controlled chronoamperometry and atomic force microscopy (AFM). The results indicated that excellent ECP effect (surfaces mean roughness Ra < 10 nm) on bulk copper could be obtained with phosphoric acid, HEDP, and phosphoric acid solutions with ethylene glycol, sodium tripolyphosphate, and copper oxide as additives. However, for copper film electroplated on trenched silicon wafer, a good ECP effect was obtained only with HEDP solutions.

ECP mechanisms have been studied and a detailed description of three possible ECP mechanisms is presented. It shows that ECP effect is strongly dependent on the surface profiles of the anode to be polished. Copper films electroplated on trenched silicon wafers consist of sine waves of short wavelength, which is more difficult (compared to copper bulk surface) to be planarized. Optimal ECP conditions for this case were determined, based on the results of this study.

Chapter 1
Introduction to Copper Electropolishing

1.1 Background

A microelectronic device is essentially composed of a number of transistors that are interconnected to perform logic functions. Continuing demand for higher speed, more functions, and lower power consumption requires faster components and denser integration of microelectronic devices. An ultra large scale integrated (ULSI) circuit may have millions of transistors on a single chip. For instance, the 2.80 GHz Intel Pentium 4 processor, with feature size (of the poly-silicon gate) of 0.13-micron, has 55 million transistors, which are interconnected on a chip of about 2 cm^2 [1, 2]. To optimize functional density and supply power to each transistor, multilevel interconnects are required and have to be interspaced with interlayer dielectrics (ILD).

For years, semiconductor manufacturers used aluminum and SiO_2 for the interconnects and ILD materials. These structures were patterned by using plasma to etch (dry etch) the fine lines. As device sizes get smaller, finer pitch of interconnects requires smaller RC delay and greater electromigration (EM) resistance. Compared to aluminum, the resistivity of copper is about 40% lower and has better EM resistance. No wonder, the interconnect RC delay of Cu / low-k materials is about half that of Al / SiO_2 [3]. Clearly, copper / low-k interconnects are the choice for deep sub-micron technologies since it provides speed enhancement with no sacrifice of device reliability.

Using new materials usually needs new processing techniques. Material removal techniques are among the key processing technologies used in the fabrication of microelectronic devices. Unlike Al / SiO2 interconnects where plasma etch can be used, copper interconnects need other techniques rather than plasma dry-etch since copper-

plasma reaction products are almost impossible to vaporize at temperatures under 400 °C [4]. Currently chemical mechanical polishing (CMP) is used with copper dual damascene process technology. Fig.1-1 illustrates copper damascene structure and extra copper removal with CMP.

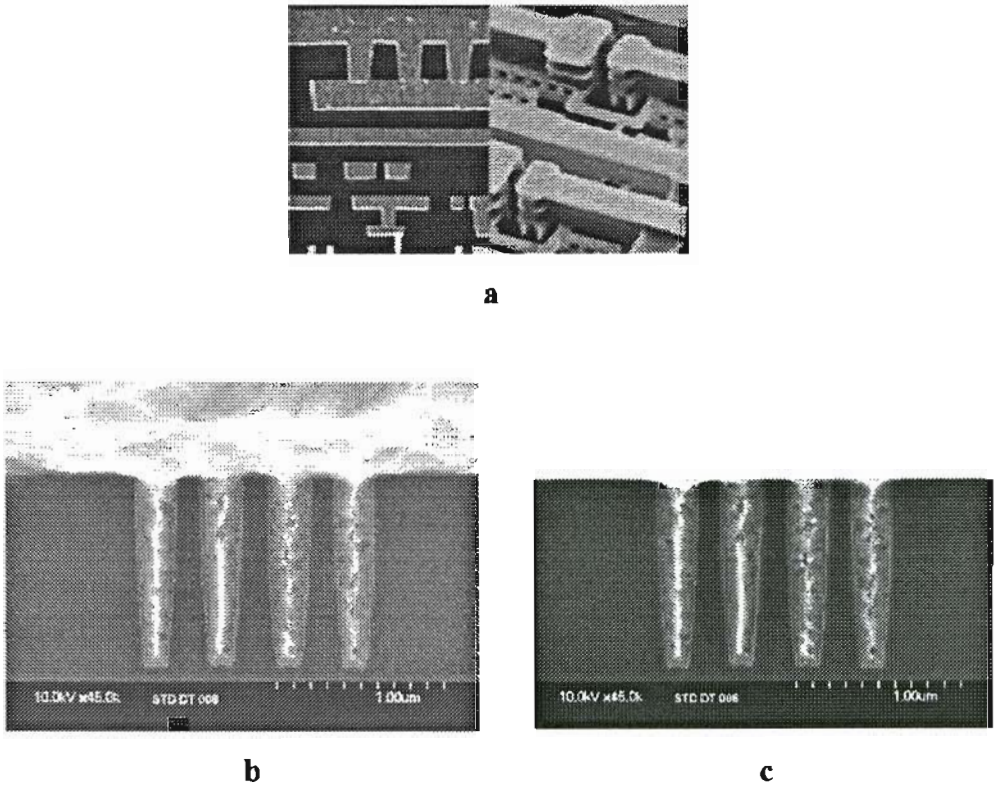

Figure 1-1 An illustration of copper dual damascene technique. a. Copper-ILD interconnects structure [3]; b. copper is electrochemically deposited in ILD trenches; c. a flat and smooth surface is obtained after CMP.

However, the effectiveness of CMP varies from material to material [5]. As the feature size of microelectronic devices continues to shrink into submicron regime, copper interconnects combined with ultra low-k interlayer dielectrics (ILD) become necessary. Ultralow-k materials, such as carbon-doped silica (SiOC) films formed by CVD and spin-on dielectric (SOD) films, are soft compared to SiO_2 and fluorosilicate glass (FSG) films. To further low down k (dielectric constant) value, air bubbles are introduced into such

materials. This makes the ILD even softer. Hence, CMP is no longer feasible due to problems such as: (1) the ILD layers can be crushed by CMP; (2) slurry particles getting embedded into the ILD materials, as a result, contaminating the materials and increasing the k value; (3) scratching of ILD; and (4) ILD layer peeling off by shear stress of CMP. Alternatively, electrochemical polishing (ECP) is a viable option that is attracting more and more interest from the semiconductor industry [6-9].

Electrochemical polishing is also called electrochemical planarization, electropolishing, or electroplanarization; and shortened as ECP. ECP is a reverse process of electroplating (EP). As shown in Fig.1-2, copper dissolution occurs on anode, which is connected to the positive pole of the power supply. Conversely, copper plating occurs on cathode, which is connected to the negative pole of the power supply. Therefore, copper electroplating results when working electrode is chosen to be cathode. And copper dissolution is accomplished when the working electrode is chosen to be the anode.

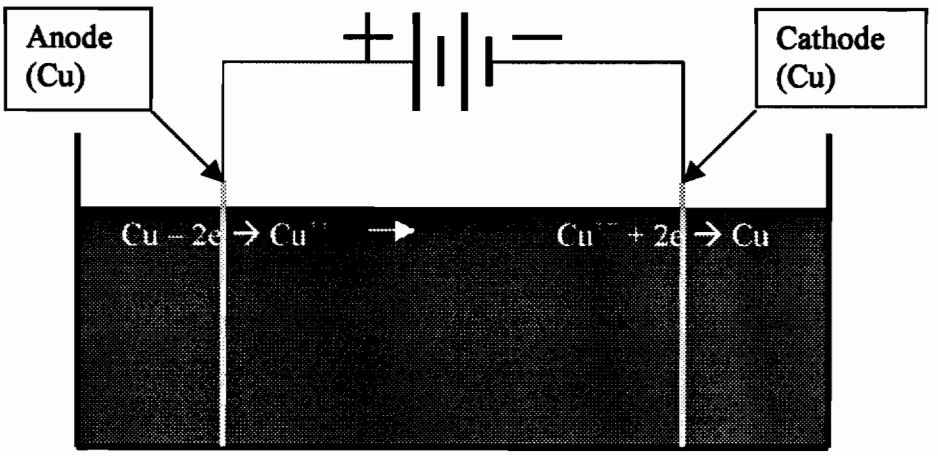

Figure 1-2 Schematic of an Electrochemical Cell

Nevertheless, electropolishing can not be achieved by simply switching the poles of the power supply of an electroplating system. In fact, when this process is applied to copper interconnects in ULSI circuit fabrication, EP and ECP have very difference mechanisms. Fig.1-3 indicates the mechanism of trench filling in copper EP.

For electroplating, the biggest challenge is void-free gap filling. This is realized by adding additives, such as accelerator, suppressor and leveler into a plating solution. Among them, accelerators have a function of catalyzing charge transfer. These rapidly diffusing small electroactive molecules accumulate onto the trench bottom as copper deposition process goes on. As a result, the current density on the trench bottom becomes higher and higher than on the top flat surface. Therefore a bottom-up filling is realized. Otherwise, voids would form due to conformal growth, as shown in Fig.1-4.

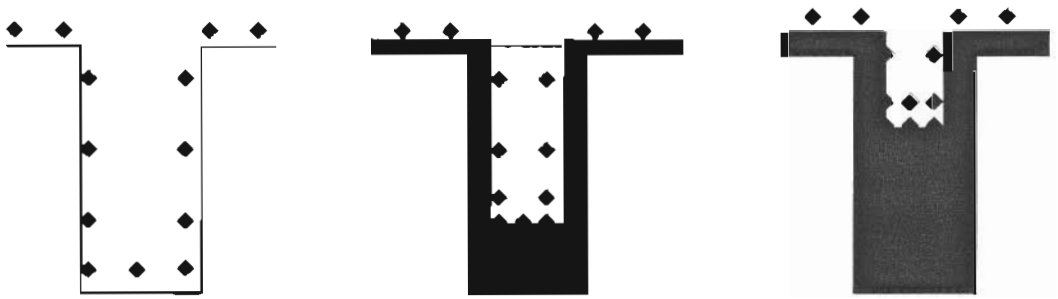

t = 0 sec. t = 5 sec. t = 10 sec.

Figure 1-3 Bottom-up trench filling is facilitated by accelerators accumulated in the trench. ◆ Represents accelerator.

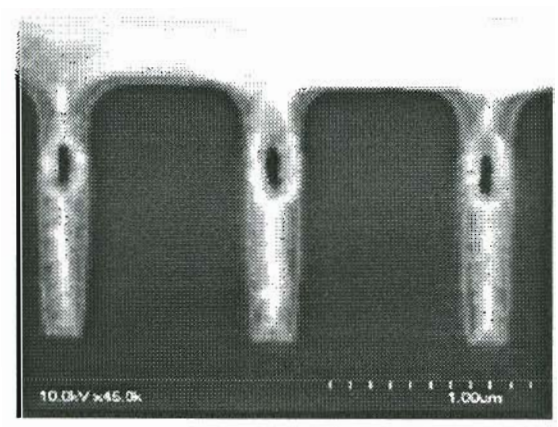

Figure 1-4 Voids formed in electroplated copper.

However, electrochemical dissolution, the reverse process of EP, does not necessarily produce a flat and smooth surface. Indeed a rough surface can be produced, at lower overpotential due to crystallographic etching mechanism, and at higher potential due to gas bubbles form on the anode surface. A smooth surface can be produced only at certain potential range in certain electrolyte solutions. A detailed discussion will be given in Chapters 2 and 3.

It is known that ECP can be subdivided into: macrosmoothing (or leveling) and microsmoothing (or brightening). Leveling, which refers to the elimination of larger surface roughness, is due to the fact that the current density (**J**) on projecting areas is greater than on recessed area on a rough surface with uniform potential (See Fig.1-5) [10]. As a result, peaks of a rough surface have higher dissolution rate than valleys.

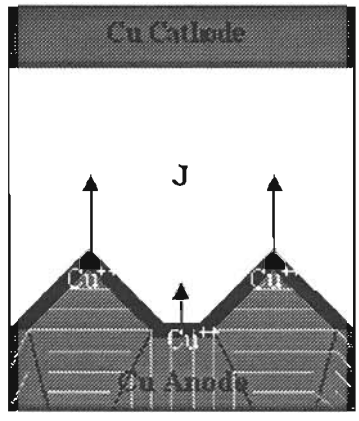

Figure 1-5 Schematic of current density variation over a rough surface and anodic resisting Cu^{++} diffusion from anode surface to wards cathode.

On the other hand, brightening, which refers to the elimination of surface roughness comparable to the wavelength of visible light, is due to the formation of certain kinds of diffusion barrier layers on the anode surface (See Fig.1-5) [10]. The barrier layer causes a shift in dissolution mechanism from surface-kinetic control to mass transport control. Under kinetic control, the dissolution speed varies from one crystallographic orientation to another. Thus a rough surface may be produced. While under mass transport control, the anodic films work as diffusion barriers and prevent

preferential dissolution at higher energy sites, such as grain boundaries and crystal planes with higher energy. In other words, the anodic dissolution is insensitive to location and crystallographic orientation. Instead, the prominences under anodic films of a rough surface are preferentially dissolved due to, a steeper concentration gradient on convex than on concave portions [11].

Copper electrochemical polishing was first reported about seventy years ago [12]. Since then a lot of work has been reported dealing with various aspects of the technology. Linear sweep voltammetry [13, 14], AC impedance spectroscopy [15, 16], Ellipsometry [17], holographic interferometry [18], XPS [19], and other techniques were used to study the anodic layers and ECP mechanisms. It is known that surface brightening can be achieved by controlling the anodic potential at limiting current plateau where the process is mass transport controlled [10, 13, 14, 17, 20-22]. Surface leveling is best achieved under primary current distribution at narrow inter-electrode distance [22]. Modeling methods have also been used to predict ECP process and facilitate the understanding of ECP mechanisms.

However, the mechanisms of electropolishing are not fully understood as yet. A detailed description of copper ECP mechanisms is not available so far.

Early work suggests that ECP process depends on many factors, such as electrolyte solution and its circulation, disk rotating speed, current density, potential, and temperature [22, 23-28]. Yet optimal ECP conditions for copper electropolishing for microelectronic applications are still not available. In fact, copper ECP technology is so far mainly used for (1) decorating purposes such as furniture arms and legs, lamps and lighting fixtures, jewelry and nameplates; (2) components with cavities such as copper cylinders and pipes; and (3) other special applications such as electrical contacts and sample preparation for materials research [29-33].

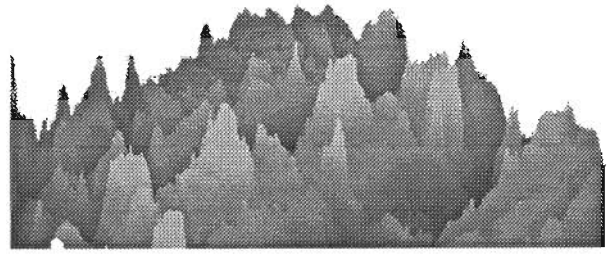

a

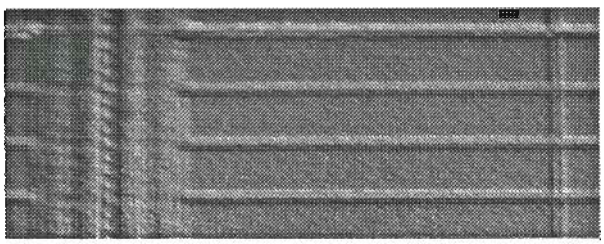

b

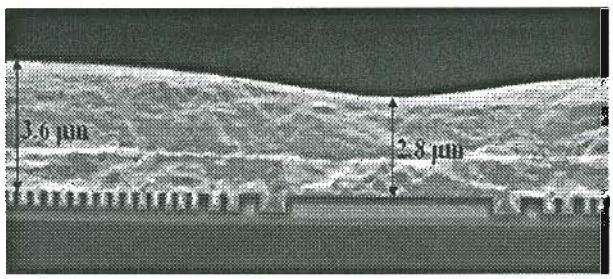

c

Figure 1-6 Copper surface profiles: a. AFM image of bulk material; b. Optical image of copper film electroplated on patterned silicon wafer; c. SEM image of cross section of copper film electroplated on patterned silicon wafer.

For microelectronic applications, there are several more issues that need to be addressed. These issues include [6, 7, 34]: (1) the patterned features of electroplated copper films are difficult to remove and may lead to non-uniform polishing; (2) over-etching of the copper in trenches because no "end-point stopping"; (3) the surface of the copper films after ECP becomes rough instead of bright as a result of inhomogeneous

etching and gas bubbles; and (4) the uniformity of ECP over a large wafer (such as 300 mm wafers) can be challenging.

In addition, it was found that ECP efficiency was influenced by the pattern of surface profile [35]. As shown in Fig.1-6, the surface profile of an electroplated (EP) copper film on a deep-trenched wafer is quite different from that of copper bulk materials. Mechanically polished surface of bulk copper material has a rough surface with protrusions involve short wavelength (Fig. 1-6a). The surface of copper film electroplated on a deep trenched wafer has a smoother surface with bumps and pads, which are corresponding to the trenches and vias under the film, See Figs. 1-6b and c. One of the biggest challenges is to even out these bumps and pads.

A better understanding of the mass transport processes and ECP mechanisms is therefore very necessary to identify the factors that are effective to ECP of copper films electroplated on trenched silicon wafers.

1.2 Research Objectives

With the goal to find optimal conditions of copper ECP for microelectronic applications, this study will investigate copper anodic behavior in various aqueous solutions, copper anodic layers and ECP efficiency in different electrolyte solutions, copper ECP mechanisms, and the factors that affect copper ECP. The following objectives are expected to be achieved:

(1) Study copper anodic behavior in various representative chemical solutions through measuring polarization curves and observing chemical and electrochemical reactions on the anode surface

(2) Measure copper anodic layers in various electrolytes with electrochemical impedance spectroscopy (EIS). Study the mechanisms of mass transport in anodic layers and solutions.

(3) Measure the efficiency of copper electropolishing in these chemical solutions.

(4) Study the mechanisms copper electropolishing. Investigate the different ECP behaviors of copper bulk material and electroplated film on patterned silicon wafer.

(5) Identify the factors that affect copper electropolishing. Find the optimal process parameters for ECP of electroplated copper films on patterned silicon wafer.

1.3 Thesis Outline

In this chapter, an introduction to copper electropolishing for microelectronic application has been presented. The organization of the rest of this dissertation is as follows.

Chapter 2, fundamental theory of copper electrochemical polishing, based on literature study, discusses various physical and chemical phenomena and processes on metal solid surface, metal-electrolyte interface, and in an electrochemical system. The mechanisms of copper electrochemical polishing in aqueous electrolyte solutions are also discussed.

Chapter 3 will discuss copper anodic behavior in an electrolyte solution. Limiting current plateau data obtained from copper anodic polarization curves, measured with a computer-controlled potentiostat, in various chemical solutions will be presented. Feasible electrical conditions for ECP of copper films electroplated on patterned silicon wafer will also be discussed.

In Chapter 4, Study the anodic layers and mass transport mechanisms in various electrolyte solutions with Electrochemical Impedance Spectroscopy (EIS). Types of the anodic layers and mass transport limiting species are identified.

In Chapter 5, results of copper ECP in various chemical solutions using chronoamperometry technique are presented. The ECP effects were evaluated using an atomic force microscope (AFM). Copper ECP efficiency in the different solutions calculated from thickness and surface roughness data measured before and after ECP. A detailed description of electropolishing mechanisms is presented. Finally, optimal conditions for ECP of electroplated copper films on patterned silicon wafers are presented.

Chapter 6 concludes the thesis work and suggests the areas of future research.

References

1. Intel® Pentium® 4 processor, Available: http://www.intel.com/home/desktop/pentium4/ [Viewed: October 22, 2002]
2. S. Wasson and A. Brown, Pentium 4 "Northwood" 2.2 GHz vs. Athlon XP 2000+ Battle of the Big Dawgs, Jan. 7, 2002. Available: http://www.tech-report.com/reviews/2002q1/northwood-vs-2000/index.x?pg=1 [Viewed: October 22, 2002]
3. Cu Damascene, Novellus Systems, Inc., 2002. Available: http://www.novellus.com/damascus/boc/boc.asp[Viewed: October 22, 2002]
4. Lesley V. Kriewald, Texas A&M Engineering News. Available: http://tlo.tamu.edu/content.cfm?Section=INDR&PageID=157 [Viewed: October 22, 2002]
5. S. Lapotin, A. Preusse, and R. Cheung, Characterization of Electrodissolving Copper in Aqueous Solution for Sub-Quarter Micron Interconnect Formation in Low k Materials, *Electrochemical Society Proceedings Volume 99-31*, 221-231.
6. D. H. Wang, S. Chiao, M. Afnan, P. Yih, M. Rehayem, Stress-Free Polishing Advances Copper Integration with Ultralow-k Dielectrics, *Solid State Technology*, 44, 10 (2001). Available: http://sst.pennnet.com/Search/ShowIssue.cfm.
7. S. Sato, Z. Yasuda, M. Ishihara, and et al, Newly Developed Electro-Chemical Polishing Process of Copper as Replacement of CMP suitable for Damascene Copper Inlaid in Fragile Low-k Dielectrics, *IEEE International Electron Devices Meeting IEDM 2001*, Dec. 2-5, 2001, Washington, DC, USA, 84-87.
8. M. H. Tsai, S. W. Chou, and C. L. Chang, et al, CMP-Free and CMP-Less Approaches for Multilevel Cu/low-k BEOL Integration, *IEEE International Electron Devices Meeting. Technical Digest*, Dec. 2-5, 2001, Washington, DC, USA, 4.3. 1-4.
9. M. Datta, Microfabrication by Electrochemical Metal Removal, *IBM J. Res. Develop.*, **42**, 5 (1998), 655-669.
10. H. Abrams and C. L. Mantell, Electrolytic Polishing of Copper and Nickel Silver, *Electrochem. Tech.*, **5**, 5-6(1967), 287-292.
11. D. Landolt, Review Article Fundamental Aspects of Electropolishing, *Electrochim. Acta*, **32**, 1 (1987), 1-11.
12. P. Neufeld and T. Zervas, The Relationship Between Polarization Characteristics and the Electropolishing Behavior of Copper, *Surf. Tech.*, **8**, (1979), 129-135.
13. I. A. S. Mansour and T. H. El Sherify, Electropolishing of Horizontal Copper Ring Disks in H_3PO_4 Solutions, *Surf. Tech.*, **19** (1983), 355-361.
14. J. Edwards, The Mechanism of Electropolishing of Copper in Phosphoric Acid Solutions, *J. Electrochem. Soc.*, **100**, 8(1953), 223C-230C.

15. M. Matlosz, S. Magaino, and D. Landolt, Impedance Analysis of a Model Mechanism for Acceptor-Limited Electropolishing, *J. Electrochem. Soc.*, **141**, 2 (1994), 410-418.

16. R. Vidal and A. C. West, Copper Electropolishing in Concentrated Phosphoric Acid, I. Experimental Findings, II. Theoretical Interpretation, *J. Electrochem. Soc.*, **142**, 8 (1995), 2682-2694.

17. M. Novak, A. K. N. Reddy, and H. Wroblowa, An Ellipsometric Study of Surface Films on Copper Electrodes Undergoing Electropolishing, *J. Electrochem. Soc.*, **117**, 6 (1970), 733-737.

18. R. J. Schaefer and J. A. Blodgett, Holographic Study of Electropolishing, *J. Electrochem. Soc.*, **123**, 11 (1976), 1701-1705.

19. J. L. Fang and N. J. Wu, Determination of the Composition of Viscous Liquid Film on Electropolishing Copper Surface by XPS and AES, *J. Electrochem. Soc.*, **136**, 12 (1989), 3800-3803.

20. P. V. Shigolev: 'Electrolytic and Chemical Polishing of Metals', 2nd edn, 7, 1974, TEL-AVIV, Israel, Freund Publishing House.

21. C. Wagner, Contribution to the Theory of Electropolishing, *J. Electrochem. Soc.*, **101**, 5(1954), 225-228.

22. R. Soutebin and D. Landolt, Anodic Leveling under Secondary and Tertiary Current Distribution Conditions, *J. Electrochem. Soc.*, **129**, 5 (1982), 946-953.

23. H. F. Walton, The Anode Layer in the Electrolytic Polishing of Copper, *J. Electrochem. Soc.*, **97**, 7 (1950), 219-226.

24. R. Soutebin H. Froidevaux, and D. Landolt, Theoretical and Experimental Modeling of Surface Leveling in ECM under Primary Current Distribution Conditions, *J. Electrochem. Soc.*, **127**, 5 (1982), 1096-1100.

25. R. Alkire and A. Cangellari, Effect of Benzotriazole on Dissolution of Copper in the Presence of Fluid Flow, *J. Electrochem. Soc.*, **136**, 4 (1989), 913-919.

26. M. Matlosz and D. Landolt, Shape Changes in Electrochemical Polishing: The effect of Temperature on the Anodic Leveling of Fe-24Cr, *J. Electrochem. Soc.*, **136**, 4 (1989), 919-929.

27. R. J. Contolini, A. F. Bernhardt, and S. T. Mayer, Electrochemical Planarization for Multilevel Metallization, *J. Electrochem. Soc.*, **141**, 9 (1994), 2503-2510.

28. R. J. Contolini et al, Removal of Field and Embedded Metal by Spray Etching, US Patent 5,486,234, Jan. 23,1996.

29. ASM International, ASM Handbook, Volume 5, *Surf. Eng.*, 815. Materials Park, Ohio, 1994.

30. M. A. Fawzy, G. H. Sedahmed, Electropolishing of inclined Cylinders under Nature Convection Condition, *Surf. Technol.*, **24**, (1985) 253.

31. A. M. Ahmed and G. H. Sedahmed, Electropolishing of Large Cavities under Free Convection Mass Transfer Controlling Conditions, *J. Mater. Sci. Lett.*, **9**, (1990) 270.

32. D. J. Dingley, T. Boal, and P. J. Phillips, The Orientation of Grain Boundaries in Annealed Copper, *Electron Microscopy and Analysis*, 1993, 377.

33. M. A. Ochando, A. Sanchez, and C. R. Serna, Mean Inner Potentials of Aluminum and Copper, *J. Physics C (Solid State Physics)*, **16**, (1983), L401.

34. M. Datta, Microfabrication by Electrochemical Metal Removal, IBM J. Res. Develop., **42**, 5 (1998), 655-669.

35. Shih-Chieh Chang, Jia-Min Shieh, Chih-Chang Huang, Bau-Tong Dai and Ming-Shiann Feng, Pattern Effects on Planarization Efficiency of Cu Electropolishing, Jpn. J. Appl. Phys. Vol. 41(12), Part 1, 7332–7337(2002).

Chapter 2

Fundamental Aspects of Electrochemical Polishing

The process of electrochemical polishing involves interaction between metal surface and electrolyte, electron transfer, electrochemical reaction, ion / molecule motion, and convection. To better understand the mechanisms of copper electrochemical polishing, it is necessary to know the state of metal surface, the chemistry of solid-liquid interface, and the electrochemical processes.

2.1 Solid Surface

Bulk metals are normally polycrystalline that are constructed by the repetition of identical structural units (crystalline cells) in space. Each unit cell consists of one or more metal atoms. These atoms vibrate around their equilibrium positions (lattices) but are tightly held together by the attractive electrostatic interactions between the negative charges of the electrons and the positive charges of the nuclei [1, 2]. The crystalline, atomic and electronic structures in a metal material determine its properties. For instance, copper has good plasticity due to its FCC crystal structure and good electrical conductivity due to its electronic structure. Metal atoms usually have one or two, but no more than three valence electrons [3]. These valence electrons can freely move inside the surface. Under electrical field (**E**), the free electrons move in the direction of applied field, resulting in conductivity.

However, the crystal periodicity is disrupted at grain boundaries and metal surfaces. Surface atoms have fewer neighbors than bulk atoms. Parts of the chemical bonds, which constitute the bulk-crystal structure, are broken to create the surface and thus the formation of a surface costs energy (surface energy). The surface of a crystalline solid in vacuum is generally defined as the few outermost atomic layers. If the surface is clean, then the top layer may be reconstructed. In addition, multilayer relaxation, i.e., interlayer spacing change, may occur at the top surface [4]. Due to these changes, in

comparison with the bulk properties, the electronic structure near the surface is markedly different. Quantum mechanics shows that localized energy levels will arise at the surface. Many macroscopic effects and phenomena on surfaces are related to this change, for example, the surface free energy, the adhesion forces, the work function, contact potential, low-energy electron diffraction, and chemical redox potential [5-7].

In addition to atom reconstruction and multilayer relaxation at the surface, crystalline defects, such as vacancies, dislocations, step edges of facets, and grain boundaries, as illustrated in Fig. 2-1, also exist at a real metal surface. Since the packing

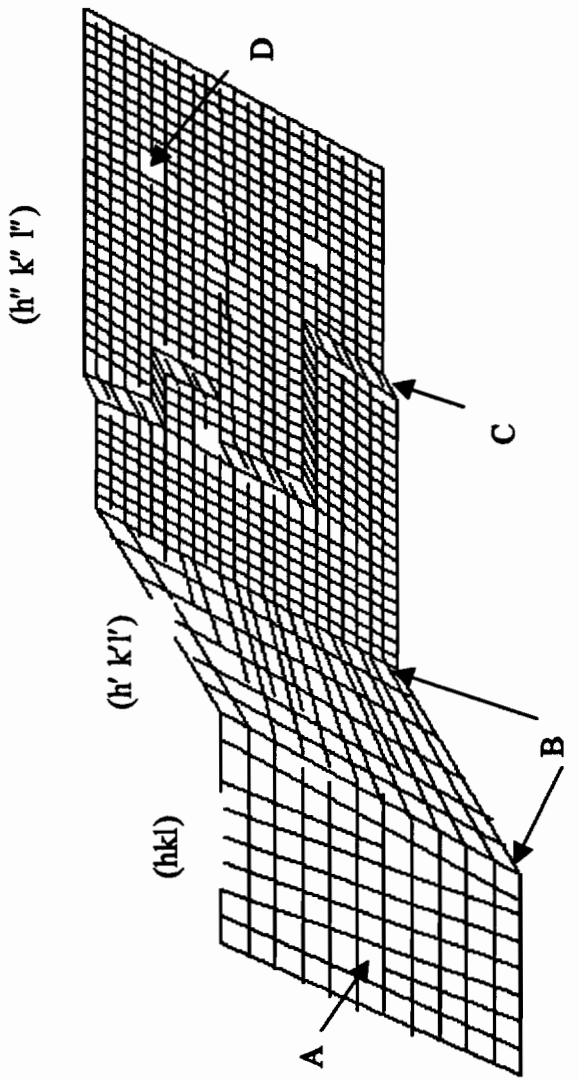

Figure 2-1 Surface profile of crystalline solid in atomic scale, illustrating crystal planes, such as (hkl); dislocations (A); grain boundaries (B); facets (C); and point defects (D).

density varies between different crystal planes, their relaxed states at a surface would imply different surface energies [8]. These surface varieties apparently affect the surface electronic structure and thus the surface physical and chemical properties as well. For example, on copper, (100) planes have the lowest and (111) planes have the highest dissolution rate in the active potential region of an electrochemical process [9].

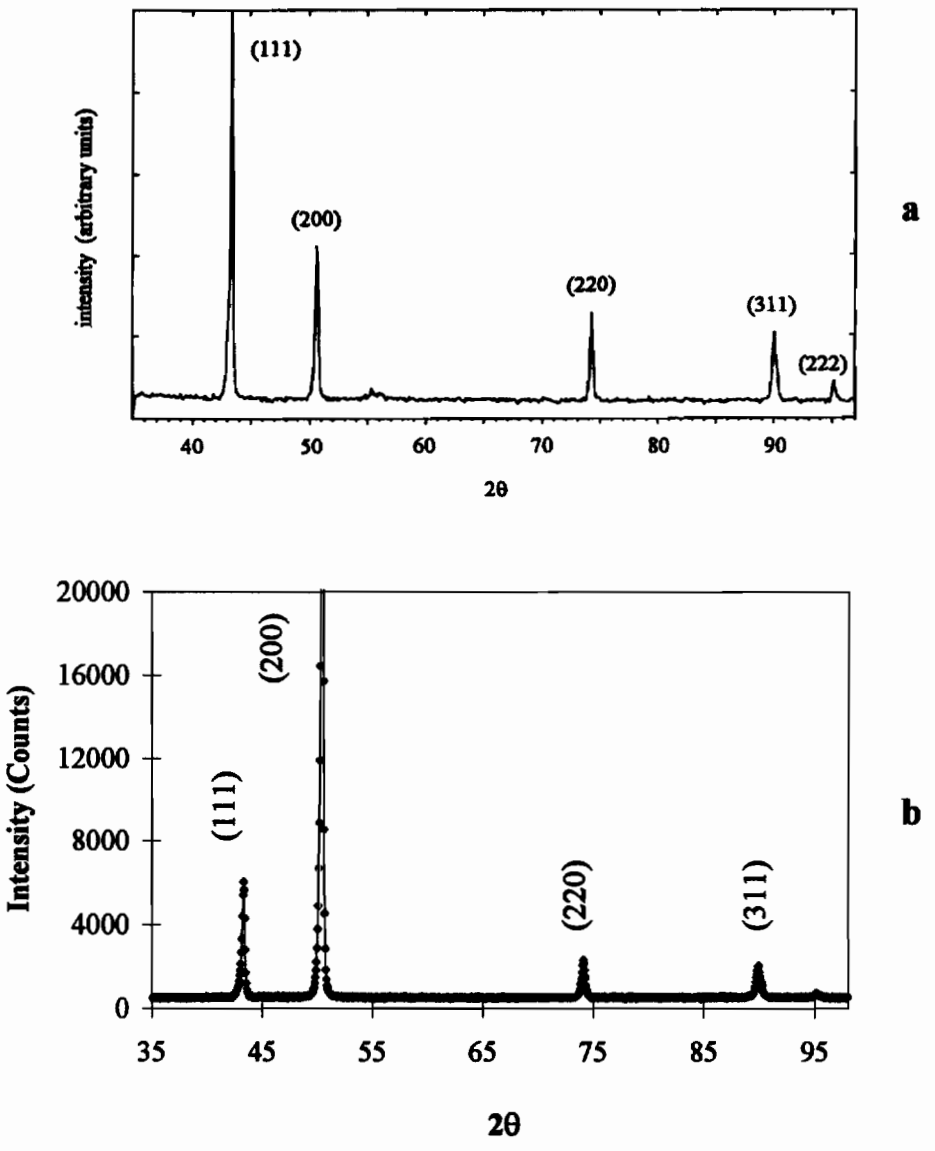

Figure 2-2 XRD spectra of ALD produced copper film (a) and of forged copper plate (b).

The orientations of crystal grains in a material depend on processing conditions the material has undergone. For example, the crystal grains of copper films produced by atomic layer deposition (ALD) have no preferential orientation while forged copper plates may have crystal grains preferentially oriented in certain directions, as shown in Fig. 2-2. In Fig. 2-2a, the x-ray diffraction (XRD) spectra of ALD copper films conform to spectra of copper powder diffraction file (PDF), which has isotropic distribution of crystals orientations. In Fig. 2-2b the (200) spectrum of forged copper plates has intensity several times higher than that of other spectrum. This indicates that a lot more crystal grains are orientated such that their (100) planes are parallel to the surface of the copper plate. These characteristics resulted from different processing conditions will affect the electrochemical behavior.

Copper is the second best electrical conductor. It is chemically stable in air and pure water [10]. In contact with electrolytes, a series of physical, chemical and electrochemical reactions may occur between copper and solutions. It can be oxidized in oxygen-containing acid solutions. Complex copper compounds may form in organic solutions under electrochemical conditions.

In macro scale, pure metals, such as copper and silver, generally exhibit low strength, high plasticity and toughness. A mechanically polished surface of copper bulk material displays characteristics similar to a tough fracture surface, as shown in Fig.2-3. In contrast, the surface profile of copper film has gentler geometrical variation. If the film is electroplated on patterned wafer, bumps and pads form on the surface due to the distribution of additives in the bottom of the trenches, vias, and flat surface.

The characteristics of surface profiles have direct effects to electrochemical polishing (ECP), which will be further discussed in Chapter 5. The ECP effect is usually evaluated by the change of mean roughness of the surface before and after ECP process. An average roughness of a solid surface is defined as following [11, 12]

$$R_a = \frac{1}{l}\int_0^l |Z(x)|dx \qquad 2\text{-}1$$

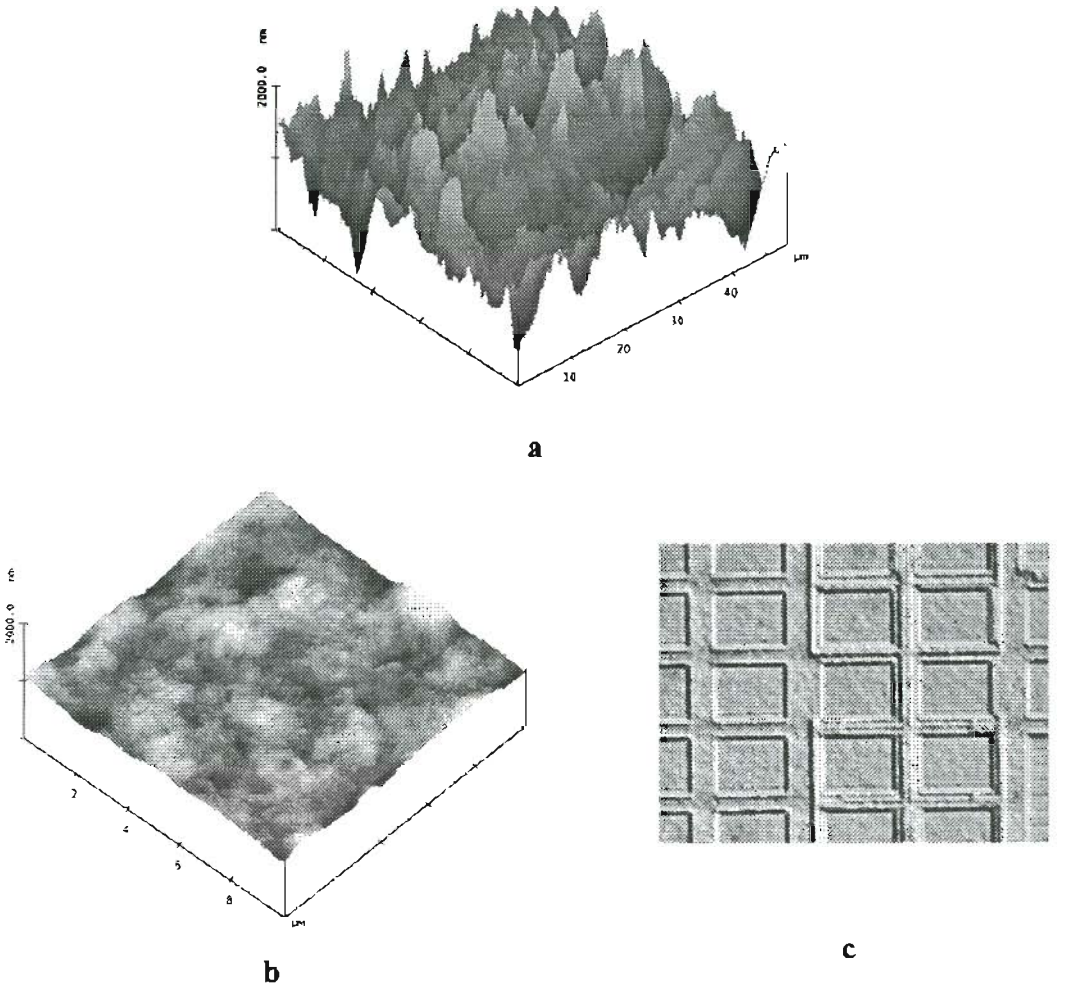

Figure 2-3 Surface topography in micro scale: (a) copper bulk material, (b) copper thin film electroplated on blanket wafer, and (c) on patterned wafer.

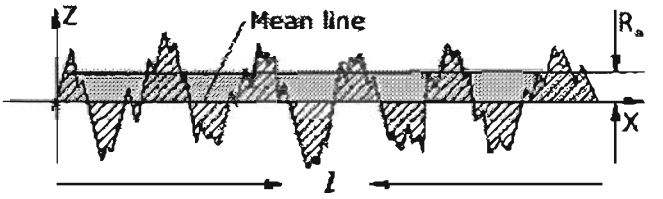

Figure 2-4 Model of Surface profile and average roughness measurement

where R_a is the arithmetic average of the absolute values of the roughness profile ordinates, l is the length of the sample (See Fig. 2-4). A discrete digital form of the above equation is

$$R_a = \frac{1}{N}\sum_{1}^{N}\left|Z_i - Z_{avrg}\right| \qquad 2\text{-}2$$

where Z is the height. Zero line is taken for the lowest Z measured by an AFM.

2.2 Aqueous electrolyte solution

An electrolyte is a substance in a solution or melt that is at least partly in the form of charged species – ions and thus conducts electricity [13, 14]. There are solid and liquid electrolyte solutions. The latter may be further classified as aqueous and non-aqueous. In an aqueous electrolyte solution, water (H_2O) is used as the solvent.

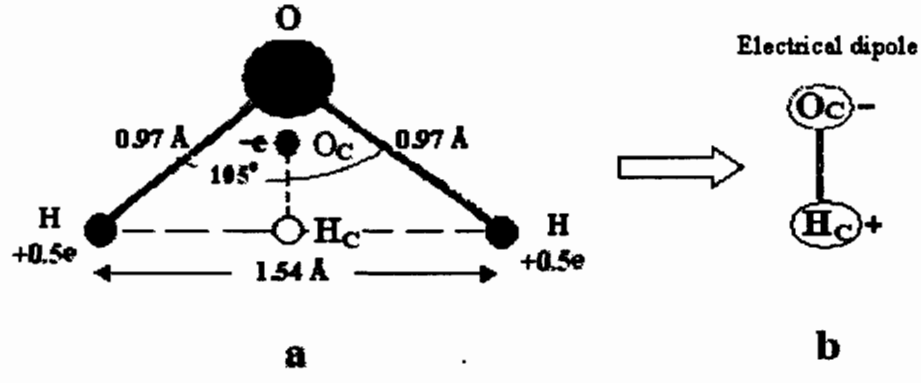

Figure 2-5 Structure and charge distribution of water (H_2O) molecule (a), and its equivalent dipole model (b).

Water is the most common solvent. Fig. 2-5 illustrate the structure and charge distribution of a water molecule [14]. The distance between oxygen and hydrogen atoms is about 0.97 Å. And the two hydrogen atoms are about 1.54 Å apart. The O-H bonds are oriented at an angle of 105°. The center of negative charge (-e) of oxygen (Oc) and the

center of positive charge (+e) of hydrogen (Hc) atoms form a dipole [14]. Such a molecular structure may break the chemical bonds of certain substances when it interacts with them.

Fig. 2-6 illustrates the electrostatic interactions between water molecules and NaCl ionic crystal [15]. The dissociation of Na^+-Cl^- bond occurs through the attracting force between Na^+ ion and the Oc^- end of water dipole (=) and between Cl^- ion and the Hc^+ end of water dipole (+). The dissolution of the crystal in water is achieved when the chemical bonding between Na^+ and Cl^- ions is overcome by the electrostatic attraction and thermal vibration energy of Na^+ and Cl^- ions in crystal.

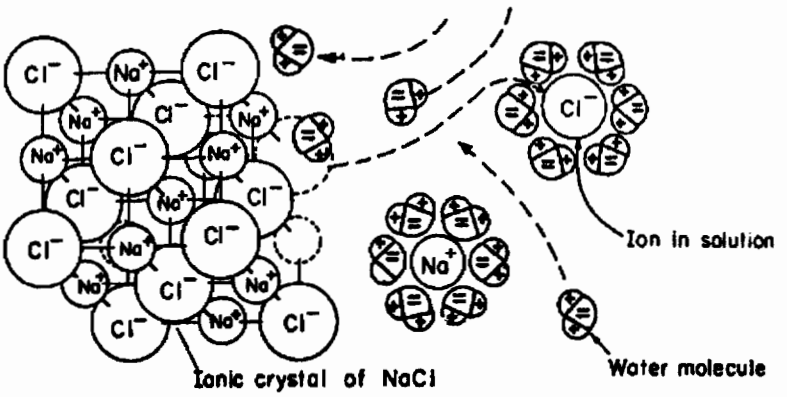

Figure 2-6 Dissolution of an ionic crystal by the action of a solvent (H_2O).

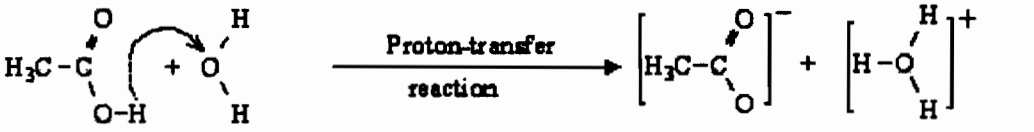

Neutral acetic acid molecule | Neutral water molecule | Acetate ion | Hydrogen ion

Figure 2-7 Ions produced by interaction of neutral molecules of water and of acetic acid.

Another way to produce mobile ions is based on the fact that some neutral (i.e., nonionic) substances can also interact with water to produce ions in solution. Fig. 2-7 illustrates how neutral molecules of water and of acetic acid interact to give an electrolytic solution of hydrogen ions and acetate ions [16].

Overall, an electrolytic solution is electrically neutral, i.e., the net charge is zero. This is due to the fact that the total charge due to the positive ions is equal to the total charge due to the negative ions. In the solution, water molecules are randomly oriented except those adjacent ions, as shown in the schematic (Fig 2-8). Of course in reality the structure is more complicated (several shells around the ions, gradually breaking up with distance).

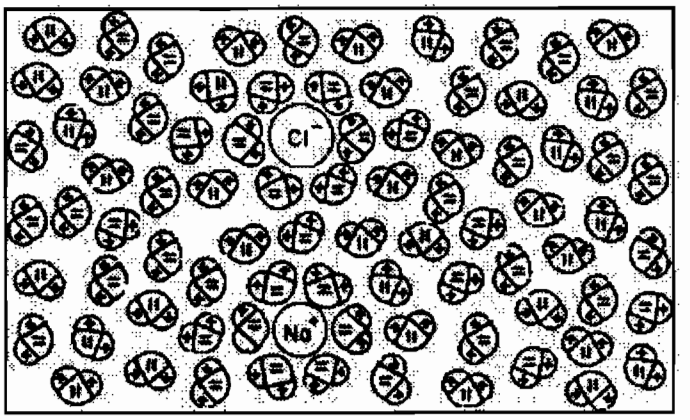

Figure 2-8 A schematic representation of the random orientation of water dipoles and the distributions of ions at an instantaneous moment in an aqueous electrolytic solution.

Ions and water molecules move around randomly in the solution (*Brownian motion*). If there is a difference in the concentration of ions in different regions of the solution, the resulting concentration gradient produces a flow of ions known as *diffusion*. If there are differences in electrostatic potential, at various points in the electrolytic solution, then the resulting field produces a flow of charge in the direction of the field. This is termed *migration* or *conduction*. The conductivity of an electrolytic solution depends on the electrolytes and their concentration in the solution [13]. Finally, if a

difference of pressure, density, or temperature exists in the solution, the liquid will move as a whole or parts of it move relative to other parts. This is *hydrodynamic* flow. These motions usually occur simultaneously in a real electrochemical system.

2.3 Solid-Liquid Interface

In an electrochemical system, electrodes are indispensable components and have to touch with electrolyte so that electrochemical processes can complete. The most important electrochemical processes, charge transfer and chemical reactions, occur at the electrolyte-electrode interfaces. Therefore, the knowledge of electrolyte-electrode interface is significant.

As stated above, an aqueous electrolytic solution exhibits electroneutrality and random orientation of water dipoles. Thus, on a time average, the ions and water molecules in aqueous solution experience forces that are independent of direction and independent of position in the electrolyte [17]. On the other hand, in the metal the valence electrons (free electrons) are highly mobile. The free electrons and atoms at the solid surface have higher energy states. Thus some of the atoms on the metal surface may lose electrons to form ions, i.e., ionization, at one moment. The ions may also recombine with electrons and become atoms at another moment. Depending on the electronic structures, some metals (such as sodium) are easier than others (such as platinum) to ionize. Copper is relatively stable. Still, some of the surface atoms may be expected to ionize at a moment.

The ionization process may be promoted when the metal is in touch with aqueous solution due to the facts that [15, 18]:

(1) Metal ions can not move in the metal electrode but can move through the solution, producing electric current in solution with an applied potential;

(2) Electrons can move freely in metal solid (electric current in a metal) but can not survive in solution and will quickly recombine with positive ions;

(3) Water dipoles and negative ions in solution may drag the surface metal ions into the solution.

As more surface metal atoms ionize, more extra electrons remain inside the metal solid. The electrostatic attraction between these electrons and the ionized metal ions make the ions to be adsorbed onto the metal surface, as shown in Fig. 2-9.

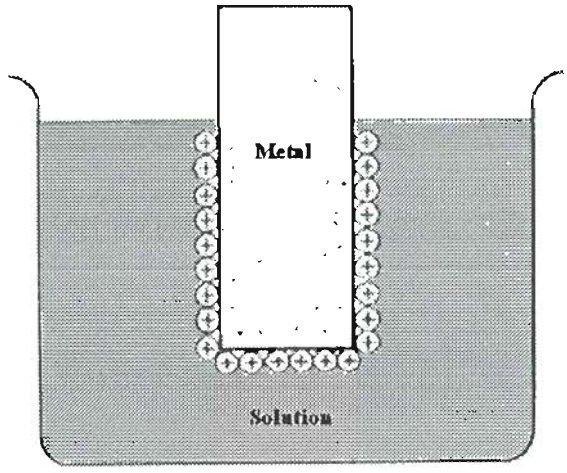

Figure 2-9 Adsorption of ionized metal ions onto the metal surface.

If a positive potential is applied to the metal (this is case an anode in an electrochemical cell), the ionization of surface metal atoms will be enhanced and thus more metal ions are produced at the surface and more electrons inside the metal.

In the solution, water molecules, positive and negative ions drift around. The adsorbed layer of positive metal ions attracts nearby water dipoles in a preferential direction, which move towards the metal surface. This forms the first layer (*hydration sheath*) – *inner Helmholtz layer*, as shown in Fig. 2-10a. While it is occupied largely by water dipoles, some negative ions can also be found in this layer. These adsorbed ions are said to be specifically adsorbed. The locus of the electrical centers of the specifically adsorbed ions is called the *inner Helmholtz plane* (IHP, at X_1) [19, 20].

Solvated ions can approach the metal only to a distance X_2; the locus centers of these nearest solvates ions is called *outer Helmholtz plane* (OHP). The interaction of solvated ions with the charged metal surface involves only long-range electrostatic force, so that their interaction is essentially independent of the chemical properties of the ions. These ions are said to be nonspecifically adsorbed. Because of thermal agitation in the

solution, the nonspecifically adsorbed ions are distributed in a three dimensional region called *diffuse layer* (δ_d), which extents from OHP into the bulk of the solution (i.e., $\delta_d = X_3 - X_2$) [19, 20].

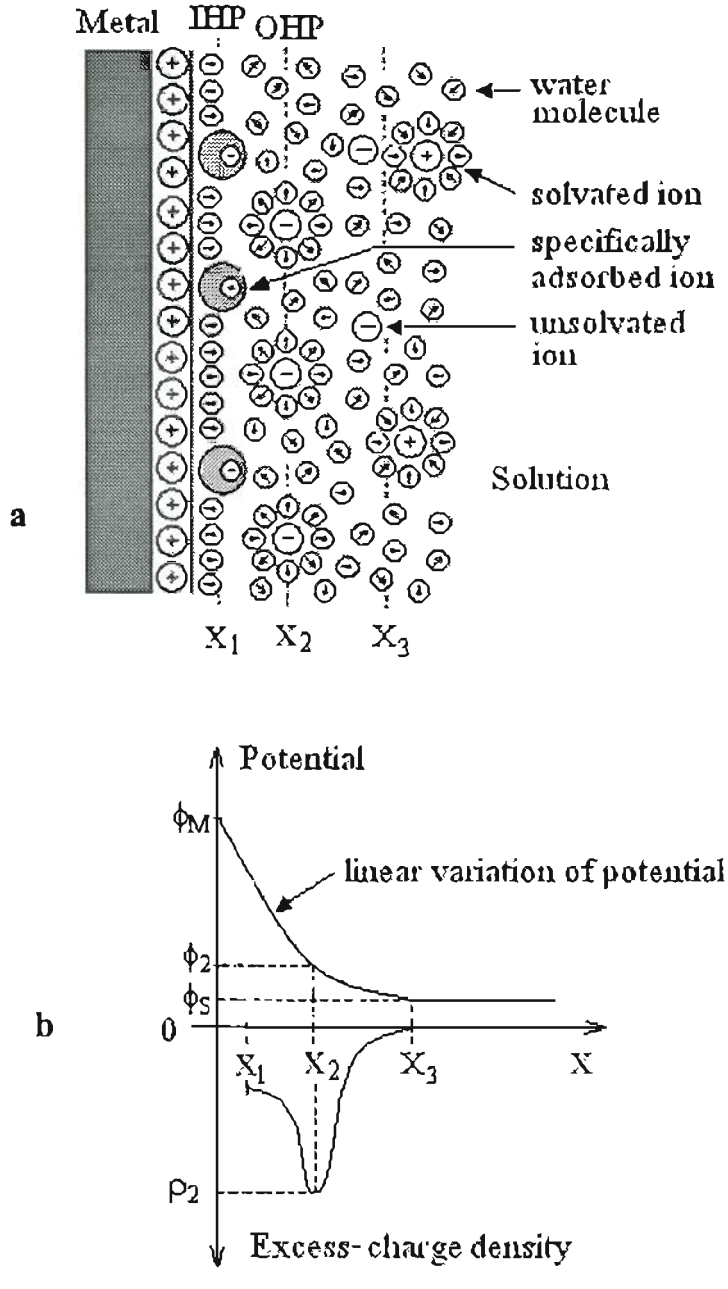

Figure 2-10 Double layer formed at the metal-solution interface (a) and the potential variation across the double layer (b).

The *diffuse layer* is loosely held there by electrostatic attraction. It is balanced by the attraction from the positive charge of the adsorbed fixed layer and the repelling from the excess of electrons inside the metal. Ions are free to move around in this layer, and to enter or leave it. Some of the ions in the diffuse layer are positive, but the net charge of the layer is negative. The excess-charge density in the diffuse layer decreases with the distance from OHP (ρ_2 at OHP) to the bulk of solution (zero at X_3) where positive and negative ions are equally likely in any region – thermal motion reigns supreme. The total excess-charge in the layer is equal to that of the adsorbed fixed layer [18, 19]. Likewise, the potential falls off into the solution, at first sharply and then asymptotically (See Fig. 2-10b).

The adsorbed fixed layer and the OHP layer (or the adsorbed fixed layer and the whole mobile diffuse layer) together are the so-called *electrical double layer*, see Fig. 2-10a. The double layer acts as a capacitor in an electrochemical system, with a 'fix plate' (the adsorbed fixed layer) and a 'moveable plate' (the double layer) [18-20]. Its structure may significantly affect the electrode processes (detailed discussion in chapters 4 and 5).

2.4 Electrochemical cell and electropolishing

2.4.1 Electrochemical cells

As stated above, when a metal bar is dipped into water or electrolytic solution, electrons and metal ions will build up respectively inside the bar and on the surfaces immersed in the solution (See Fig. 2-9). Different metals have different tendencies of such electron / ion build-up and thus may have different electric potentials. For example, when copper and iron bars are put into same solution, more electrons build-up in iron than that in copper. So iron is more negative in potential than copper. If an electrical connection is made between the copper and iron bars, electrons will flow from iron to copper, as shown in Fig. 2-11. The process may continue until all the iron has corroded away or until all the hydrogen ions (obtain electrons at copper surface and form hydrogen gas) in the solution have been used up. In the process, iron atoms are said to be oxidized and hydrogen ions are said to be reduced. This is how a battery (power supply) cell works.

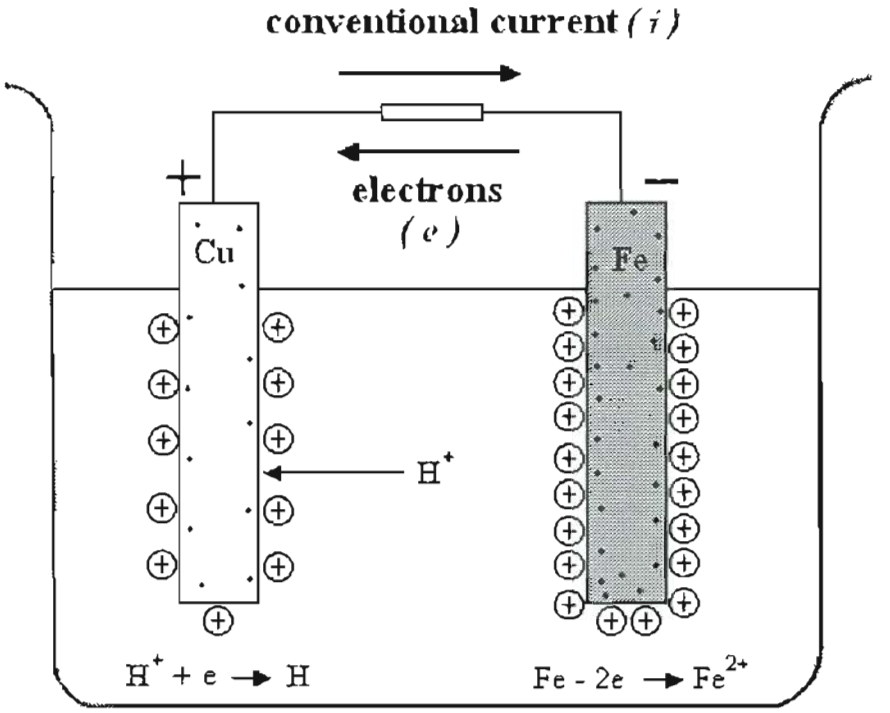

Figure 2-11 A battery cell.

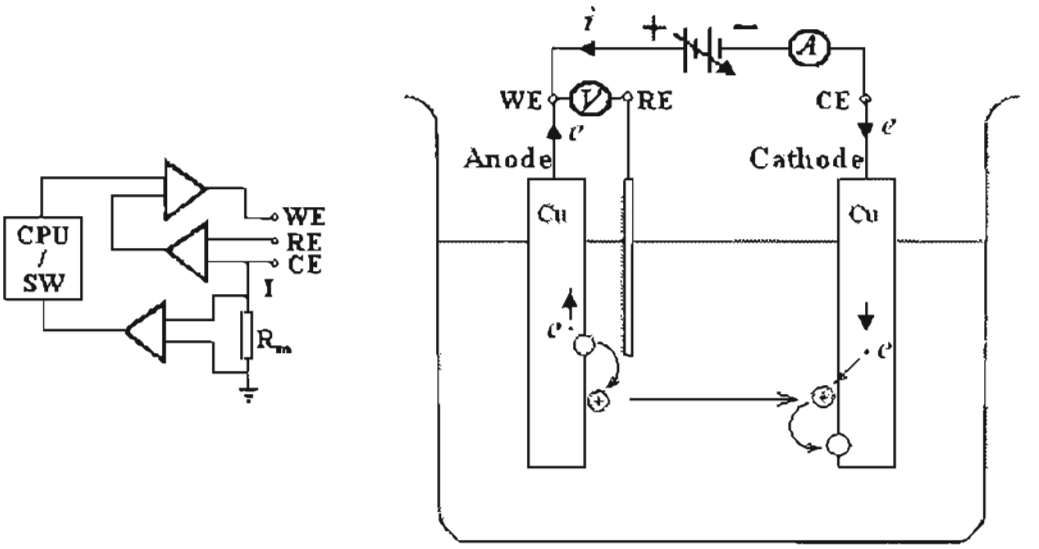

Figure 2-12 A copper electrochemical deposition / polishing cell.

The present study focuses on another kind of electrochemical cell, which forces the oxidation / reduction processes to occur by an external power supply, as illustrated in Fig. 2-12. An external voltage is applied to the two electrodes. The electrode connected to the positive pole of the power supply is called *anode*. And the one connected to the negative pole of the power supply is called *cathode*. When the applied voltage is high enough, electrons in the anode may be pumped out and the metal atoms on the anode surface will be oxidized (e.g., $Cu - 2e \rightarrow Cu^{++}$) and dissolved into the electrolyte solution. Under electrical field, the positive ions (*cations*) move towards cathode and negative ions (*anions*) move towards anode. The cations may get electrons and be reduced to atoms (e.g., $Cu^{++} + 2e \rightarrow Cu$) again at the cathode surface, as illustrated in Fig. 2-12. Therefore, electron transfer between the two electrodes is carried out via the ion drift in the electrolyte and electron conduction in metal wire. When the working electrode (WE) is set to be anode, dissolution is processed at certain potential. Likewise, when the working electrode is set to be cathode, it can result in deposition. For electropolishing of copper, the copper part to be polished is set to be anode while the cathode can be any conductive material (e.g., copper).

The potential of the working electrode may be measured and controlled with a system shown in Fig.2-12. The critical potential at which the oxidation / reduction starts to occur is related to the *standard redox potential*, E^0, for a specific anode material. The redox potential is a measure (in volts) of the affinity of a substance for electrons - its electronegativity - compared with hydrogen (which is set at 0). Substances more strongly electronegative (i.e., capable of oxidizing or accepting electrons) than hydrogen have positive redox potentials (e.g., Cu / Cu^{++}: $E^0 = 0.34$ V). Substances less electronegative (i.e., capable of reducing or giving up electrons) than hydrogen have negative redox potentials (e.g., Cr^{3+} / Cr^{2+}: $E^0 = -1.07$ V) [21, 22, 23].

2.4.2 Kinetics of electrode reactions

For an electrochemical process involving oxidized species "ox" (e.g., Cr^{3+}) and reduced species "re" (e.g., Cr^{2+})

$$ox + n\,e \rightleftharpoons re \qquad 2\text{-}3$$

the dynamics of the process in equilibrium may be characterized by the *Nernst equation* [24, 25]

$$E = E^0 + \frac{RT}{nF}\ln\frac{a_{ox}}{a_{re}} \qquad 2\text{-}4$$

where a_{ox}, a_{re}, and $a_{M^{n+}}$ are the activities of ox and re. In a simple case (so called "first-class" electrodes), when a metal is immersed in a solution that contains the metal ion, reactions

$$M^{n+} + n\,e \rightleftharpoons M(s) \qquad 2\text{-}5$$

may occur and the Nernst equation is

$$E = E^0 + \frac{RT}{nF}\ln a_{M^{n+}} \qquad 2\text{-}6$$

where E is the electrode potential, R = 8.317 J mol^{-1} K^{-1} is the gas constant, T is the temperature of the system in kelvins (K), n is the number of electrons transferred in the electrochemical reactions, F = 9.64853×10^4 C is Faraday constant, a_{ox}, a_{re}, and $a_{M^{n+}}$ are the activities of ox, re, and M^{n+} in the electrolyte solution respectively. The quantity $[M^{n+}]$ is equal to the concentration of the species times the activity coefficient:

$$a_{M^{n+}} = \gamma_{\pm} C_{M^{n+}} \qquad 2\text{-}7$$

The mean activity ($\gamma_{\pm}$) at low concentration (usually < 0.01 M) is given by

$$\log\gamma_{\pm} = -0.509 z^2 \frac{\sqrt{\mu}}{1+\sqrt{\mu}} \qquad 2\text{-}8$$

where z is the charge on the ion and μ is the ionic strength

$$\mu = \frac{1}{2}\sum C_i z_i^2 \qquad 2\text{-}9$$

These equations describe the relationship between the applied electrode potential (E), standard potential E^0, and the product concentrations of electrode reactions 2-3 and 2-5.

Driven by the applied electrical field, the ionic products, together with other existing ions in the solution, move towards electrodes according to the signs of their charges. The ion drift forms a current flow in the solution. Electrons are transferred at the electrode surfaces through electrode reaction, and travel along the conductive wires in the closed circuit of the cell. As a result, an electric current flow is realized under the

externally applied voltage. Since current is much easier to measure than the ionic concentration of the electrolyte, it is a better parameter than concentration to depict the dynamics of electrode reactions. Early study indicates that in case of low current and efficient stirring, in which mass transport is not a factor determining the current, the current-potential relation is given by Tafel equation [26]

$$\eta = E - E^{0\,\square} = a + b \log i \qquad 2\text{-}10$$

where η is the over potential, $E^{0\,\square}$ is formal potential at which the interface is at equilibrium with a solution (i.e., $C_{ox} = C_{re}$), i is current, a and b are constants.

Introducing the correlation between concentrations C_{ox} / C_{re} and current (i) into the above equation leads to the well known Butler-Volmer formulation of electrode kinetics [27]

$$i = i_0[\frac{C_{ox}(0,t)}{C_{ox}} e^{-\alpha f\eta} - \frac{C_{re}(0,t)}{C_{re}} e^{(1-\alpha)f\eta}] \qquad 2\text{-}11$$

with

$$i_0 = F\,A\,k^0\,C_{ox}^{(1-\alpha)}\,C_{re}^{\alpha} \qquad 2\text{-}12$$

and

$$f = \frac{F}{RT} \qquad 2\text{-}13$$

where C_{ox} and C_{re} are bulk concentrations, $C_{ox}(0, t)$ and $C_{re}(0, t)$ are the concentrations of ox and re at the electrode / solution interfaces at time t, α (=0 ~ 1) is transfer coefficient, A is the area of the electrode, and k^0 is standard rate constant (i.e., the reaction rate constant at E^0 at which the rate of the forward process (v_f, M/s) and backward process (v_b, M/s) are equal: $v_f = k_f C_{re} = v_b = k_b C_{ox}$ and thus $C_{re} = C_{ox}$ and $k_f = k_b = k^0$).

Equation 2-11 gives a quantitative relation between current and overpotential, which reflects the dynamics of electrode reaction at low current. A graphic illustration of the equation is shown in Fig. 2-13 with constant vales: $i_0 = 10^{-7}$ A/cm^2; α = 0.3, 0.5; T = 298 K; F = 96500 C/mol, and R = 8.3144 J/(mol K). The condition "low current" means that mass transport is not the limiting process and interfacial electrochemical reaction process is dominant.

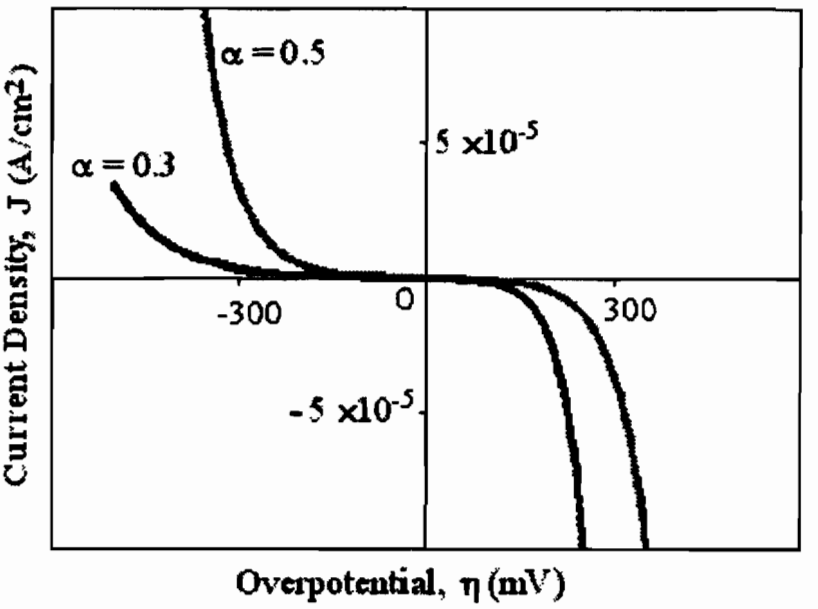

Figure 2-13 current-overpotential curves for redox reaction 2-3 with $i_0 = 10^{-7}$ A/cm^2 at 25 ^{0}C.

2.4.3 Mass transport in electrolyte solution

Mass transport is an important process in an electrochemical system. With stirring or other type of forced circulation, mass transport occurs by three mechanisms in an electrochemical cell [28]:

(1) Migration, motion of ions driven by electrical field $\frac{\partial \phi}{\partial x}$;

(2) Diffusion, motion of species (ions, atoms, molecules) driven by concentration gradient $\frac{\partial C}{\partial x}$; and

(3) Convection, driven by pressure (P).

Thus, in general, a flux J_j (mol s^{-1} cm^{-2}) of species j will occur due to the above the three types of motions. The flux may be described by Nernst-Planck equation [29]

$$J_j = -D_j \frac{\partial C_j(x)}{\partial x} - \frac{z_j F}{RT} D_j C_j \partial \frac{\phi(x)}{\partial x} + C_j \mathrm{v}(x) \qquad 2\text{-}14$$

where C_j, z_j, and D_j are respectively the concentration, number of valence electrons, and diffusion coefficient of species j; and $v(x)$ is the velocity of solution in x direction.

If j is an ionic species, then the flux J_j is equivalent to a current density. Thus, the current (i, C s^{-1}) for a solution flow through a cross-section area, A, normal to the axis of mass flow, is

$$i_j = i_{d,j} + i_{m,j} + i_{c,j} = J_j z_j F A \qquad 2\text{-}15$$

where $i_{d,j}$ is diffusion current, $i_{m,j}$ is migration current, and $i_{c,j}$ is convection current, which represent the contribution of diffusion, migration and convection respectively.

In bulk solution (away from electrode), concentration gradients, $\frac{\partial C_j(x)}{\partial x}$, are generally small, and the total current is carried mainly by migration, i.e.,

$$i_j = i_{m,j} = \frac{z_j^2 F^2 A D_j C_j}{RT} \cdot \frac{\partial \phi}{\partial x} \qquad 2\text{-}16$$

and the total current is

$$i = \sum_j i_j \qquad 2\text{-}17$$

The transference number of species j, defined as the fraction of total current that ionic species j carries is given by [29]

$$t_j = \frac{i_j}{i} = \frac{\kappa_j}{\kappa} = \frac{|z_j| C_j \lambda_j}{\sum_k |z_k| C_k \lambda_k} \qquad 2\text{-}18$$

where κ is the conductivity of the solution, κ_j and λ_j are the ionic conductivity and mobility for ion j.

For an electrochemical cell shown in Fig. 2-14, assume: the electrolyte solution contains 0.3M $CuSO_4$ and 0.001M H_2SO_4; the mobilities of Cu^{2+}, SO_4^{2-}, and H^+ are $\lambda_{Cu^{++}}$ = 50, $\lambda_{SO_4^{--}}$ = 80, and λ_{H^+} = 350 respectively; an applied potential difference (voltage) ΔE produces a total current equivalent to 200 electrons per unit time passing through the cell, i.e., i = 200 eq/s; and no convection (i.e., $i_{c,j}$ = 0). Then from Eq. 2-18, $t_{Cu^{++}}$ = 0.380, $t_{SO_4^{--}}$ = 0.611, and t_{H^+} = 0.009; and $i_{m,\,Cu^{++}} = i_{Cu^{++}}$ = 76 eq/s, $i_{m,\,SO_4^{--}} = i_{SO_4^{--}}$ = -122 eq/s, and $i_{m,\,H^+} = i_{H^+}$ = 2 eq/s, as shown in Fig. 14. Accordingly, the diffusion current of reactant species, Cu^{++}, may be calculated from Eq. 2-15: $i_{d,\,Cu^{++}} = i - i_{m,\,Cu^{++}}$ = 124 eq/s. However, for non reactant species SO_4^{2-} and H^+, to maintain the electroneutrality and the balance of

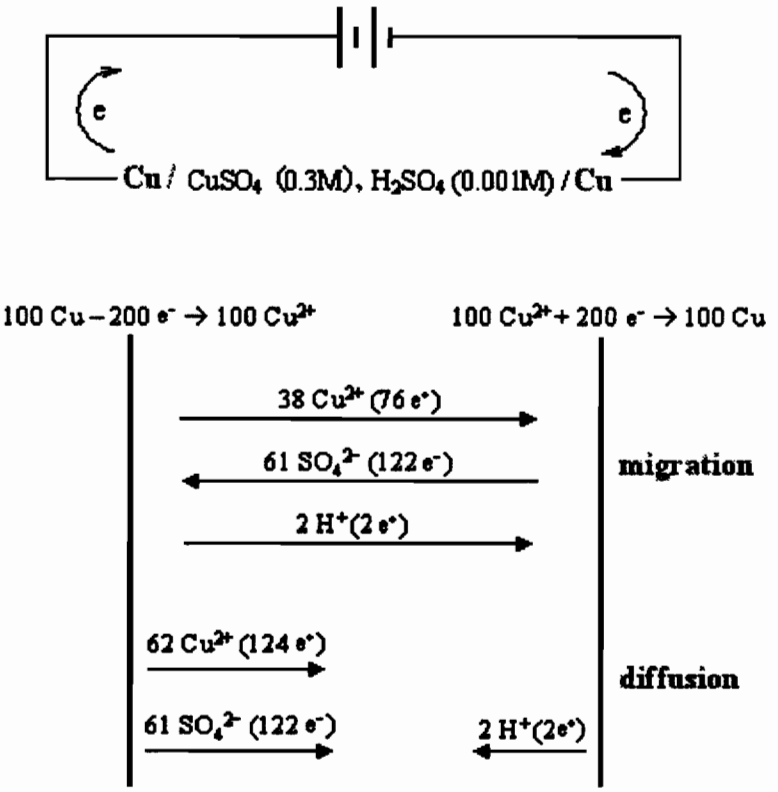

Figure 2-14 Schematic of an electrochemical deposition / polishing cell and ion motions in the solution.

concentration, same amount of ions have to diffuse to the opposite direction, i.e., $i_{d,\,SO_4^{--}} = -i_{m,\,SO_4^{--}} = 122$ eq/s, and $i_{d,\,H^+} = -i_{m,\,H^+} = i_{H^+} = -2$ eq/s. See Fig. 2-14.

In the above example, convection is neglected. Nevertheless, in a real electrochemical system, convection is usually introduced by methods such as rotating electrode, stirring, or other forced circulation strategies. In such a system, the velocity of solution flow is generally a constant (v_∞) in bulk solution (far from the electrode surface and the wall of solution container) and decreases while approaching the solid surfaces due to the friction between the fluid and the solid surface [30]. For rotating disk electrode, as employed in this study, the important velocities are radial velocity (v_r) and and normal velocity (v_y). They are shown in Fig. 2-15 and given by [31]

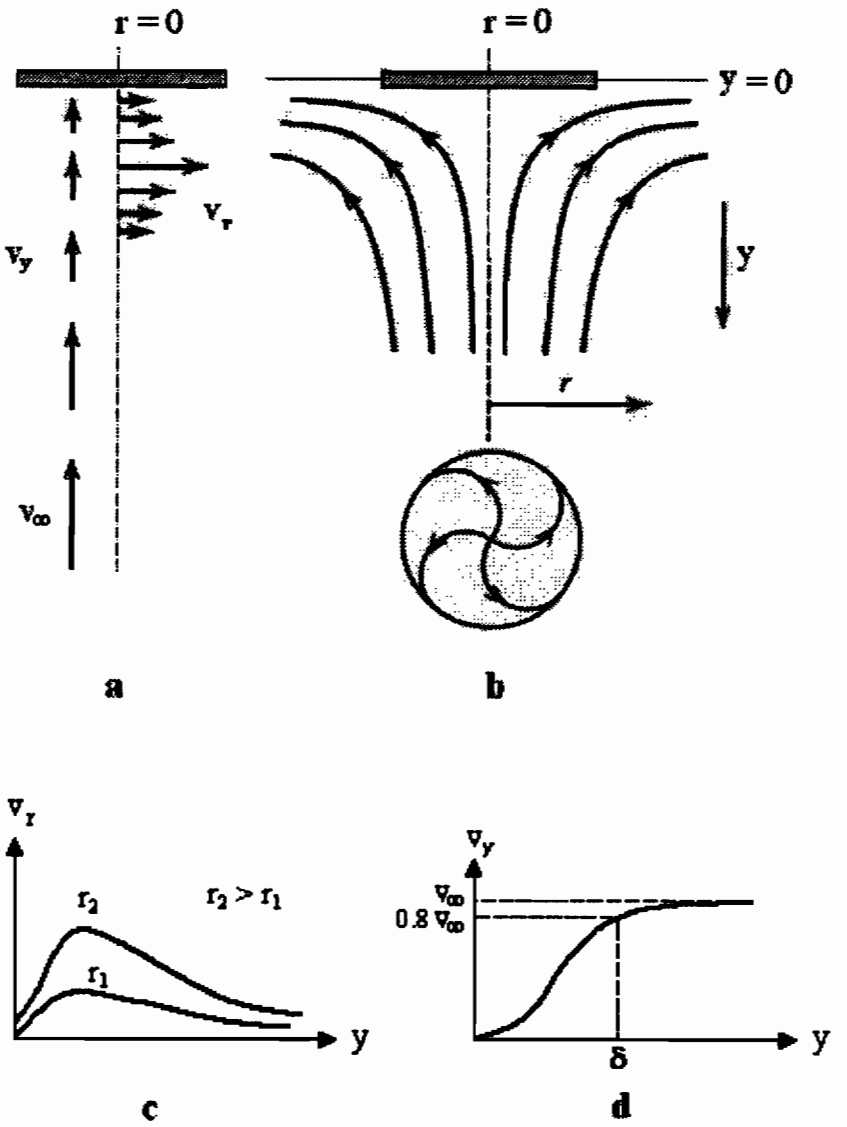

Figure 2-15 Fluid velocities near a rotating disk: a. Vector representation, b. Schematic resultant streamlines (or flows), c. Variation of radial fluid velocity (v_r) as a function of y and r, d. Variation of normal fluid velocity (v_y) as a function of y.

$$v_y = -0.51\,\omega^{3/2}\,\nu^{-1/2}\,y^2 \qquad 2\text{-}19$$

$$v_r = 0.51\,\omega^{3/2}\,\nu^{-1/2}\,r\,y \qquad 2\text{-}20$$

where $\omega = 2\,\pi$ rps (s^{-1}, rps represents resolution per second) is the angular velocity of rotating disk, ν is kinematic viscosity, y is the distance from the electrode surface, and r is the radius from the center of electrode disk.

The limiting velocity in y direction, v_∞, is

$$v_\infty = \lim_{y\to\infty} v_y = -0.88447\,(\omega\nu)^{1/2} \qquad 2\text{-}21$$

The distance $\delta = 3.6\,(\frac{\nu}{\omega})^{\frac{1}{2}}$, corresponding to $v_y = 0.8\,v_\infty$, is called the *hydrodynamic (or Prandtl) boundary layer thickness* and roughly represents the thickness of the layer of liquid dragged by the rotating disk.

The material flux during convective diffusion due to forced convection can be described by [32]

$$\mathbf{J_d} + \mathbf{J_c} = -\,D\,\mathrm{grad}\,C + C\,\mathbf{v} \qquad 2\text{-}22$$

where C is the material concentration, $\mathbf{J_d}$ is the diffusion and $\mathbf{J_c}$ the convection material flux. In case of rotating disk, Eq. 2-22 leads to

$$v_y \frac{dC}{dy} = D\frac{d^2C}{dy^2} \qquad 2\text{-}23$$

Under steady-state ($\frac{\partial C}{\partial t} = 0$); assuming that the fluid is incompressible and concentration in y direction (C_y) is much larger that the concentration in r direction (C_r); and with boundary conditions:

$y = 0$: $\quad C = C^*$;

$y \rightarrow \infty$: $\quad C = C^o$, $\frac{dC}{dy} = 0$

one gets the solution from Eqs. 2-19 and 2-23 [32]

$$J = -D(\frac{dC}{dy})_{y=0} = 0.62\,D^{2/3}\,\nu^{-1/6}\,\omega^{1/2}\,(C^o - C^*) \qquad 2\text{-}24$$

Thus,

$$i_L = n\,F\,A\,J_L = 0.62\,n\,F\,A\,D^{2/3}\,\nu^{-1/6}\,\omega^{1/2}\,(C^o - C^*) \qquad 2\text{-}25$$

for ionic species.

Since the forced convection diffusion effect is limited inside the Prandtl layer, a concentration gradient will be developed if the electrochemical reaction is faster than diffusion. In such a case (so called *limiting current* condition), the oxidized ions produced every second are more than diffusion can remove from the anode surface into the bulk solution. Consequently, the concentration at the anode surface is higher than that in the bulk solution, as illustrated in fig. 2-16. The concentration variation occurs only in a thin layer within the Prandtl layer (δ), i.e., $\delta_c < \delta$. The quantity δ_c is termed the thickness of *Nernst layer* (δ_c). This layer has significant importance to electrochemical polishing and will be further discussed in Chapter 5.

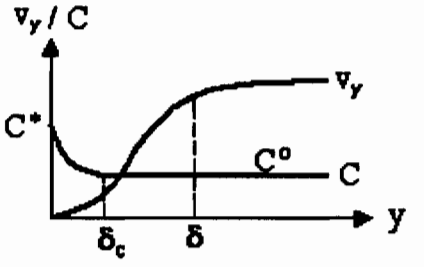

Figure 2-16 Prandtl layer (0~δ) and Nernst layer (0~δ_c) formed at the boundary between the anode surface and flowing solution.

2.4.4 Electrochemical polishing

The preceding two sections discussed the relationship between current and overpotential, and the effects of migration, diffusion, and convection. To a copper electrochemical polishing / deposition system as shown in Fig. 2-12, if the current flow through the cell is known, one can calculate the rate of copper dissolution (from the anode) or deposition (onto the cathode). Assuming that

(1) at anode, $Cu - 2e \rightarrow Cu^{++}$ 2-26

(2) at cathode, $Cu^{++} + 2e \rightarrow Cu$ 2-27

are the only reactions occurring in the system, then, the current flow of every two electrons results in one copper atom dissolved on the anode and deposited on the cathode. Since 1 A = 1 C/s, the charge of one electron e = 1.60218×10^{-19} C, so the number of electrons (per second) in 1 A current is $N_e = i / e$; the number of copper atoms being oxidized or reduced $N_a = N_e / 2 = i / 2e$, the number of moles $N_m = N_a / N_A = i / (2 e N_A)$ $= i / (2 F)$ where Avogadro's number $N_A = 6.02214 \times 10^{23}$ mole-1; the weight of N_m mole copper $W = N_m M = i M / (2 F)$ where M is the molecular weight; in volume, $V = W / d =$ $i M / (2 F d)$ where d is the density of copper. Thus 1 A current produces a dissolution / deposition rate in thickness (cm/s)

$$R_d = \frac{M}{2FdA} i \qquad 2\text{-}28$$

where A is the area of the electrode surface.

From Eq. 2-11 we can see that current increases with increasing overpotential $\eta = E - E^0$ □. Therefore, for a certain applied potential E, higher standard redox potential E^0 and so higher E^0 □ will result at lower current. According to Eq. 2-28, this will lead to lower dissolution rate. As stated in section 2.1, on a polycrystalline metal surface there are sites, such as defects and grain boundaries, where atoms are at higher energy states. In addition, due to arbitrary crystal orientation, there are different crystalline planes with different energy states of atoms on the electrode surface. Therefore, atoms at all these different sites and planes have different standard redox potential E^0, and as a result, have different dissolution rate according to Eq. 2-28. Such an anodic dissolution will not lead to polishing. Instead, a crystallographic etching is produced [9, 33-35]. This is true at lower current (or applied potential).

However, when the applied potential of anode electrode is increased to certain value, Eq. 2-11 will no longer be valid since the reaction rate is so high that the system becomes mass transport controlled. In other words, the Cu^{++} ion flux (J) and so the current (i_L) is determined by diffusion process instead of applied potential over a range of E_L (See Fig. 2-17). Previous study [36-40] indicated that a polishing effect could be achieved in this range. Further discussion will be presented in the following chapters.

With continuing increase of applied potential, other reactions than Cu oxidation / reduction may occur and contribute to the increasing current. These reactions produce H_2

and O_2 bubbles, which occur at or reach the anode surface and produce a rough surface. A whole range of $i \sim E$ curve, *polarization curve* and surface characteristics after anodic dissolution are shown in Fig. 2-17 and will be further studied in next chapter.

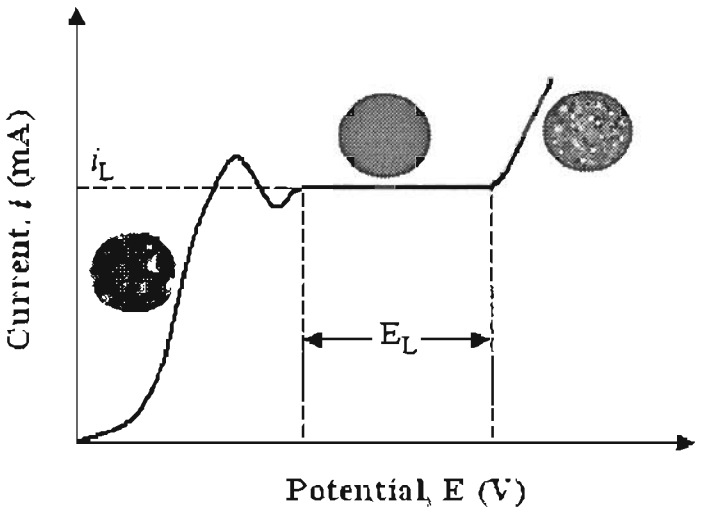

Figure 2-17 Polarization curve and surface topography after anodic dissolution at different potential range.

References

1. G. Busch and H. Schade, **Lectures on Solid State Physics**, Pergamon Press, New York, 1975, 45.
2. C. Kittel, **Introduction to Solid State Physics**, 7th ed. John Wiley & Sons, Inc., New York, 1996, 55.
3. J. R. Hook and H. E. Hall, **Solid State Physics**, 2nd ed. John Wiley & Sons, Inc., New York, 1991, 31.
4. C. Kittel, **Introduction to Solid State Physics**, 7th ed. John Wiley & Sons, Inc., New York, 1996, 555.
5. H. Lüth, **Solid Surfaces, Interfaces and Thin Films**, 4th ed. Springer, New York, 2001, 265.
6. N. W. Ashcroft and N. D. Mermin, **Solid State Physics**, Holt, Rinehart and Winston, New York, 1976, 353.
7. S. R. Morrison, **Chemical Physics of Surfaces**, 2nd ed. Plenum Press, New York, 1990, 3-4.
8. M. J. Jaycock and G. D. Parfitt, **Chemistry of Interfaces**, John Wiley & Sons, Inc., New York, 1981,157.
9. D. Landolt, Review Article Fundamental Aspects of Electropolishing, *Electrochim. Acta*, **32**, 1 (1987), 1-11.
10. K. Cui, Iron, **Steel and Non-ferrous Metal Materials**, Machinery Industry Press, Beijing, P. R. China, 1980, 414. [Chinese]
11. http://www.mahr.com/en/content/products/glossary/surface/mittenrauhwerte.html [Viewed: April 14, 2003].
12. http://www.project.slac.stanford.edu/lc/local/systems/MainLinac/High_Gradient/100901XPS_spect.pdf [Viewed: April 14, 2003].
13. Freitag, Creighton University, Fall 2002, CHM 203 G: General Chemestry I, Available http://freitag.creighton.edu/CHM203/notes/9.13.02.pdf [Viewed: April 14, 2003].
14. J. Koryta, J. Dvořák, and L. Kavan, **Principles of Electrochemistry**, 2nd ed. John Wiley & Sons, Inc., New York, 1993, 1.
15. R. A. Robinson and R. H. Stokes, **Electrolyte Solutions**, 2nd ed. Butterworths Publications Limited, London, UK, 1959, 2.
16. J. O'M. Bockris and A. K.N. Reddy, **Modern Electrochemistry**, Vol.1, Plenum Press, New York, 1970, 45-47.
17. J. O'M. Bockris and A. K.N. Reddy, **Modern Electrochemistry**, Vol.2, Plenum Press, New York, 1970, 623.
18. Solartron Analytic, Understanding Electrochemical Cells, Technical report 17.

19. J. O'M. Bockris and A. K.N. Reddy, **Modern Electrochemistry**, Vol.2, Plenum Press, New York, 1970, 629-636.

20. A. J. Bard and L. R. Faulkner, **Electrochemical Methods Fundamentals and Applications**, 2nd ed. John Wiley & Sons, Inc., New York, 2001, 12.

21. S. R. Morrison, **Chemical Physics of Surfaces**, 2nd ed. Plenum Press, New York, 1990, 311.

22. D. R. Lide, CRC Handbook of Chemistry and Physics, 81st Edition, CRC Press2000, 5-5 – 5-23.

23. http://users.rcn.com/jkimball.ma.ultranet/BiologyPages/R/RedoxPotentials.html [Viewed: April 14, 2003].

24. D. T. Sawyer, A. Sobkowiak, and J. L. Roberts, **Electrochemistry for Chemists**, 2nd ed. John Wiley & Sons, Inc., New York, 1995, 24-28.

25. J. Koryta, J. Dvořák, and L. Kavan, **Principles of Electrochemistry**, 2nd ed. John Wiley & Sons, Inc., New York, 1993, 178.

26. A. J. Bard and L. R. Faulkner, **Electrochemical Methods Fundamentals and Applications**, 2nd ed. John Wiley & Sons, Inc., New York, 2001, 92.

27. A. J. Bard and L. R. Faulkner, **Electrochemical Methods Fundamentals and Applications**, 2nd ed. John Wiley & Sons, Inc., New York, 2001, 99.

28. L.-W. Pan, P. Yuen, L. Lin, 3D electroplated microstructures fabricated by a novel height control method, *Microsystem Technologies* 8 (2002) 391–394.

29. A. J. Bard and L. R. Faulkner, **Electrochemical Methods Fundamentals and Applications**, 2nd ed. John Wiley & Sons, Inc., New York, 2001, 138.

30. F. P. Incropera, D. P. DeWitt,**Fundamentals of Heat and Mass Transfer**, 4th edn, Jone Willey & Sons, Inc., New York, 1996, 294-351.

31. A. J. Bard and L. R. Faulkner, **Electrochemical Methods Fundamentals and Applications**, 2nd ed. John Wiley & Sons, Inc., New York, 2001, 337.

32. J. Koryta, J. Dvořák, and L. Kavan, **Principles of Electrochemistry**, 2nd ed. John Wiley & Sons, Inc., New York, 1993, 134-139.

33. R. Soutebin and D. Landolt, Anodic Leveling under Secondary and Tertiary Current Distribution Conditions, *J. Electrochem. Soc.*, **129**, 946-953(1982).

34. H. Abrams and C. L. Mantell, Electrolytic Polishing of Copper and Nickel Silver, *Electrochem. Tech.*, **5**, 287(1967).

35. M. Matlosz, S. Magaino, and D. Landolt, Impedance Analysis of a Model Mechanism for Acceptor-Limited Electropolishing, *J. Electrochem. Soc.*, **141**, 410-418(1994).

36. P. V. Shigolev: **Electrolytic and Chemical Polishing of Metals**, 2nd edn, 1974, TEL-AVIV, Israel, Freund Publishing House, 7.

37. J. Edwards, The Mechanism of Electropolishing of Copper in Phosphoric Acid Solutions, *J. Electrochem. Soc.*, 1953, **97**, 223C-230C.

38. C. Wagner, Contributions to the Theory of Electropolishing, *J. Electrochem. Soc.*, 1954, **101**, 225-228.

39. M. Novak, A. K. N. Reddy, and H. Wroblowa, An Ellipsometric Study of Surface Films on Copper Electrodes Undergoing Electropolishing, *J. Electrochem. Soc.*, 1970, **117**, 733-737.

40. P. Neufeld and T. Zervas, The Relationship Between Polarization Characteristics and the Electropolishing Behavior of Copper, *Surface Technology*, 1979, **8**, 129-135.

Chapter 3

Copper Anodic Behavior and Polarization Curves in Various Aqueous Electrolyte Solutions

It was discussed in last chapter that electropolishing can be achieved only in the range of the limiting current plateau of a current-potential (polarization) curve. Therefore, a practical search for electropolishing electrolytes and favorable experimental conditions is best started with a determination of current-potential curves under controlled mass transport conditions, e.g., by using a rotating disk [1]. This chapter will discuss and present the anodic behavior and polarization curves of copper rotating disks in various aqueous electrolyte solutions.

3.1 Anodic Behavior and Polarization Curve of Copper in General

When a voltage is applied to an electrochemical system (anode-electrolyte solution-cathode-power supply / control), the following processes may occur [2]:

(1) Charge transfer between the electrode and an ion or molecule across the double layer in the electrolyte solution next to the electrode surface;

(2) Mass transport, in the forms of convection, migration, and diffusion of limiting species between the cathode and anode across anodic layers and the bulk solution;

(3) Chemical reactions, e.g. $2H^+ (aq) + 2e^- \rightarrow H_2 (g)$, at the electrode-solution interfaces; and

(4) Crystallization, which involves incorporation into or removal of atoms from crystal lattice.

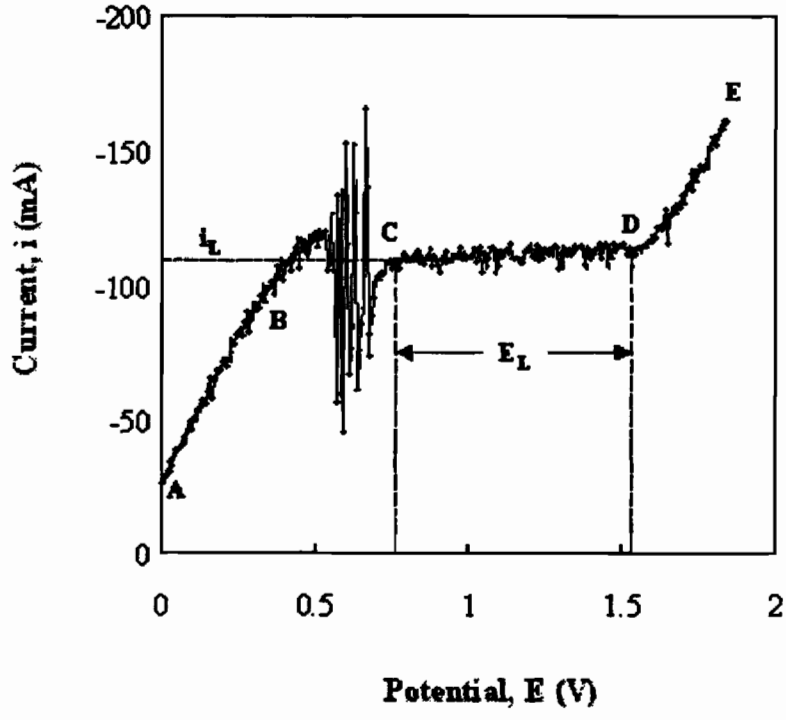

Figure 3-1 Copper anodic polarization curve obtained from solution 10 % H_3PO_4 + 30% HEDP + 60 % H_2O, with electrode area of 1 cm^2 and rotating speed of 100 rpm, at room temperature.

In AB region, the anode potential is relatively low. So the electrochemical process is kinetics dominated. The current is linearly proportional to electrode potential. $i \sim E$ relation obeys Butler-Volmer equation (Eq.2-11) and may be approximated to [3]

$$i = \frac{\eta}{R_p} \qquad 3\text{-}1$$

with

$$R_p = \frac{RT}{nFi_0} \qquad 3\text{-}2$$

where $\eta = E - E^\circ$ is the over potential, E is applied potential on anode, E° and i_o are equilibrium potential and equilibrium current (i.e., when the cathodic current and anodic current have equal amplitude and therefore the net current is zero), R_p is termed the *polarization resistance*, R is the gas constant, T is temperature, F is Faraday constant, and n is the number of valence electrons.

In this region, the reactions

$$2H^+ (aq) + 2e^- \rightarrow H_2 (g);\ E^\circ = 0.00\ V \qquad 3\text{-}3$$

may occur at the cathode and

$$Cu + 2OH^- \rightarrow CuO (c) + H_2O + 2e^-;\ E^\circ = 0.29\ V \qquad 3\text{-}4$$

at the anode [4]. Due to the low redox potential (0V), reaction 3-3 occurred and so hydrogen bubbles were observed on the copper cathode (counter electrode) in all the experiments in this study. Black CuO films were also observed in this region for certain solutions [5].

In BC region of the polarization curve, current – potential deviates from linear relationship. As the potential continues to increase, the increase of the current slows down until it reaches a maximum and then decreases to a minimum point, and finally increases to the limiting current plateau. This is a transition from kinetics (of charge transfer / chemical reaction) domain to mass transport domain. When a black solid film formed in AB region, the film was observed to break down and strip off in this (BC) region. For most phosphoric acid containing solutions, a current – potential oscillation was observed, as shown in Fig.3-1. The oscillations are very likely related to the formation and breakdown of the black anode film. Experiments indicate that the oscillations depend on potential and the amount of phosphoric acid and water [5]. More details of the oscillation phenomena in copper - phosphoric acid system have been discussed in literature [6-8].

CD region is the limiting current plateau. In this region, the potential is so high that Cu^{++} ions produced on copper anode per second are more than mass transport processes can remove from the anode surface into the bulk solution. Thus the Cu^{++} concentration at the anode surface is higher than that in the bulk solution, as illustrated in fig. 2-16. In other words, a concentration gradient of Cu^{++} is developed in the anode boundary layer (Nernst layer). The current in this case, termed *limiting current*, depends on the diffusion of Cu^{++} ions from anode surface to bulk solution across anodic layers [9, 10]:

$$i_L \propto 0.62\, n\, F\, A\, D^{2/3}\, \nu^{-1/6}\, \omega^{1/2}\, (C^\circ - C^*) / \delta \qquad 3\text{-}5$$

where D is the diffusion coefficient, C° and C^* are the Cu^{++} concentrations in bulk solution and at the electrode, $\omega = 2\,\pi$ rps (s^{-1}, rps represents revolution per second) is the angular velocity of rotating disk, ν is kinematic velocity, A is the area of anode surface,

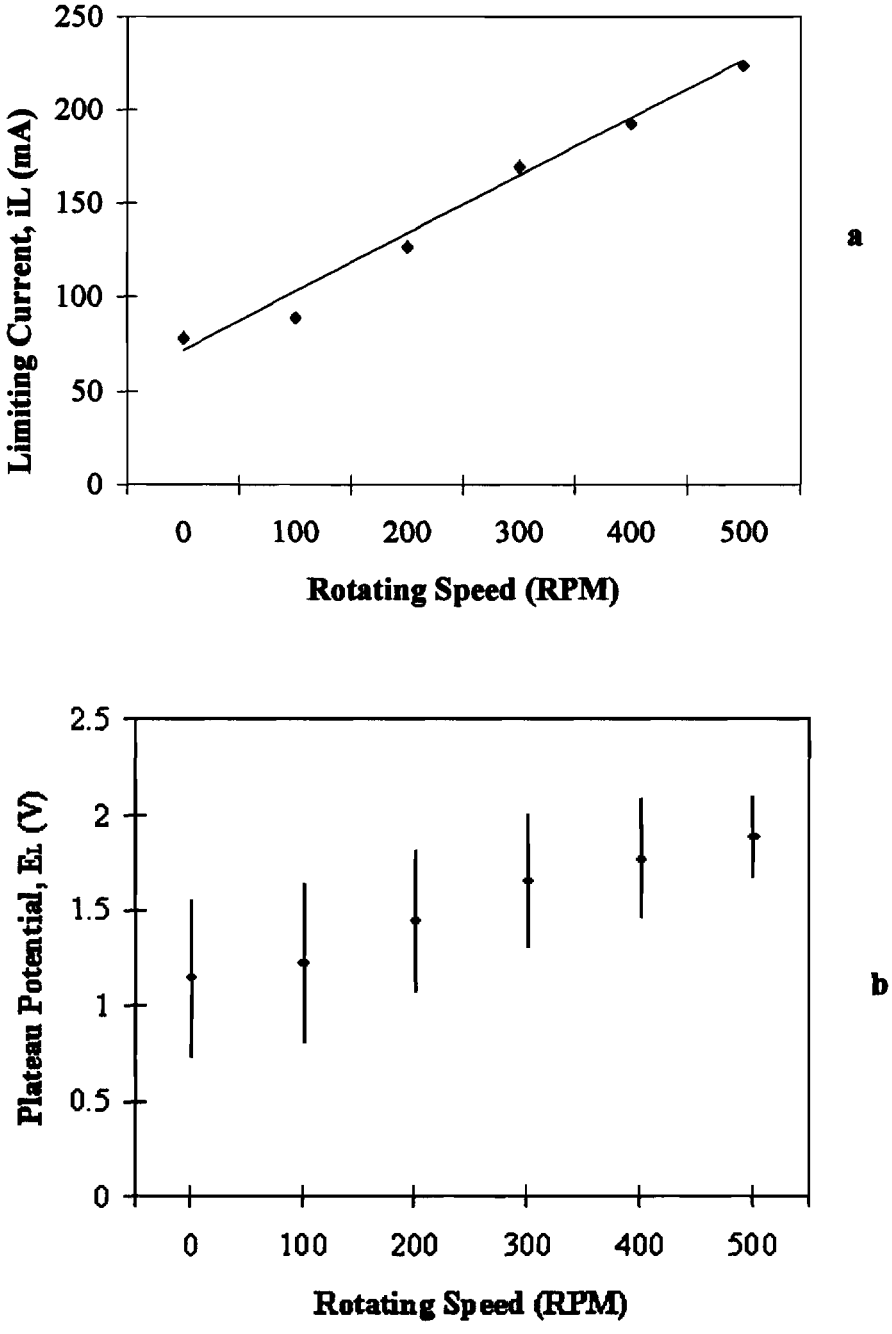

Figure 3-2 Influence of rotating speed on limiting current i_L (a) and the potential range E_L of limiting current plateau (b). Solution: 54% H_3PO_4 + 1.2M CuO + 46% H_2O.

and δ is the thickness of the diffusion layer. It should be point out that acceptors (such as water molecules) instead of Cu^{++} are the mass transport limiting species in some cases (See Chapter 4).

Equation 3-5 describes the influences of concentration gradient and diffusion coefficient of Cu^{++}, viscosity of solution, and disk rotating speed on limiting current. Higher diffusion coefficient, concentration gradient, disk rotating speed, lower viscosity, and thinner diffusion layers facilitate the diffusion and therefore higher limiting current can be expected. Fig. 3-2 shows the influence of disk rotating speed (RPM) on i_L and E_L. Increasing rotating speed results in higher limiting current and narrower range of limiting current plateau (E_L).

Increasing limiting current by increasing the disk rotating speed is due to the decreasing thickness of the boundary layer. When disk rotating speed is so high that the anodic layers vanish, the limiting current plateau will no longer exist. As shown in Fig.3-3, decent limiting current plateaus were obtained from phosphoric acid solution at disk rotating speed lower than 200 rpm.

As the disk rotating speed increases, the limiting current plateaus shift to higher potentials and tilt away from horizontal orientation. This indicates that the diffusion layers are critical for holding the process in mass transport controlled regime.

If a potential difference exists in the anodic layers (for example, when a salt film is formed on the anode surface), ion migration is also one of the mass transport controlled processes [11].

As stated in last chapter, electrochemical polishing can be achieved under mass transport condition in the potential range of limiting current plateau. Higher limiting current (i_L) produces higher dissolution rate (R_d), as expressed in Eq. 2-28. Larger range (E_L) of limiting current plateau gives wider operation window for electrochemical polishing process. Therefore, a decent limiting current plateau (level and large E_L) is important for electrochemical polishing.

In DE range of the polarization curve, current increases again almost linearly with increasing potential. This is most likely due to the occurrence of reactions such as [12]

$$4OH^- - 4e^- \rightarrow O_2 + 2H_2O \qquad 3\text{-}6$$

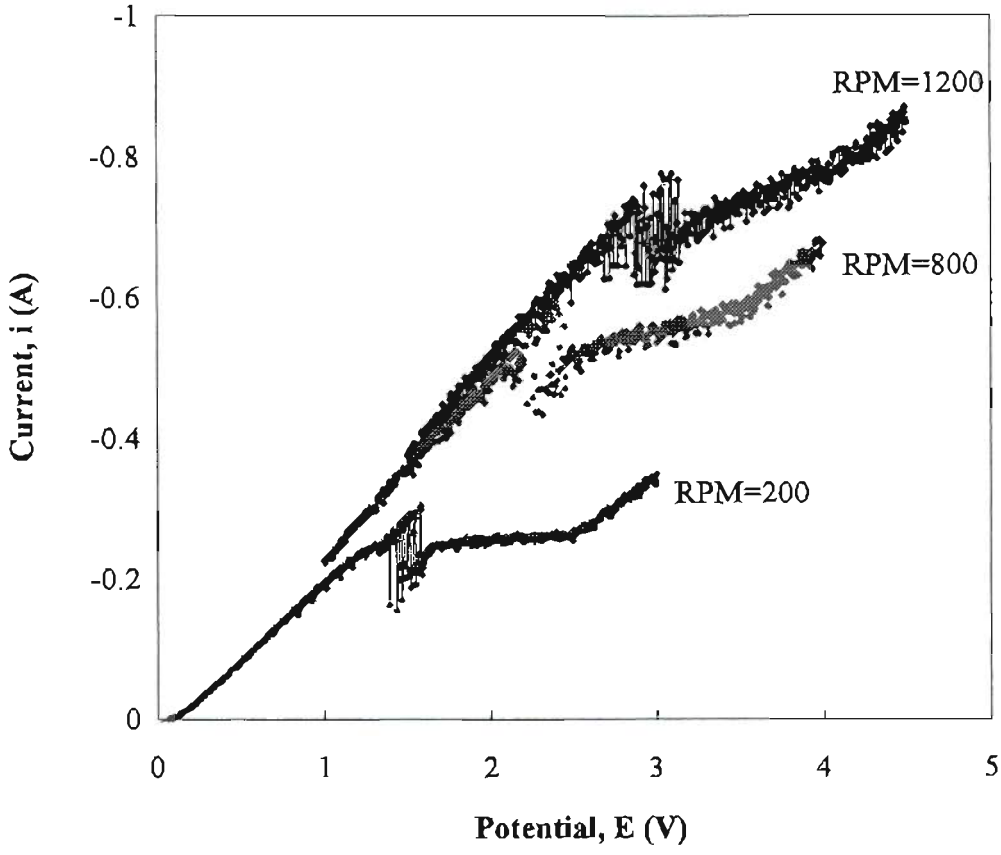

Figure 3-3 Copper anodic polarization curves obtained from solution: 37% H_3PO_4 + 63% H_2O, with rotating speed 200, 800, and 1200 rpm.

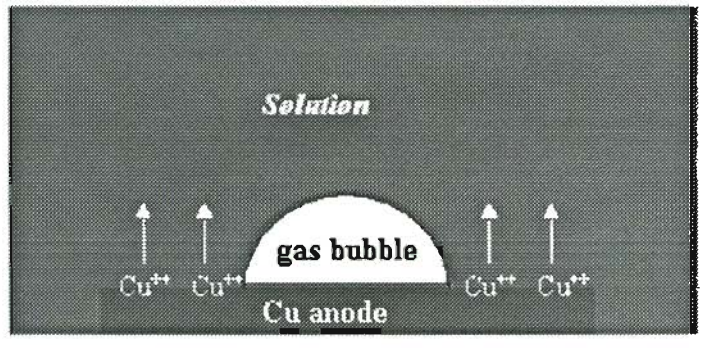

Figure 3-4 Gas bubble formed on anode surface terminates electrochemical dissolution process and produces rough surface.

in addition to faster copper dissolution (on anode) and deposition (on cathode) reactions (Eqs. 2-26 and 2-27). All the reactions contribute to charge transfer and therefore the increasing current. OH^- ions tend to move to anode. Reaction 3-6 occurs on anode surface and produce O_2. When more and more oxygen is produced, bubbles may form on the anode surface.

These gas (oxygen or hydrogen) bubbles may block Cu^{++} ion transport and therefore terminate the electrochemical dissolution process on the area inside the bubbles, as illustrated in Fig.3-4. However, the residual solution on the surface area inside the bubbles may react with Cu atom and result in chemical etching. Depending on the chemical property of the electrolyte solution and the value of current density at which the electrochemical dissolution is occurring, the etching speed can be higher than the rate of electrochemical dissolution. In this case, pits will be produced on the anode surface, as

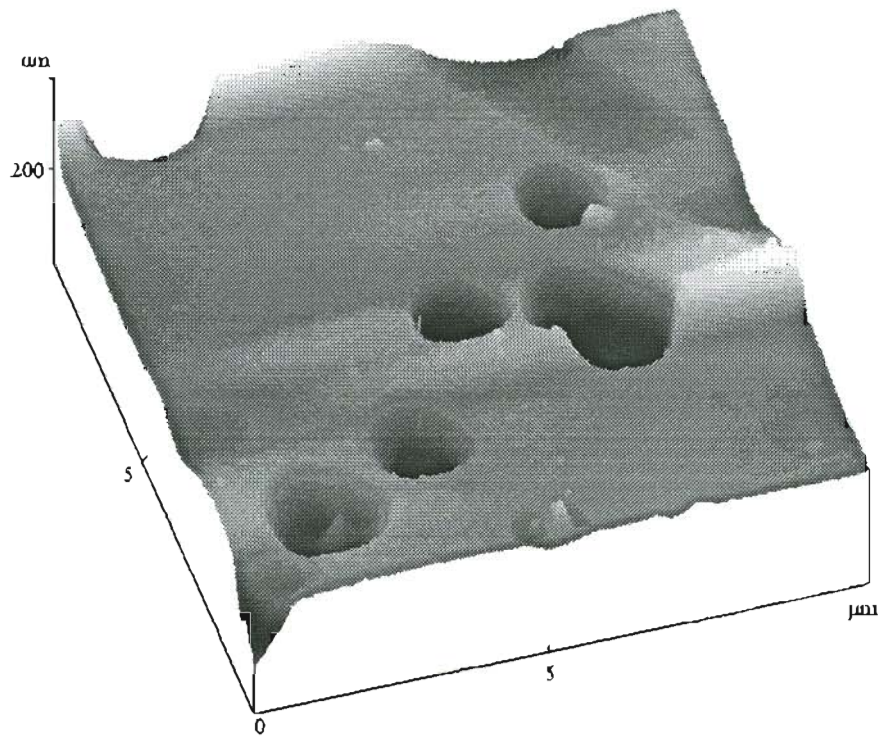

Figure 3-5 AFM topography image of the copper rotating disk after 20 seconds of electropolishing at 2V in 70 % phosphoric acid + 2.0 M CuO.

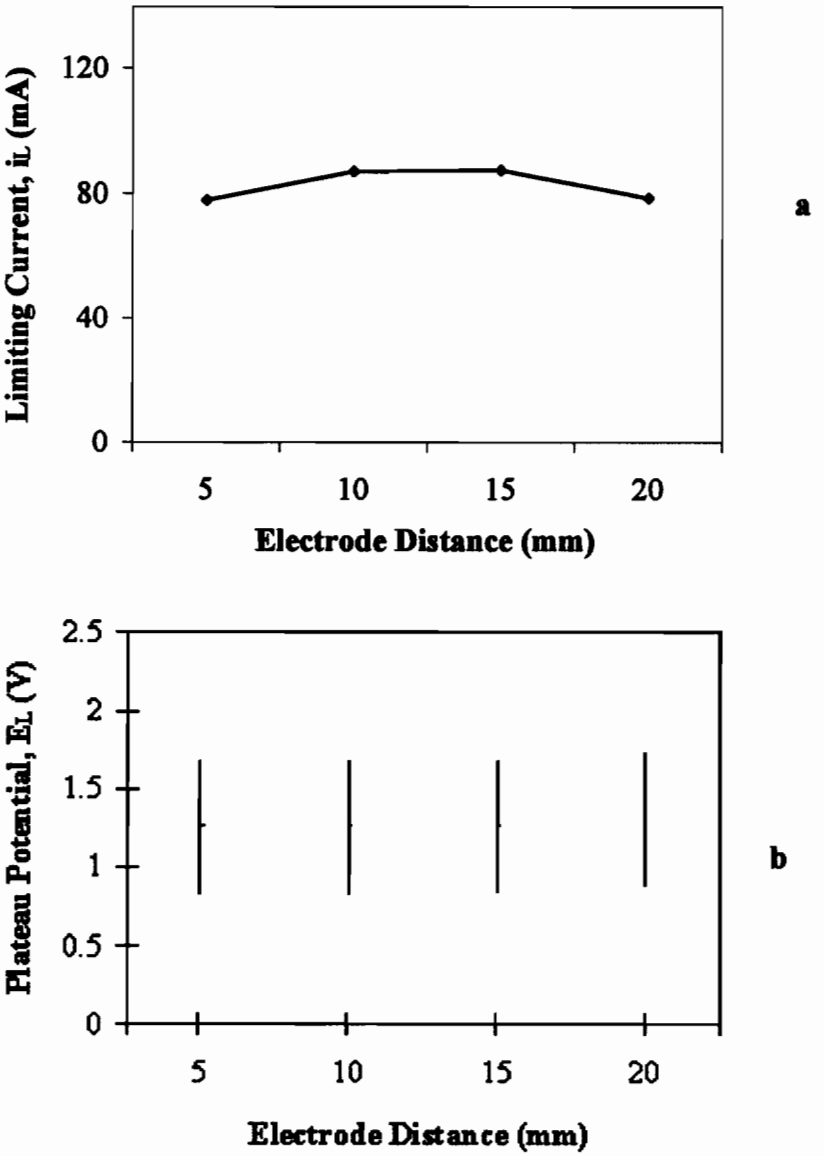

Figure 3-6 Influence of inter electrode distance on limiting current i_L (a) and the potential range E_L of limiting current plateau (b). Solution: 54% H_3PO_4 + 1.2M CuO + 46% H_2O.

shown in Fig. 3-5. In contrast, if etching does not occur inside the bubbles, or if its speed is slower than that of electrochemical dissolution process, the area inside the bubbles will remain and appears as protruding particles after the electrochemical dissolution process. In either case, a rough surface is produced.

Overall, the values of i_L and E_L of the limiting current plateau and the shape of a polarization curve depends on electrolyte solution, anode material, disk rotating speed, solution circulation, temperature, and the distance between anode and cathode. Fig. 3-6 shows the influence of the distance between anode and cathode on i_L and E_L. The influence is very small over the range of inter electrode distance studied here.

Of all the factors, electrolyte is the most important one determining the polarization curve. Therefore, this work investigated several electrolytes and the influences of their concentrations on polarization curve.

3.2 Measurement of Polarization Curves - Experiment Details

The experimental system used for the measurement of copper anodic polarization curves is illustrated in Fig. 3-7. The measurements were performed using 273A Princeton Applied Potentiostat under computer control with Linear Sweep Voltammetry (LSV). A customized rotating-disk electrode with copper disks was used. The copper disks were 11.3 mm in diameter (1 cm^2), with a thickness of 1.5 mm. The counter electrode consisted of a copper plate 12 mm thick and 43 mm in diameter. A reference electrode (Ag/AgCl in 3M KCl) was also used. A teflon cylinder, with acid resistant filter at the bottom, was used to prevent hydrogen bubbles (formed on the counter electrode) from reaching the copper disk (working electrode) surface.

The scan range of potential was 0 V ~ 4 V, and the scan rate was 5 mV/sec. The disk rotating speed was 100 rpm. The distance between working and counter electrodes was about 15 mm. All experiments were carried out in a 200 mL glass container at room temperature. 100 mL electrolyte solution was used for each experiment.

As stated in last chapter, the electrochemical properties are very sensitive to the state of anode surface. Thus in this study, all the copper disk samples were hand polished with 1 μm sand paper and cleaned with acetone before the LSV experiments. Limiting

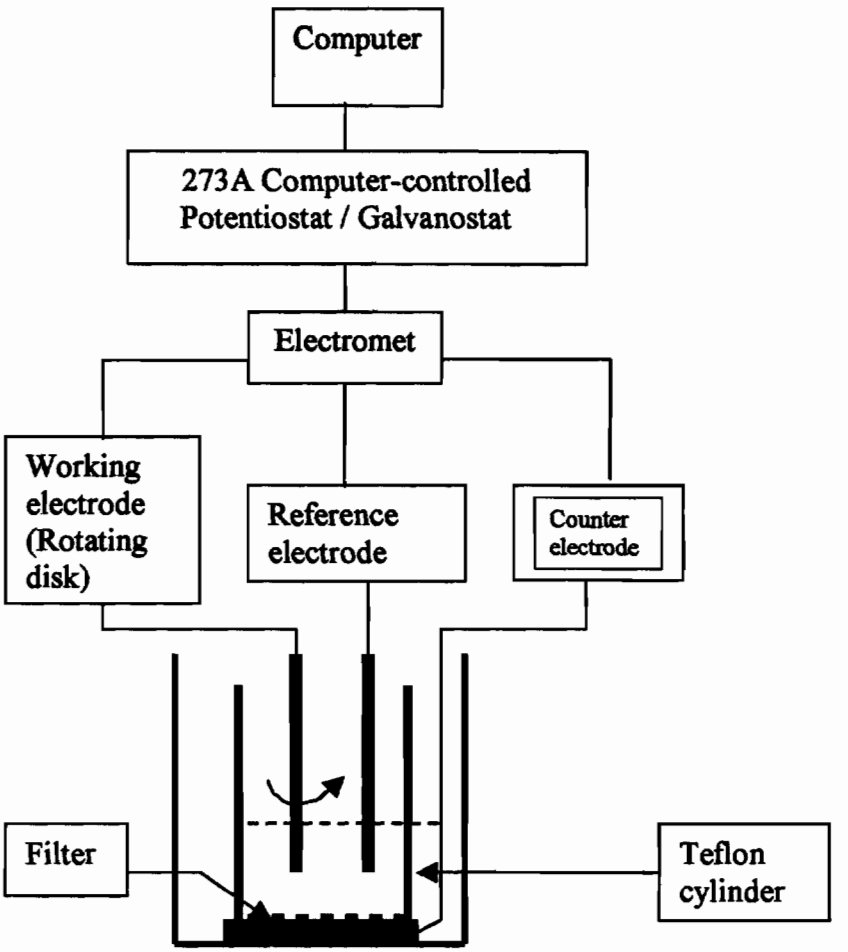

Figure 3-7 A schematic of the system used for the measurement of polarization curves.

current (i_L) and plateau range (E_L) were obtained from the polarization curves. The electrolyte solutions studied were listed in Table 3-1. All the concentration data reported are in terms of percentage by volume for liquid ingredients and mole/liter for solid ingredients. "Phosphoric acid" in this study means commercial o-phosphoric acid (85% H_3PO_4).

To validate that the process in limiting current plateau is mass transport control, Steady-State Experiments were performed. That is, conduct LSV at different rotating speed and plot $1/i_L \sim 1/\omega^{1/2}$ curve.

Table 3-1 Electrolytes Used for *i* ~ E curve Measurements

Solution No.	Chemical 1	Concentration (% Volume)	Chemical 2	Concentration (Mole / L)
1	Phosphoric acid (85% H_3PO_4)	13 ~ 100	Copper oxide (CuO)	0 ~ 2
2	Phosphoric acid (85% H_3PO_4)	6.25 ~ 56.25	Ethylene glycol ($C_2H_6O_2$)	6.25 ~ 56.25 (% vol)
3	Phosphoric acid (85% H_3PO_4)	10 ~ 90	Sodium tripolyphosphate ($Na_5P_3O_{10}$)	0.1 ~ 0.5
4	Hydroxyethyliden ediphosphonic acid (HEDP)	0 ~ 100	Phosphoric acid (85% H_3PO_4)	0 ~ 30 (% vol)
5	Ethylene glycol ($C_2H_6O_2$)	0 ~ 100	Sodium chloride (NaCl) / Sodium Nitrate ($NaNO_3$)	1 ~ 5 / 1 ~ 4
6	Sulphuric acid (95.7% H_2SO_4)	1 ~ 20	Sodium Nitrate ($NaNO_3$)	0 ~ 2.5
7	Sulphuric acid (95.7% H_2SO_4)	1 ~ 20	Potassium Nitrate (KNO_3)	0 ~ 2.5

3.3 Results and Discussion

Due to the significance of limiting current plateau to electropolishing as stated above, the purpose of measuring polarization curve of an electrolyte solution is to find out if there is a limiting current plateau and the values of the limiting current (i_L) and the potential range (E_L) of the plateau if there is one. Therefore, this section presents only i_L and E_L data from measure polarization curves while polarization curves themselves are not presented.

3.3.1 Phosphoric acid – copper oxide solutions

There are several articles about copper electropolishing with phosphoric acid solution [6, 13-17]. Dianatkhah [18] studied the Passivation behavior of copper thin films in phosphoric acid – copper oxide (CuO) solutions. However, systematic research on the correlation of limiting current, concentrations of phosphoric acid and additives, such as CuO, has not been reported yet.

Table 3-2 H_3PO_4-CuO Solutions Used for $i \sim E$ Curve Measurements

Chemical 1	Concentration (% Volume)	Chemical 2	Concentration (Mole / L)
Phosphoric acid (85% H_3PO_4)	13, 24, 37, 54, 70, 100	Copper oxide (CuO)	0
Phosphoric acid (85% H_3PO_4)	24, 37, 54, 70, 100	Copper oxide (CuO)	0.5
Hydroxyethyliden ediphosphonic acid (HEDP)	37, 54, 70, 100	Copper oxide (CuO)	1.2
Phosphoric acid (85% H_3PO_4)	54, 70, 100	Copper oxide (CuO)	2.0

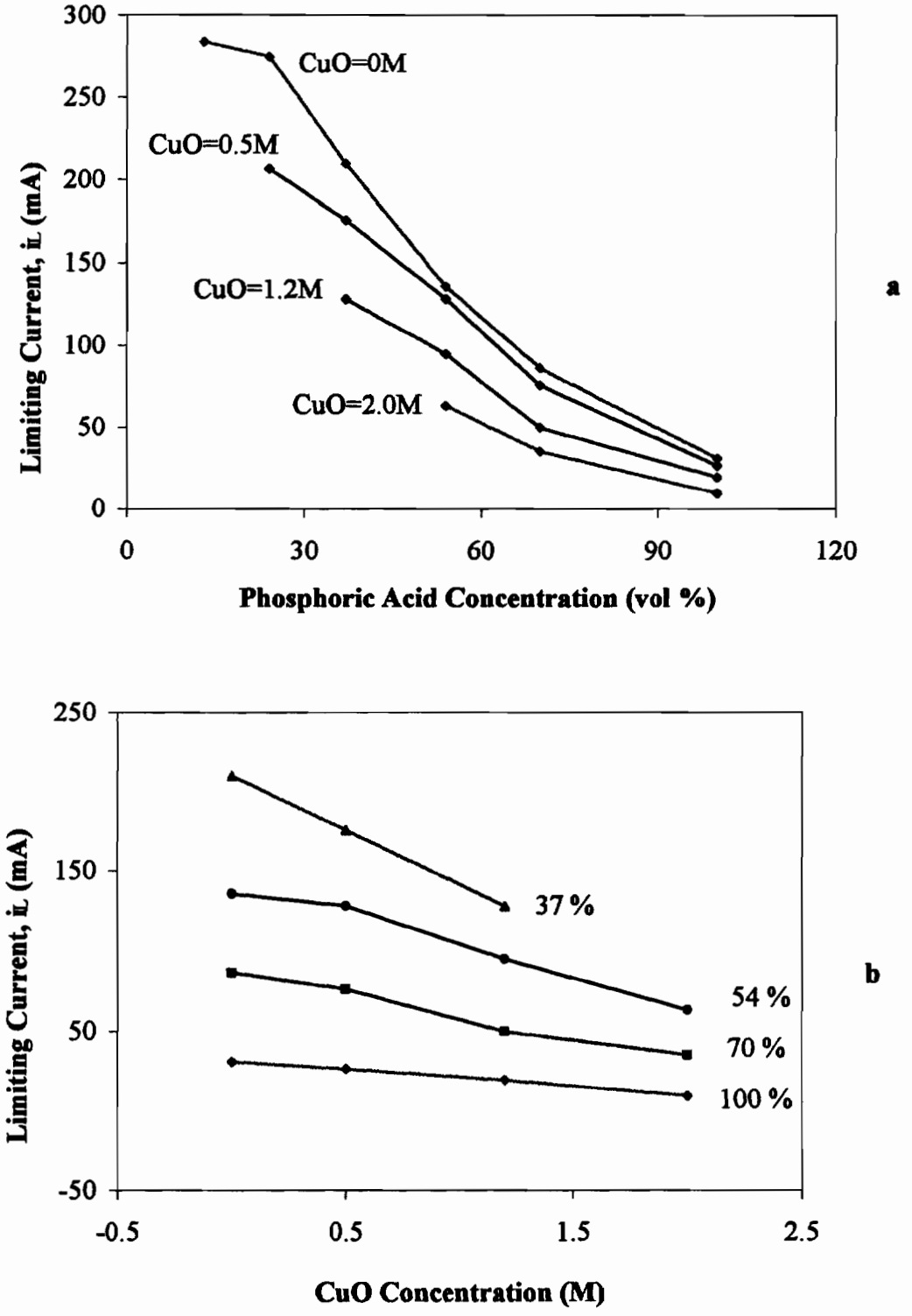

Figure 3-8 Limiting current versus concentrations of phosphoric acid with certain CuO concentrations (a) and limiting current versus concentrations of CuO with certain phosphoric acid concentrations (b).

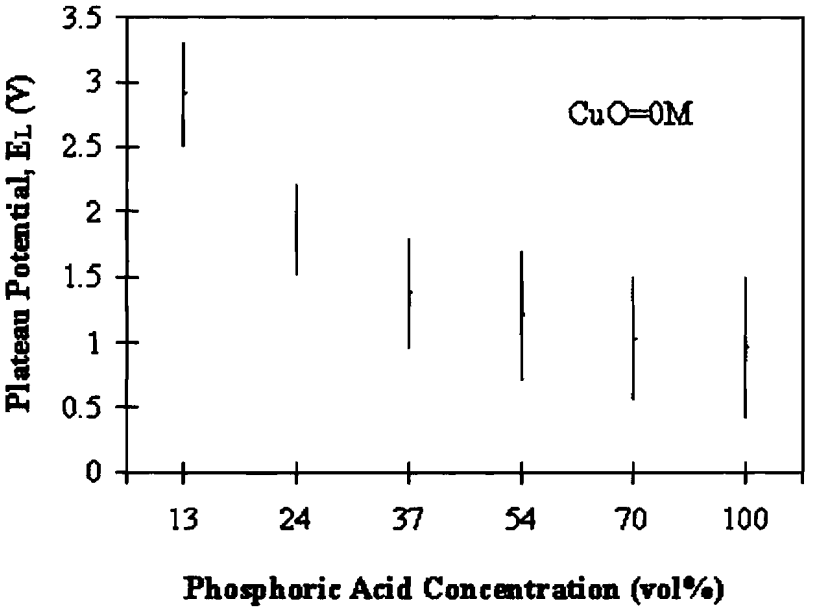
3.5
3
2.5
2
1.5
1
0.5
0
Plateau Potential, EL (V)
CuO=0M
13
24
37
54
70
100
Phosphoric Acid Concentration (vol%)

a

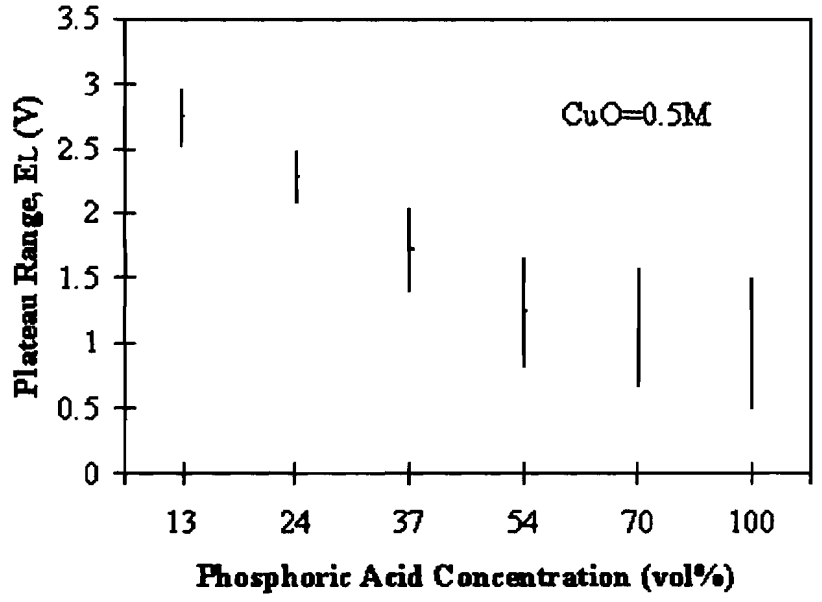
3.5
3
2.5
2
1.5
1
0.5
0
Plateau Range, EL (V)
CuO=0.5M
13
24
37
54
70
100
Phosphoric Acid Concentration (vol%)

b

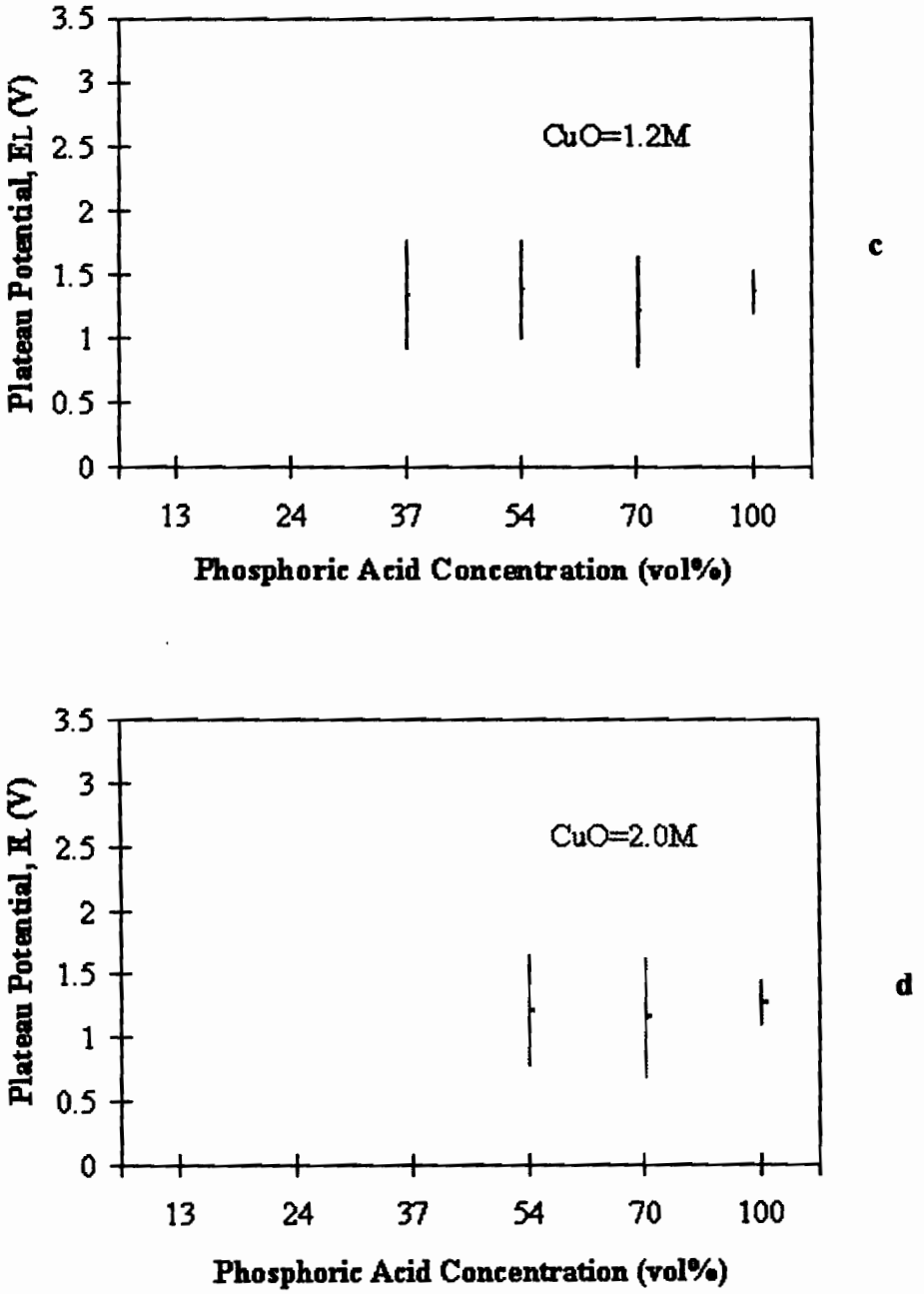

Figure 3-9 Potential of limiting current plateau versus phosphoric acid concentration: (a) without CuO, (b) with 0.5M CuO, (c) with 1.2M CuO and (d) with 2.0M CuO.

In this study, CuO powder was added in phosphoric acid solutions. The solutions exhibit nice blue color when the black CuO powder is well dissolved. The solubility of CuO in a phosphoric acid solution is directly proportional to the concentration of phosphoric acid. Phosphoric acid – copper oxide solutions in the concentration range of solubility were investigated. The solutions studied are listed in Table 3-2.

Polarization curves with decent limiting currents plateau were obtained from all the solutions (in Table 3-2). The values of the limiting current (i_L) and the potential range (E_L) of the plateaus were obtained from the measured polarization curves and plotted in Figs. 3-8 and 3-9.

From Fig.3-8, we can see that: (1) limiting current decreases with the increase of H_3PO_4 concentration in all the solutions with or without CuO; (2) limiting current is decreased by adding CuO in $H_3PO_4 + H_2O$ solutions and the higher CuO concentration the lower limiting current; (3) the influence of CuO becomes smaller for solutions with higher H_3PO_4 concentration.

The influence of H_3PO_4 concentration on limiting current is very likely due to the change of the thickness of the boundary layer. Higher H_3PO_4 concentration results in higher viscosity and thus thick boundary layer and lower limiting current. The effect of CuO may be caused by increasing the concentration of copper in the bulk electrolyte, thereby reducing the concentration gradient across the Nernst layer. Consequently decreases the diffusion rate of Cu^{++}.

Fig.3-9 indicates that: (1) for phosphoric acid solutions without CuO or with low concentration (0.5M) of CuO, the limiting current plateau becomes narrower and shifts to higher potential as H_3PO_4 concentration decreases; solutions of 37% ~ 100% phosphoric acid have the range of limiting current plateau larger than 0.6V; (2) higher CuO concentration (>1.2M) has little influence on limiting current plateau except 100% phosphoric acid solution; in which case, the range of limiting current plateau < 0.35V.

3.3.2 Phosphoric acid – ethylene glycol solutions

Ethylene glycol (CH_2OHCH_2OH) is a clear, colorless, odorless, viscous liquid with a sweet taste, and can produce dramatic toxicity. It is an organic solvent and found most commonly in antifreeze, automotive cooling systems, and hydraulic brake fluids

[19]. It was reported [13] that ethylene glycol (EG) could improve copper polishing in phosphoric acid solution. Yet, it is not clear how EG affects the polishing and what is its optimal concentration for copper electropolishing.

In this work, polarization curves of phosphoric acid – ethylene glycol solutions with EG concentration ranging over 6.25 ~ 56.25% were measured. The concentrations of EG and phosphoric acid of the solutions are listed in Table 3-3.

Table 3-3 H_3PO_4-EG Solutions Used for $i \sim E$ Curve Measurements

Solution Set	Phosphoric acid (85% H_3PO_4) (% vol)	EG (% vol)	Water (% vol)
1	25, 50, 75, 100.	75, 50, 25, 0.	0
2	18.75, 37.5, 56.25.	56.25, 37.5, 18.75.	25
3	12.5, 25.0, 37.5.	37.5, 25.0, 12.5.	50

The values of the limiting current (i_L) and the potential range (E_L) of the plateaus obtained from the measured polarization curves are plotted in Figs. 3-10 and 3-11. In Fig. 3-10, curves 1, 2, and 3 represents respectively the solution sets 1, 2, and 3 in Table 3-3.

Fig. 3-10 indicates that adding EG into phosphoric acid solutions decreases limiting current. More EG added the lower limiting current. This is true for both undiluted and diluted (with water) phosphoric acid solutions. Diluting phosphoric acid – EG solutions with water (25%, curve 2 in Fig. 3-10) increases limiting current. Further diluting phosphoric acid – EG solutions with water (50%, curve 3 in Fig. 3-10) decreases limiting current. Limiting current plateau disappears at solution "12.5% phosphoric acid + 37.5% EG + 50% water".

Fig. 3-11 indicates that limiting current plateaus slightly shift to higher potential with increasing EG concentration or decreasing phosphoric acid concentration.

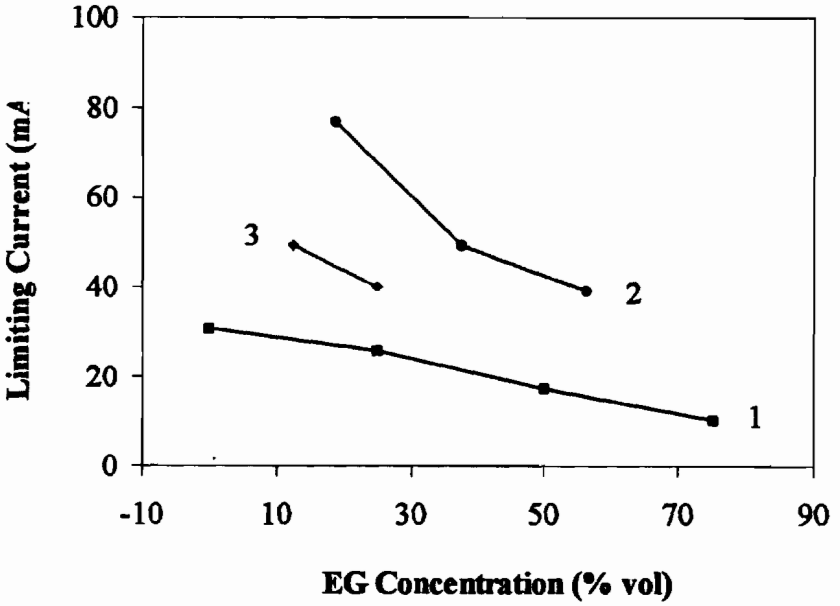

Figure 3-10 Limiting current versus EG concentration in phosphoric acid – EG solutions: (1) undiluted phosphoric acid + EG; (2) 25% water; and (3) 50% water diluted phosphoric acid – EG.

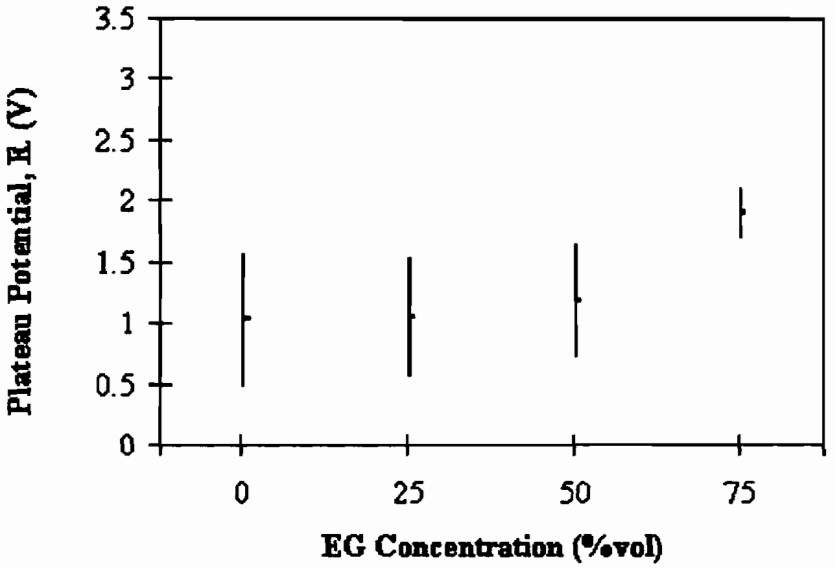

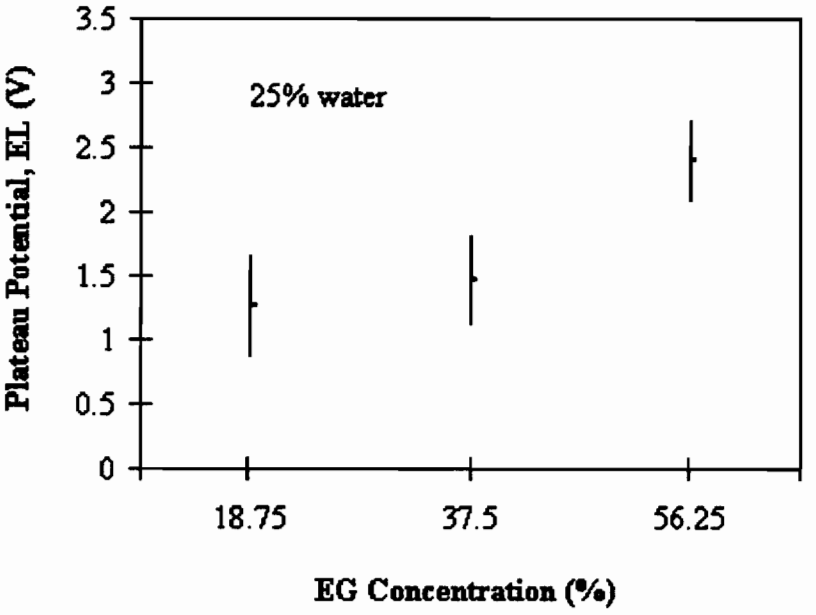

b

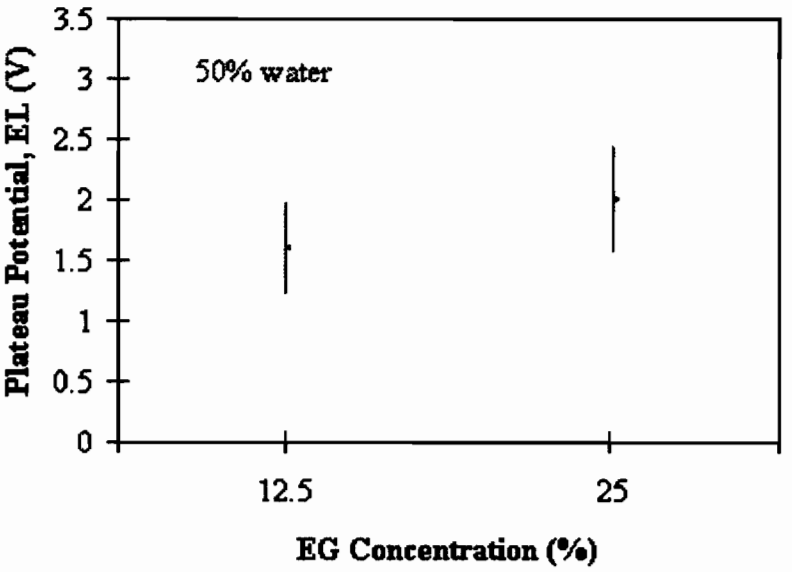

c

Figure 3-11 Potential of limiting current plateau versus EG concentration: (a) without water, (b) with 25% water, and (c) with 50% water dilution.

3.3.3 Phosphoric acid – sodium tripolyphosphate solutions

Sodium tripolyphosphate ($Na_5P_3O_{10}$) is used mainly as a water softening agent because of its excellent heavy metal sequestration properties [20]. Its molecular structure is shown in Fig. 3-12 [21]. Sodium tripolyphosphate was mentioned as copper electropolishing agent with phosphoric acid in Fang and Wu's work [22], but no detailed information is available.

Hereupon, polarization curves were measured from 10% ~ 90% phosphoric acid solutions with respectively 0.1, 0.25, and 0.50M sodium tripolyphosphate as additive (See Table 3-4). Data of limiting current and the potential range of limiting current plateaus were extracted from the measured polarization curves and plotted in Figs. 3-13~15.

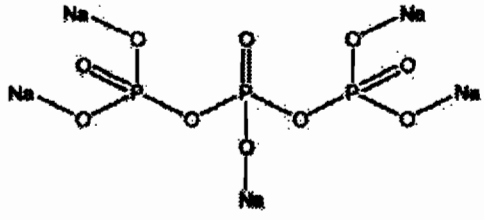

Figure 3-12 Molecular structure of $Na_5P_3O_{10}$.

Table 3-4 H_3PO_4 - $Na_5P_3O_{10}$ Solutions Used for $i \sim E$ Curve Measurements

Solution Set	Phosphoric acid (85% H_3PO_4) (% vol)	Sodium tripolyphosphate (M)
1	13 ~ 100	0
2	10 ~ 90	0.10
3	10 ~ 90	0.25
4	10 ~ 90	0.50

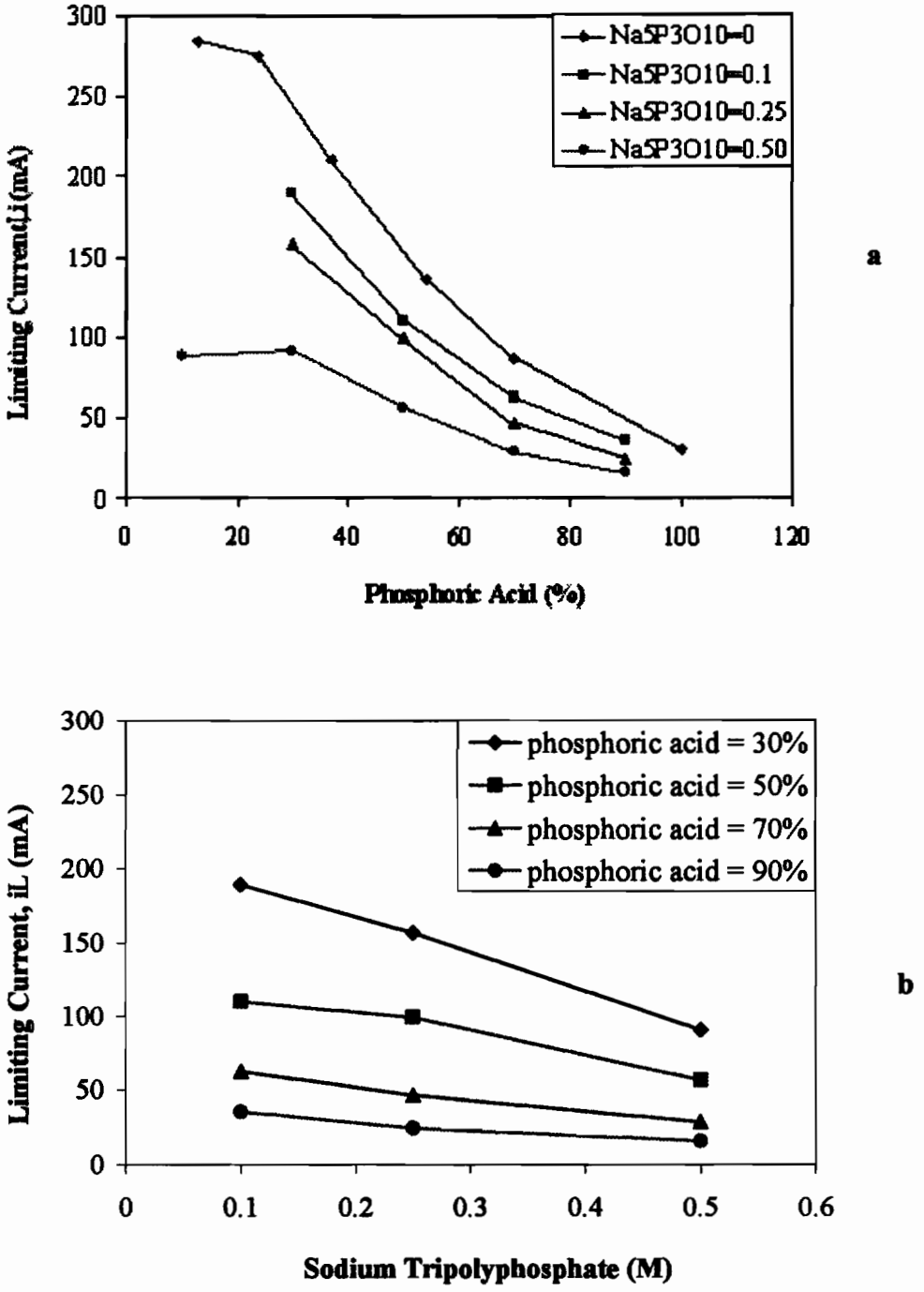

Figure 3-13 Limiting current versus concentration of phosphoric acid (a) and versus concentration of sodium tripolyphosphate (b).

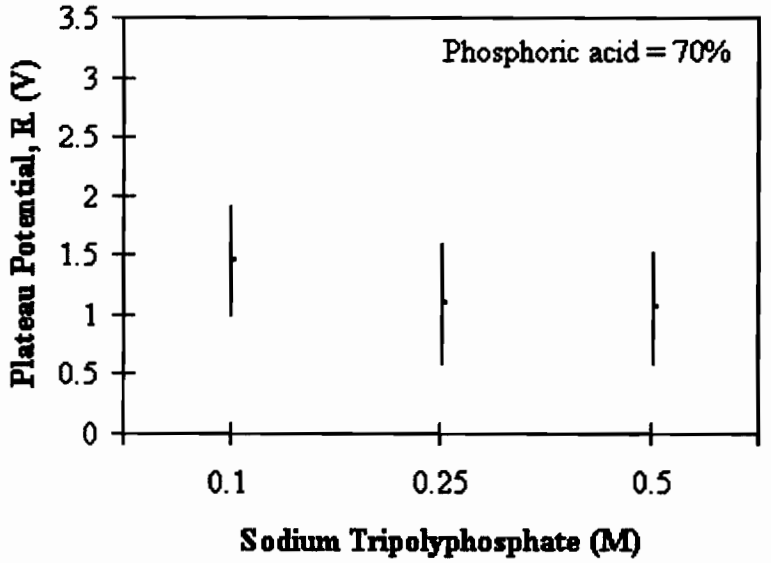

a

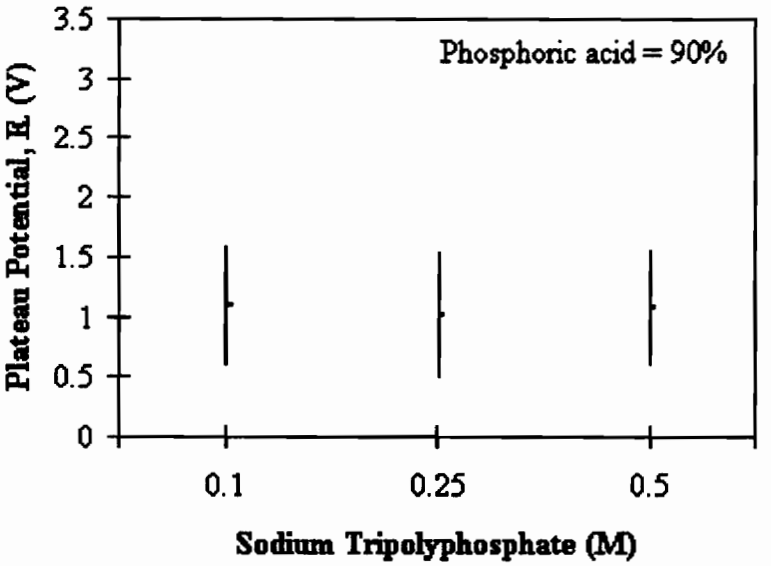

b

Figure 3-14 Potential of limiting current plateau versus Sodium tripolyphosphate concentration with: (a) 70% phosphoric acid, (b) 90% phosphoric acid.

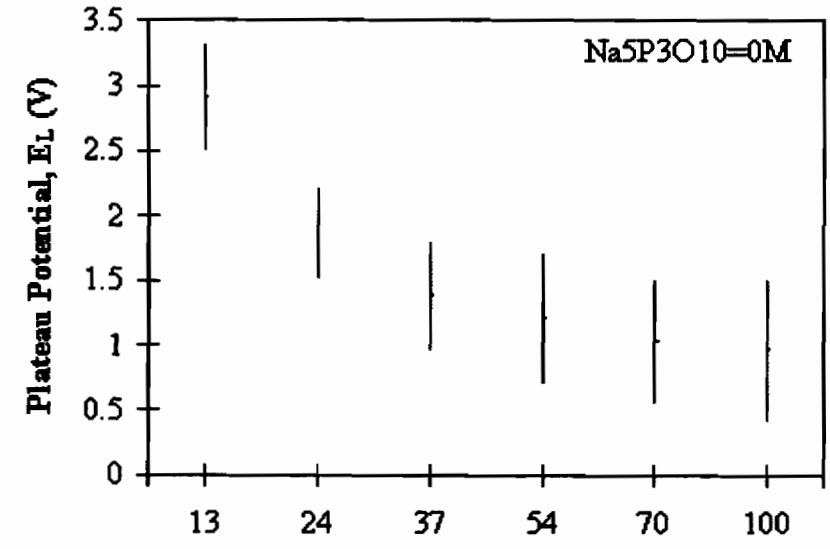

a

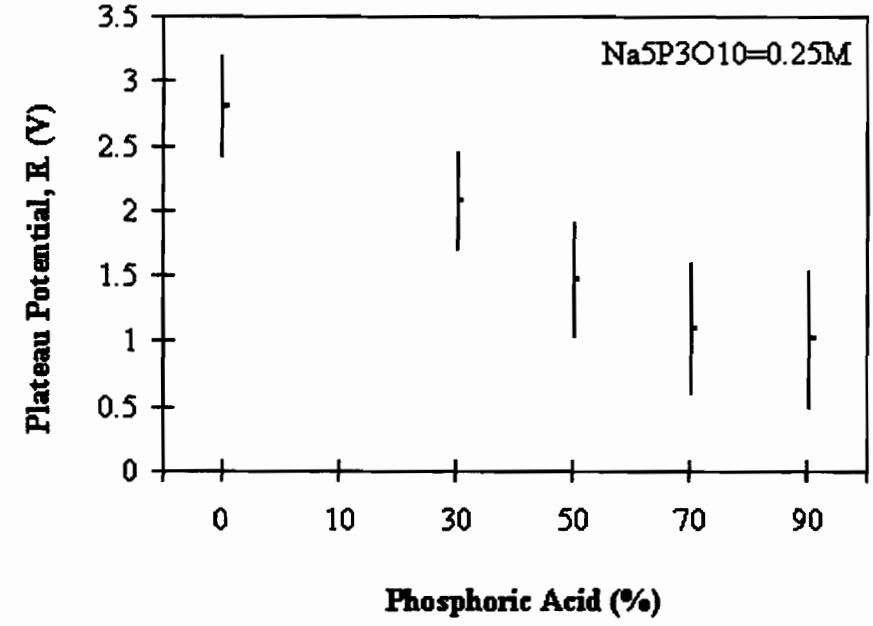

b

Figure 3-15 Potential of limiting current plateau versus phosphoric acid concentration with (a) no sodium tripolyphosphate and (b) 0.25 M sodium tripolyphosphate

The experimental data indicate that limiting current decreases with the increase of phosphoric acid concentration in solutions with or without sodium tripolyphosphate (See Fig. 3-13a). Adding sodium tripolyphosphate into phosphoric acid solution decreases limiting current, and more sodium tripolyphosphate was added the lower limiting current was measured (See Fig. 3-13b). This is similar to the effect of CuO on the limiting current in phosphoric acid solutions. A limiting current plateau was not shown in the measured polarization curves of solutions 10% phosphoric acid with 0.1M and 0.25M sodium tripolyphosphate. Nevertheless, a limiting current was observed in 10% phosphoric acid with 0.5M sodium tripolyphosphate. This suggests that limiting current depends on the concentration of PO_4^{3-} in the solution.

Figs. 3-14 and 3-15 indicates that sodium tripolyphosphate does not have obvious impact on the potential ranges of limiting current plateaus.

3.3.4 Hydroxyethylidenediphosphonic acid – phosphoric acid solutions

Hydroxyethylidenediphosphonic acid (HEDP: $C_2H_8O_7P_2$, 1-Hydroxyethylidene-1, 1-Diphosphonic) is clear, colorless to pale yellow, and odorless liquid [23]. Its molecular structure is shown in Fig. 3-15 [24]. HEDP is a good metal (such as iron, copper, and zinc) complexing agent and widely used for water treatment, boiler and water pipe cleaning [25, 26]. Fang and Wu [22, 27] reported that HEDP is both an excellent electropolishing sequestering agent for copper and an electroplating complexing agent for various metals. They investigated the composition of the viscous liquid film formed on electropolished copper surface with XPS and AES. However, no systematic study of polarization curves or of electropolishing performance in HEDP has been reported.

In this work, polarization curves of HEDP solutions and HEDP - phosphoric acid solutions were measured. The chemical ingredients of solutions are listed in Table 3-5.

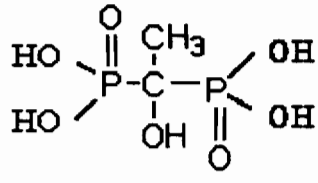

Figure 3-16 Molecular structure of HEDP

Table 3-5 H_3PO_4-EG Solutions Used for $i \sim E$ Curve Measurements

Solution Set	HEDP (60% $C_2H_8O_7P_2$) (% vol)	Phosphoric acid (85% H_3PO_4) (% vol)	Water (% vol)
1	2.5 ~ 100	0	97.5 ~ 0
2	0 ~ 90	10	90 ~ 0
3	0 ~ 70	30	70 ~ 0

Data of limiting current (i_L) and the potential range (E_L) of limiting current plateaus were extracted from the measured polarization curves.

The effect of HEDP on the limiting current is shown in Fig. 3-17a. In the case without phosphoric acid, limiting current increases with the increase of HEDP concentration (when < 20 %) and reaches a maximum at 20 % ~ 40 % HEDP. The limiting current then slowly decreases with an increase of HEDP concentration in the range of 40 % ~ 100 %.

When phosphoric acid was added to HEDP solution, the limiting current largely increased at lower HEDP concentration (< 30 %). The limiting current decreased with an increase of HEDP concentration in the whole range though the trend was slower at higher HEDP concentrations (>40%).

The effect of phosphoric acid on limiting current is demonstrated in Fig. 3-17b. At lower HEDP concentration (≤ 30 %), the limiting current increases with an increase of phosphoric acid and then reverses this trend as phosphoric acid concentration continues to increase (≥30%). At higher HEDP concentration (≥ 50 %), limiting current simply decreases with the increase of phosphoric acid.

As shown in Fig. 3-18, the limiting current plateaus have a wide range (E_L) when HEDP concentration is higher than 40%. This is true both for HEDP and HEDP - phosphoric acid solutions. The limiting current plateau becomes narrower and shifts to higher value as the HEDP concentration decreases.

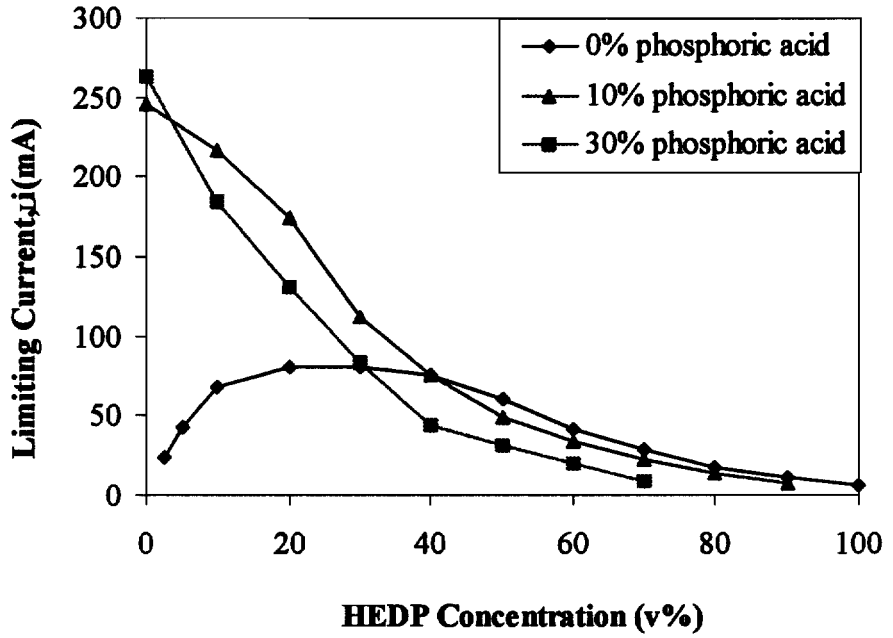

a

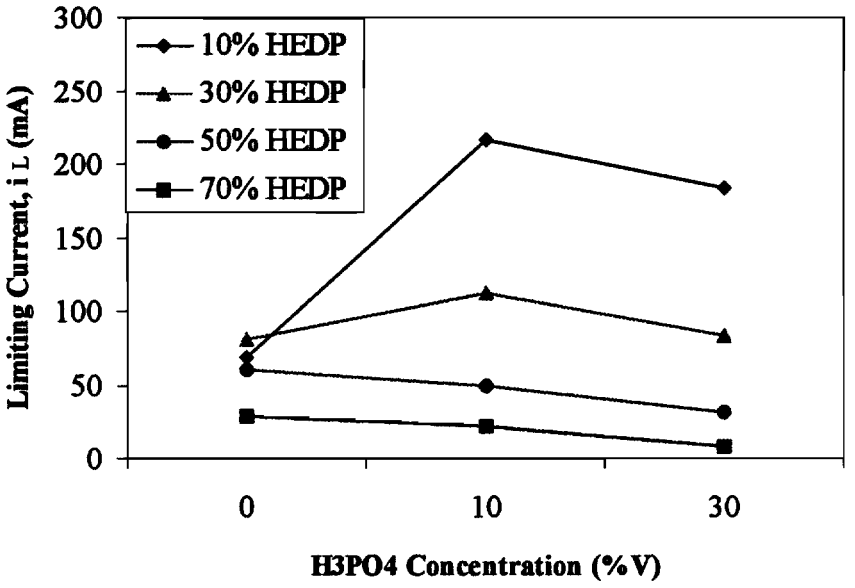

b

Figure 3-17 Limiting current versus HEDP concentration with different phosphoric acid concentration (a) and Limiting current versus phosphoric acid concentration with different HEDP concentration (b).

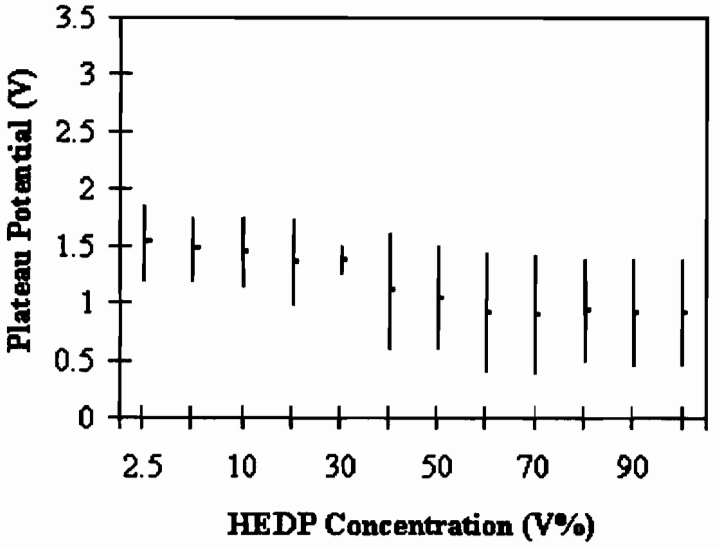
Plateau Potential (V)
3.5
3
2.5
2
1.5
1
0.5
0
2.5
10
30
50
70
90
HEDP Concentration (V%)

a

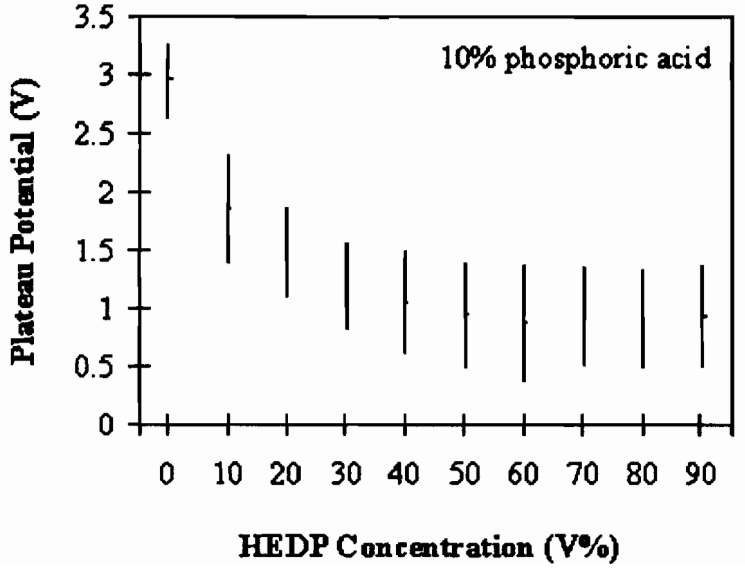
10% phosphoric acid
Plateau Potential (V)
3.5
3
2.5
2
1.5
1
0.5
0
0
10
20
30
40
50
60
70
80
90
HEDP Concentration (V%)

b

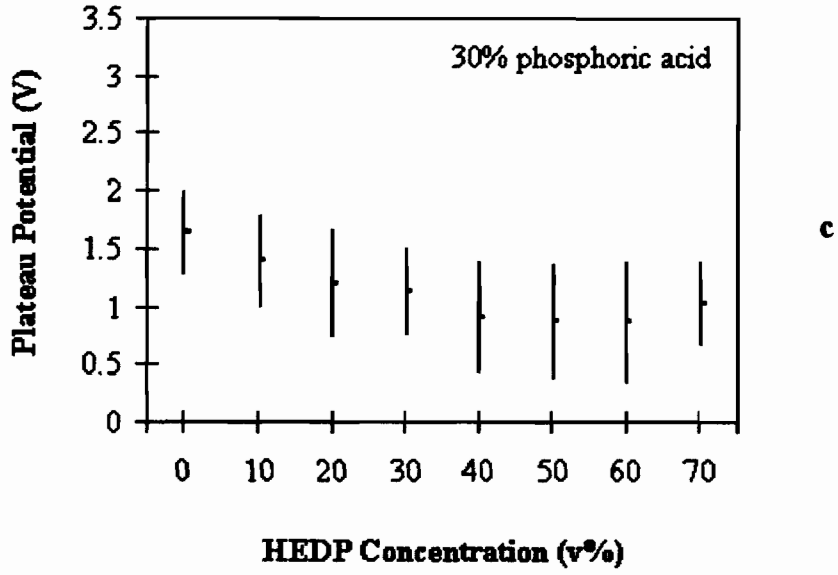

Figure 3-18 Potential of limiting current plateau versus HEDP concentration: (a) without phosphoric acid, (b) with 10% phosphoric acid and (c) with 30% phosphoric acid.

3.3.5 Sodium chloride / sodium nitrate – ethylene glycol solutions

Sodium chloride (2~4M) and sodium nitrate (2~4M) solutions with ethylene glycol (1~3M or 5~15% vol) as additive were reported having electrochemical planarization effect on copper film plated on silicon wafers and patented by IBM in 1996 [28]. To compare the electrochemical planarization effect of the above solutions with this patented electrolyte solution, this work studied 1~5M sodium chloride solutions with 0~50% ethylene glycol as additive, 2~4M sodium nitrate solutions with 10% ethylene glycol, and 1~3M sodium chloride + 1~3M sodium nitrate solutions with 10~20% ethylene glycol as additive.

The limiting current and plateau potential data of sodium chloride – ethylene glycol solutions extracted from measured polarization curves are plotted in Fig. 3-19 and 3-20. It is shown that limiting current increases with increasing sodium chloride concentration. In contrast, adding ethylene glycol into sodium chloride solutions decreases limiting current. In other words, adding ethylene glycol increases the resistance of the solution. This agrees to the results in [28]. Ethylene glycol also affects the solubility of sodium chloride in the solutions. When more ethylene glycol was added, less

sodium chloride dissolved in the solution. When 50% EG was added in solution, 3M NaCl is a little beyond the solubility.

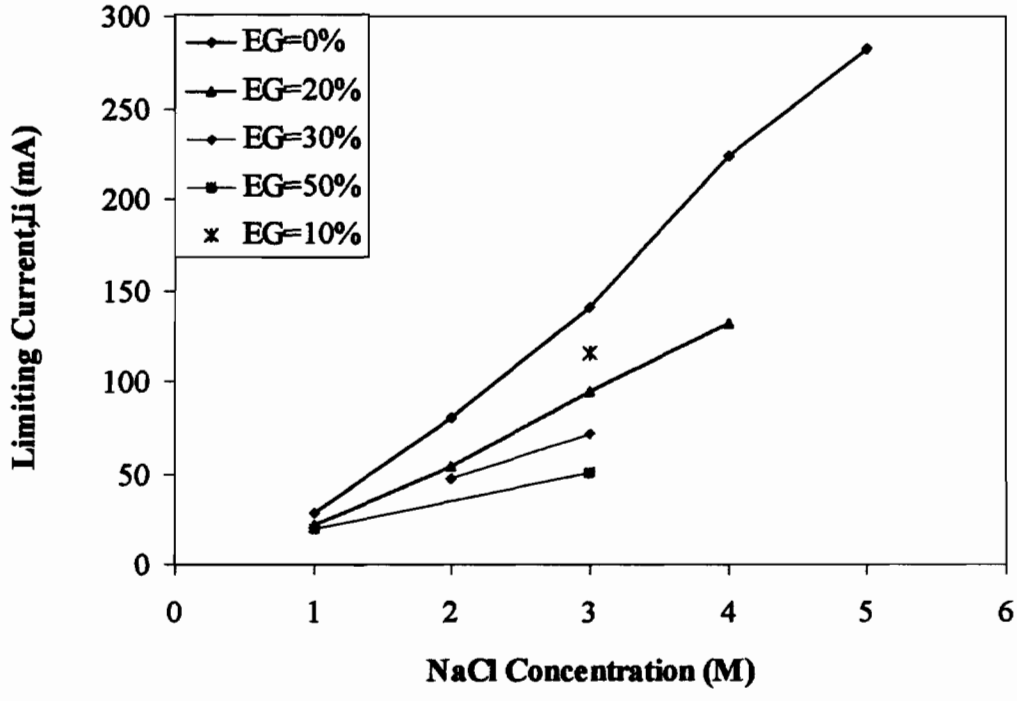

Figure 3-19 Limiting current versus NaCl concentration with different ethylene glycol concentrations.

Sodium chloride – ethylene glycol solutions have wide range of limiting current plateau. As shown in Fig. 3-20, all solutions have a limiting current plateau from 2V or lower up to maximum voltage of the scanning range, 4V. Varying the concentrations of NaCl and EG did not apparently influence the potential range of the limiting current plateaus.

A decent limiting current plateau was not shown in the measured polarization curves of 2~4M sodium nitrate + 10% ethylene glycol solutions, nor in the polarization curves of 1~3M sodium chloride + 1~3M sodium nitrate solutions + 10~20% ethylene glycol.

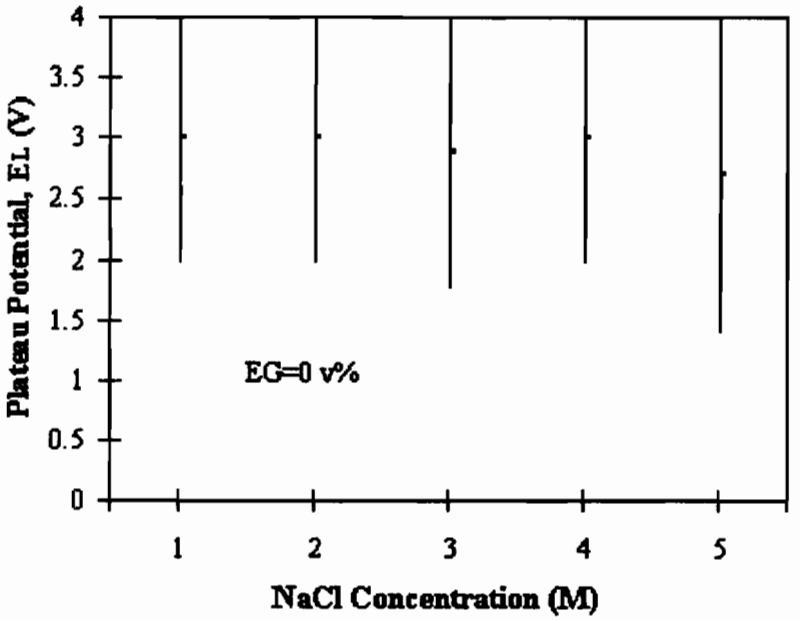

a

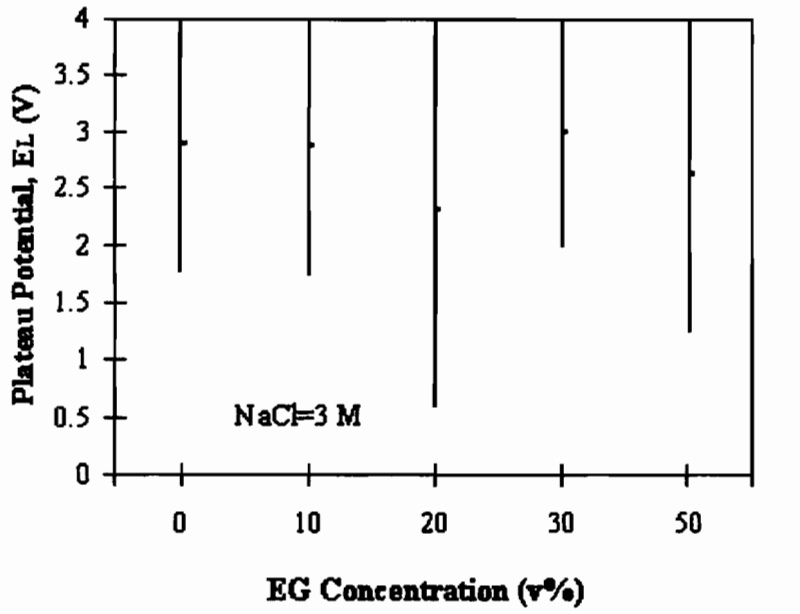

b

Figure 3-20 Potential of limiting current plateau versus NaCl concentration (a) and versus EG concentration (b).

3.3.6 Sulphuric acid – sodium nitrate solutions

Sulphuric acid is a popular electrolyte. Sulphuric acid solution with 2M sodium nitrate as additive was used to study copper anodic leveling under secondary and tertiary current conditions [29]. To further explore the electrochemical behavior and ECP effect of Cu with sulphuric acid – sodium nitrate solutions, polarization curves of 1 ~ 20% Sulphuric acid (H_2SO_4) solutions with 0 ~ 2.5M sodium nitrate ($NaNO_3$) were measured. The limiting current and plateau potential data were plotted in Figs. 3-21 and 3-22.

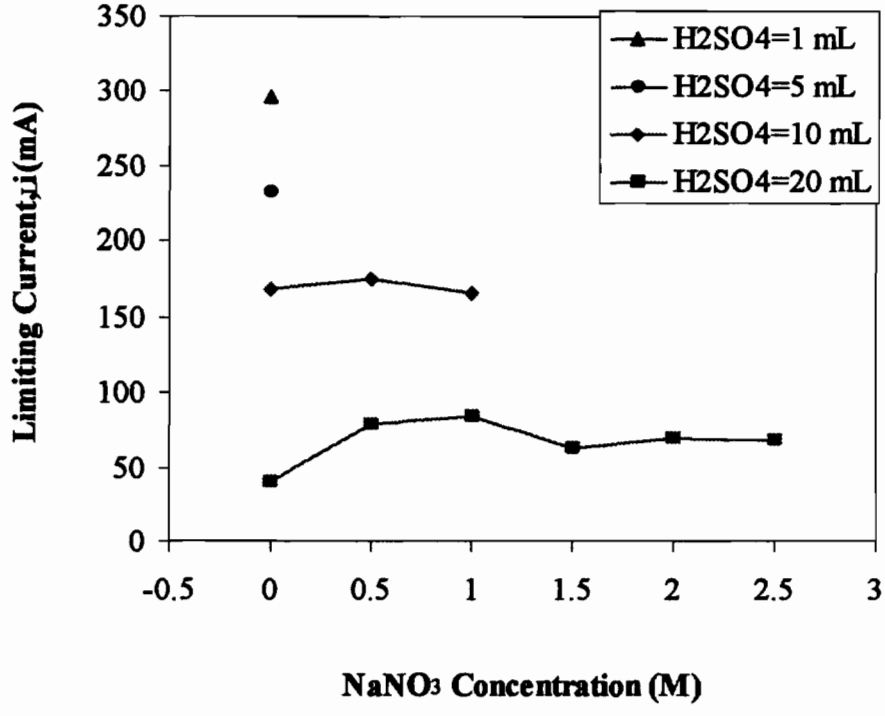

Figure 3-21 Limiting current versus sodium nitrate concentration with different sulphuric acid concentrations.

From Fig. 3-21 we can see that limiting current decreases with increasing concentration of sulphuric acid. The influence of sodium nitrate is not significant. However, increasing sodium nitrate concentration narrows the potential range of limiting current plateau and shifts them to higher values (See Fig. 3-22b). On the contrary,

increasing the concentration of sulphuric acid widens the potential range of limiting current plateau (See Fig. 3-22a).

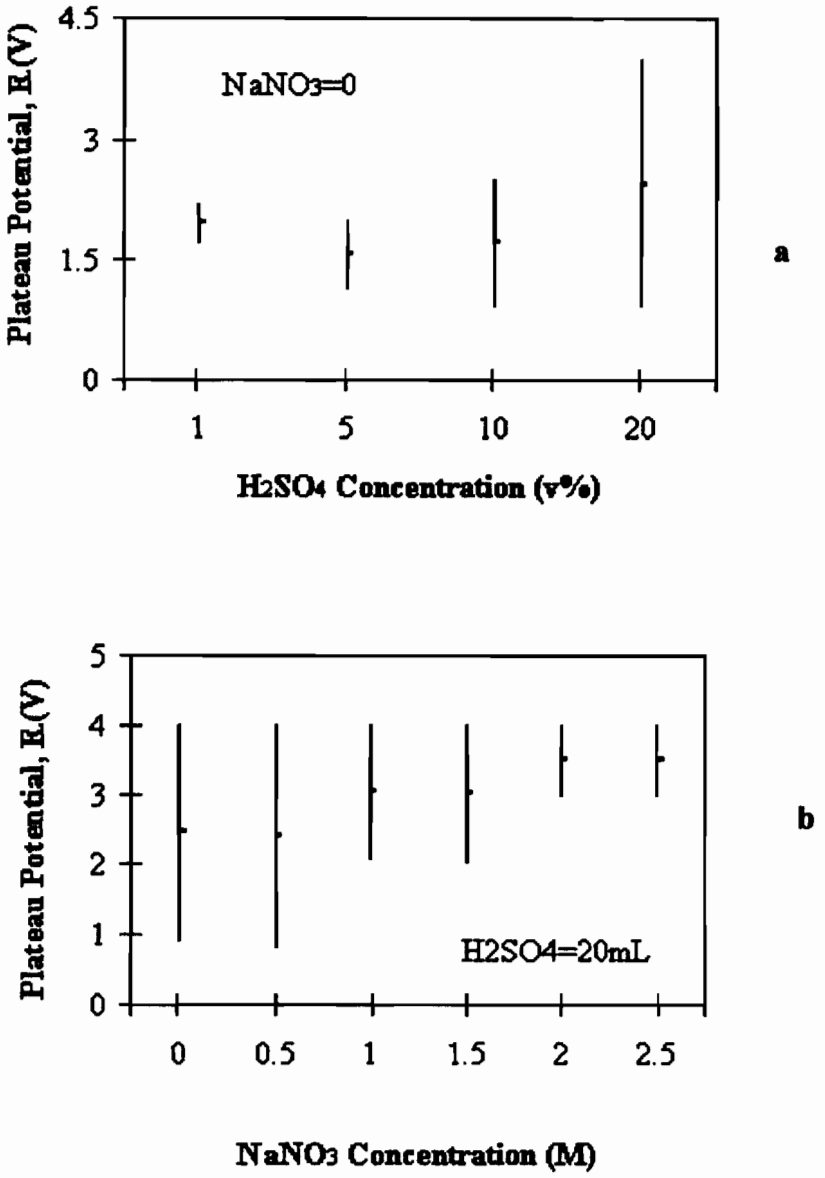

Figure 3-22 Potential of limiting current plateau versus (a) sulphuric acid concentration and (b) sodium nitrate concentration.

There was no limiting current plateau observed on the measured i~V curves for 10% sulphuric acid solutions with sodium nitrate concentration larger than 1.5M and for 1 ~ 5% sulphuric acid solutions with sodium nitrate concentration larger than 0.5M.

3.3.7 Sulphuric acid – potassium nitrate solutions

Potassium (KNO_3) nitrate has similar chemical properties as sodium nitrate. High rate anodic dissolution of copper with 2M KNO_3 solutions was reported by Landolt and his coworkers [30]. To further explore its effects to copper anodic polarization behavior and ECP effect in sulphuric acid solutions, polarization curves of 1 ~ 20% sulphuric acid (H_2SO_4) solutions with 0 ~ 2M potassium nitrate were measured. The limiting current and plateau potential data are plotted in Figs. 3-23 and 3-24.

It is shown that limiting current increases with increasing KNO_3 concentration in solutions with lower sulphuric acid concentration (5%). At higher sulphuric acid concentration (≥ 10%), KNO_3 concentration seems not affect the limiting current much. Similar to sulphuric acid – sodium nitrate system, sulphuric acid influences limiting current inversely.

Increasing KNO_3 concentration shifts the limiting current plateau to higher value. However, this trend reverses at 2M for 10% sulphuric acid solutions. While KNO_3 concentration equal to or higher than 2.5M, limiting current plateau disappears in 5% and 10% sulphuric acid solutions. In 1% and 20% sulphuric acid solutions, current plateau disappears with KNO_3 concentration equal to or higher than 0.5 and 1.5M respectively.

3.3.8 Limiting current feasible to electrochemical planarization for microelectronic applications

Copper anodic polarization curves with limiting current plateau were obtained for most of the electrolyte solutions listed in Table 3-1. The limiting current and plateau potential data is a guide for designing a practical ECP solution and process. The anode potential has to be in the potential range of limiting current plateau, E_L. It will be discussed in Chapter 5 that even in this range, different applied potential may result in different ECP effect.

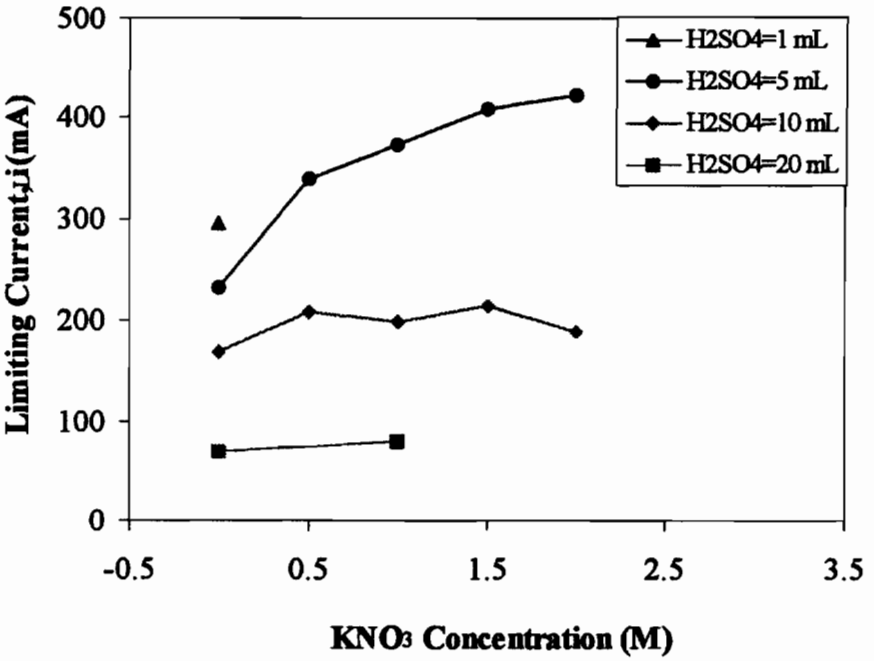

Figure 3-23 Limiting current versus KNO_3 concentration.

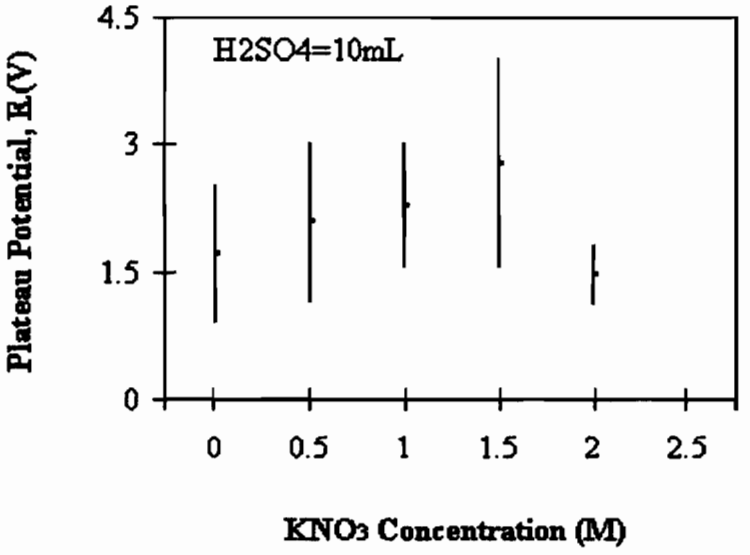

Figure 3-24 Potential of limiting current plateau versus KNO_3 concentration.

Table 3-6 Summary of i_L and E_L data and the trend of i_L affected by increasing the electrolytes

Solutions	i_L (mA)	Typical E_L (V)	Effect of conc. on i_L
Phosphoric acid (H_3PO_4) 13 ~ 100 %	31 ~ 284	0.7 ~ 1.7	H_3PO_4 ↓
phosphoric acid - copper oxide (H_3PO_4) 24 ~ 100 % (CuO) 0.5 ~ 2 M	9 ~ 206	0.8 ~ 1.7	H_3PO_4 ↓ CuO ↓
phosphoric acid - ethylene glycol (H_3PO_4) 13 ~ 75 % ($C_2H_6O_2$) 13 ~ 75 %	10 ~ 77	1.1 ~ 1.8	H_3PO_4 ↑ $C_2H_6O_2$ ↓
phosphoric acid - sodium tripolyphosphate (H_3PO_4) 10 ~ 90 % ($Na_5P_3O_{10}$) 0.1 ~ 0.5 M	16 ~ 190	0.6 ~ 1.6	H_3PO_4 ↓ $Na_5P_3O_{10}$ ↓
HEDP ($C_2H_8O_7P_2$) 2.5 ~ 100 %	6 ~ 81	0.5 ~ 1.4	$C_2H_8O_7P_2$ ↑↓
HEDP - hosphoric acid ($C_2H_8O_7P_2$) 0 ~ 90 % (H_3PO_4) 10 ~ 30 %	8 ~ 217	0.5 ~ 1.4	$C_2H_8O_7P_2$ ↓ 85% H_3PO_4 ↓
ethylene glycol - sodium chloride ($C_2H_6O_2$) 10 ~ 50 % (NaCl) 1 ~ 4 M	20 ~ 131	2 ~ 4	$C_2H_6O_2$ ↓ NaCl ↑
sulphuric acid - sodium nitrate (H_2SO_4) 1 ~ 20 % ($NaNO_3$) 0.5 ~ 2.5 M	63 ~ 175	2 ~ 4	H_2SO_4 ↓
sulphuric acid - potassium nitrate (H_2SO_4) 1 ~ 20 % (KNO_3) 0.5 ~ 2 M	69 ~ 422	1.6 ~ 3	H_2SO_4 ↓

Note: "↓" indicates that i_L decreases with increasing the electrolyte concentration and "↑" indicates that i_L increases with increasing the electrolyte concentration.

From Eq. 2-28, we know that higher limiting current results in higher dissolution rate and therefore higher productivity of electropolishing. However, to realize electropolishing effect, it has to be under mass transport control condition. For a fresh copper surface to form anodic layer(s), which control(s) mass transport, usually a transient time about 50 ~ 100 seconds is required (Refer to Chapter 5). For electropolishing of patterned copper films electroplated on silicon wafers, the thickness of extra film to be removed is about 1μm or so. If the current is too high, the extra copper film will be totally dissolved before the anodic layer(s) is formed. Thus polishing effect will not be reached. That is, a rough surface of the copper interconnects in trenches and vias will be produced. According to Eq.2-28, we can calculate the proper current for this case and it should be no more that 15 mA. Even if the film thickness is increased to 2 μm, the limiting current needs to be lower than 30 mA.

A summary of the i_L and E_L data obtained from studied solutions and the influence of the electrolytes on i_L are listed in Table 3-6.

3.4 Validation of Mass Transport Control

ECP can be achieved only in condition of mass transport control. However, the presence of a current plateau with an anodic film on the surface is not a sufficient criterion for mass transport control [1]. Validation of mass transport control can be performed by steady-state experiments with rotating disk. It is known [31] that under pure mass transport control, limiting current obeys Levich equation (Eq.2-25).

According to Eq.2-25, Levich-Koutecky plot ($1/i_L$ vs $1/\omega^{1/2}$) is a straight line as long as the process is mass transport controlled. Fig. 2-25 is the Levich-Koutecky plots of steady-state data obtained from phosphoric acid solution and HEDP solution. Both of the plots fall on a straight line. This indicates that they are mass transport controlled in the potential range of limiting current plateaus.

In addition, the plot obtained from phosphoric acid solution (54% phosphoric acid + 1.2M CuO) passes through origin. The plot obtained from HEDP solution (80% HEDP) has a nonzero intercept with $1/i_L$ axis, which indicates the existence of additional series resistance to mass transport [31]. Similar results were obtained in Cu - H2SO4 + BTA and Si - HF systems where anodic salt films existed [31, 32].

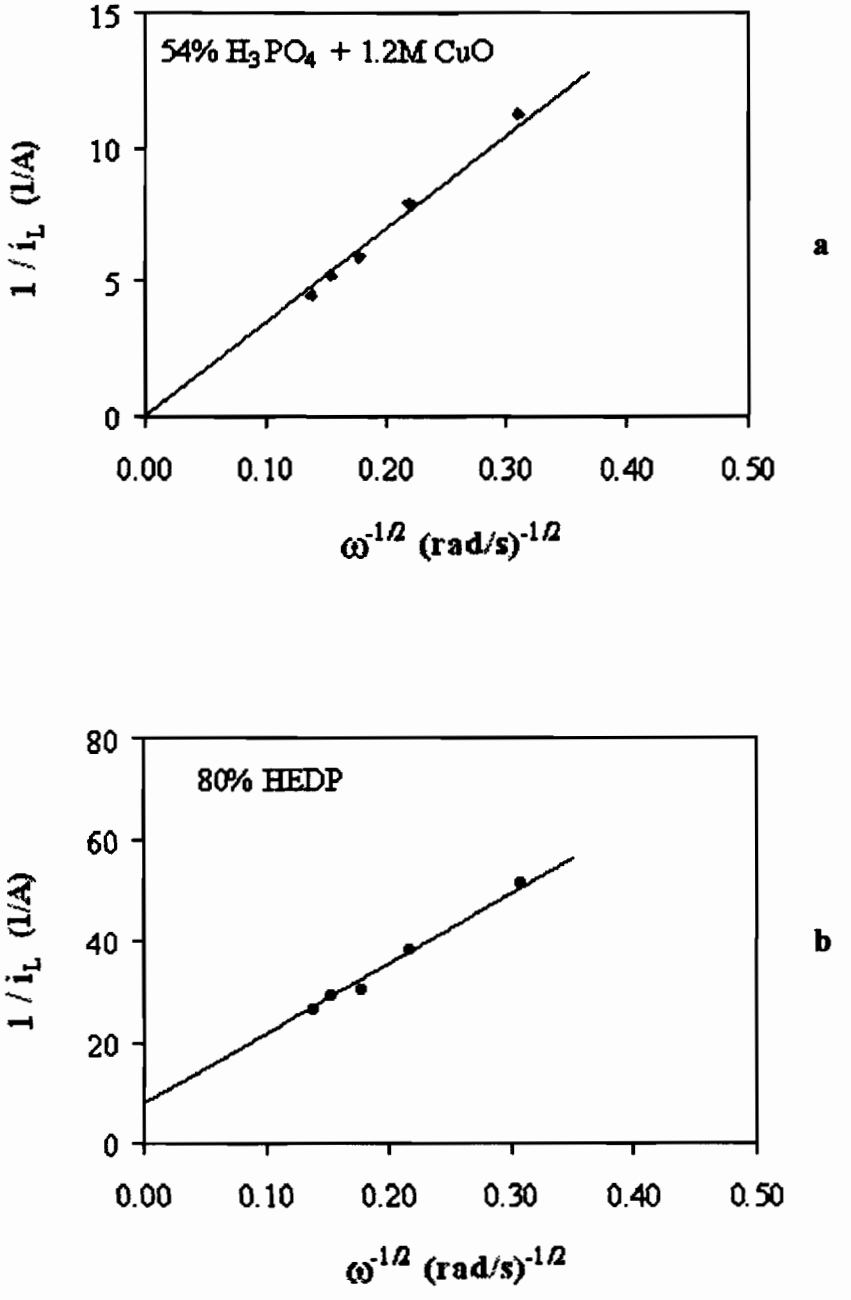

Figure 3-25 Levich-Koutecky plot of solutions: (a) 54% phosphoric acid + 1.2M CuO, (b) 80% HEDP.

References

1. D. Landolt, Review Article Fundamental Aspects of Electropolishing, *Electrochim. Acta*, **32**, 1 (1987), 1-11.
2. M. Paunovic and M. Schlesinger: **Fundamentals of Electrochemical Deposition**, John Wiley & Sons, Inc., New York, 1998, 73-97.
3. J. Koryta, J. Dvořák, and L. Kavan, **Principles of Electrochemistry**, 2nd ed. John Wiley & Sons, Inc., New York, 1993, 259.
4. A. J. Bard, R. Parsons, and J. Jordan: **Standard Potentials in Aqueous Solution**, Marcel Dekker, Inc., International Union of Pure and Applied Chemistry, New York, 1985, 41, 292.
5. J. Huo, R. Solanki, and J. McAndrew, Electrochemical Polishing of Copper for Microelectronic Applications, *Surface Engineering*, vol.19, no.1, 11-16, 2003.
6. V. A. Dmitriev and E. V. Rzhevskaya, Periodic Phenomena in the Anodic Dissolution of Copper in Phosphoric Acid, *Russian J. Phys. Chem.*, **35** (1961), 425-429.
7. S. H. Glarum and J. H. Marshall, The Anodic Dissolution of Copper into Phosphoric Acid, I. Voltammetric and Oscillatory Behavior, *J. Electrochem. Soc.*, **132**(1985), 2872-2878.
8. S. H. Glarum and J. H. Marshall, The Anodic Dissolution of Copper into Phosphoric Acid, II. Impedance Behavior, *J. Electrochem. Soc.*, **132**(1985), 2878-2885.
9. J. Koryta, J. Dvořák, and L. Kavan, **Principles of Electrochemistry**, 2nd ed. John Wiley & Sons, Inc., New York, 1993, 134-139.
10. M. Paunovic and M. Schlesinger, **Fundamentals of Electrochemical Deposition**, John Wiley & Sons, Inc., New York, 1998, 73-97.
11. J. Huo, R. Solanki, and J. McAndrew, Study of anodic layers and their effects on electropolishing of bulk and electroplated films of copper, *Journal of Applied Electrochemistry*, to be published.
12. L. J. Korb, D. L. Olson, J. R. Davis, and et al: **Metals Handbook**, 9th ed., Vol.13, ASM International, Metals Park, Ohio, 1978, 35.
13. H. F. Walton, The Anode Layer in the Electrolytic Polishing of Copper, *J. Electrochem. Soc.*, **97**(1950), 219-226.
14. J. Edwards, The Mechanism of Electropolishing of Copper in Phosphoric Acid Solutions, *J. Electrochem. Soc.*, **100**(1953), 223C-230C.
15. R. J. Schaefer and J. A. Blodgett, Holographic Study of Electropolishing, *J. Electrochem. Soc.*, **123**(1976), 1701-1705.

16. R. Vidal and A. C. West, Copper Electropolishing in Concentrated Phosphoric Acid, I. Experimental Findings, II. Theoretical Interpretation, *J. Electrochem. Soc.*, **142**(1995), 2682-2694.

17. K. Kojima and C. W. Tobias, Solution-Side Transport Processes in the Electropolishing of Copper in Phosphoric Acid, *J. Electrochem. Soc.*, **120**(1973), 1026-1033.

18. K. Dianatkhah, **Passivation behavior of copper thin films for electrochemical planarization application,** Thesis of Oregon Graduate Institute of Science and Technology, Dept. of Materials Science and Engineering, 1999.

19. A. Nashed, G. Fink, The Emergency Medicine and Primary Care, Triple Star Systems, Inc., Available: http://www.embbs.com/cr/alc/alc7.html [Viewed: June 30, 2003].

20. Detergent, Bleach, Cleaner, and Sanitizer Applications, Occidental Chemical Corporation, Available: http://www.oxychem.com/products/handbooks/ACLHB.pdf [Viewed: June 30, 2003].

21. Sodium tripolyphosphate tech., 85%, 2003 Fisher Scientific International, Available: https://www1.fishersci.com/Coupon?gid=42507&cid=1334 [Viewed: June 30, 2003].

22. J. L. Fang and N. J. Wu, Determination of the Composition of Viscous Liquid Film on Electropolishing Copper Surface by XPS and AES, *J. Electrochem. Soc.*, **136**(1989), 3800-3803.

23. ProductInformation, North Metal and Chemical Company, Available: http://nmc-nic.com/spec_sheets/HEDPtechdataSHEETrev_1.pdf [Viewed: June 30, 2003].

24. 1-Hydroxyethylidene-1,1- Diphosphonic Acid (HEDP), Wuzhou International Co., Ltd. Available: http://www.chinax.com/pages/wuzhou/hedp.htm [Viewed: June 30, 2003].

25. Lily Yu, Water Treatment Chemicals, Compass Chemical International, Inc. Available: http://www.compasschemical.com/Page3.html [Viewed: June 30, 2003].

26. YuSi, Circulating Cooling Water treatment System, Jiangsu, P.R. China, Available: http://www.yusi.org/china/ys7662.htm [Viewed: June 30, 2003].

27. J. L. Fang, X. Ma, and W. Lu, Study of Zinc Electroplating Mechanisms with Zn^{2+} - HEDP – CO_3^{2-} System, *Chem. J. Chinese Univ.*, **2**(1981), 285-292.

28. Datta et al, Electrochemical Metal Removal Technique for Planarization of Surfaces, US Patent 5,567,300, Oct. 22,1996.

29. R. Soutebin and D. Landolt, Anodic Leveling under Secondary and Tertiary Current Distribution Conditions, *J. Electrochem. Soc.*, **129**(1982), 946-953.

30. R. Soutebin H. Froidevaux, and D. Landolt, Theoretical and Experimental Modeling of Surface Leveling in ECM under Primary Current Distribution Conditions, *J. Electrochem. Soc.*, **127**(1982), 1096-1100.

31. R. Alkire and A. Cangellari, Effect of Benzotriazole on Dissolution of Copper in Presence of Fluid Flow, *J. Electrochem. Soc.*, **136**(1989), 913-919.

32. C. Serre, S. Barret, and r. Herino, Characterization of the Electropolishing Layer during Anodic Etching of p-Type Silicon in Aqueous HF Solutions, *J. Electrochem. Soc.*, 141 (1994) 2049-2053.

Chapter 4

Study of Copper Anodic Layers and Mass Transport Mechanisms with Electrochemical Impedance Spectroscopy

As stated earlier, electropolishing occurred in the potential range of limiting current plateau and the process is mass transport controlled. In such conditions, the speed of anodic dissolution reaction is higher than that of mass transport process. As a result, a layer with concentration gradient of the anodic reaction product is developed between the anode surface and bulk solution. In some electrochemical system, such as Fe – $FeCl_2$ [1], Ni – HCl [2], and Cu – HCl [3], a salt film can form on the anode surface due to the precipitation of the dissolved metal ions when its concentration exceeds a solubility limit.

Under mass transport controlled condition, continuing anodic dissolution proceeds through either the dissolved metal ions diffusing / migrating through the anodic layer(s) into bulk solution, or acceptor species (anions or water) in solution passing the anodic layer(s) to form a complex with the dissolved metal ions adsorbed on the anode surface [4-9].

Although electrochemical polishing (ECP), applied to bulk metal materials so far, can be achieved through either of the above mechanisms, results of this research suggest that the effect of electropolishing is strongly dependent on the ECP mechanism and anode surface profile. An anodic salt film could be crucial to ECP effect in certain conditions, for example, the electrochemical planarization of patterned copper film electroplated on silicon wafer [10]. Additionally, anodic salt film was found to be responsible for controlling the rate of corrosion pit growth and crack growth in stress corrosion [1, 11]. Therefore, measuring anodic films and identifying the existence of salt film have significant importance to electrochemical polishing and corrosion study.

However, probing such anodic layers is very challenging since it may break down when the potential is switched off and the anode is taken out of the electrolyte. Several

techniques have been tried to study the anode layers, such as linear sweep voltammetry [12, 13], ellipsometry [14], holographic interferometry [15], XPS [16], and AC impedance spectroscopy. Among them, electrochemical impedance spectroscopy (EIS) has been proved effective for the study of anodic layers [1, 9, 10, 17, 18].

4.1 Electrochemical Impedance Spectroscopy

4.1.1 Definition and applications of EIS

Electrochemical impedance spectroscopy (EIS) is a method in which a small ac signal is applied to an electrode and the resulting current is measured. The measuring instrument processes the current – time and voltage – time measurements to provide the impedance at different frequencies, i.e., the impedance spectrum [19]. The electrode studied can be a corroding metal, for corrosion study, or an anode electrode in an electrochemical cell, for characterizing the anodic layers and electrochemical processes.

Impedance is the term used to describe the ac equivalent of dc resistance. With dc methods, such as LSV used in last chapter, the total resistance of the system (polarization resistance R_p) can be obtained. When an ac signal is applied, an electrochemical cell or even a simple corrosion system behaves more complicated. One has to consider polarization resistance R_p, solution resistance R_s, and double layer capacitance C_{dl} (See detailed discussion in section 4.2). EIS can be used to identify and quantify these components and thus characterize the anodic layers and electrochemical processes.

4.1.2 Principle of EIS

AC (alternating current) signal is voltage or current that cyclically flows in one direction and then in another. Voltage or current varies continuously with time. Fig. 4-1 shows a dc and a sinusoidal ac signal.

DC signal can be regulated by Ohm's law:

$$V = I R \qquad 4\text{-}1$$

where V, in volts, is the voltage across a resistor, R, in ohms, and I, in amps, is the current flow through the resistor.

For AC signal,

$$V = I Z \qquad 4\text{-}2$$

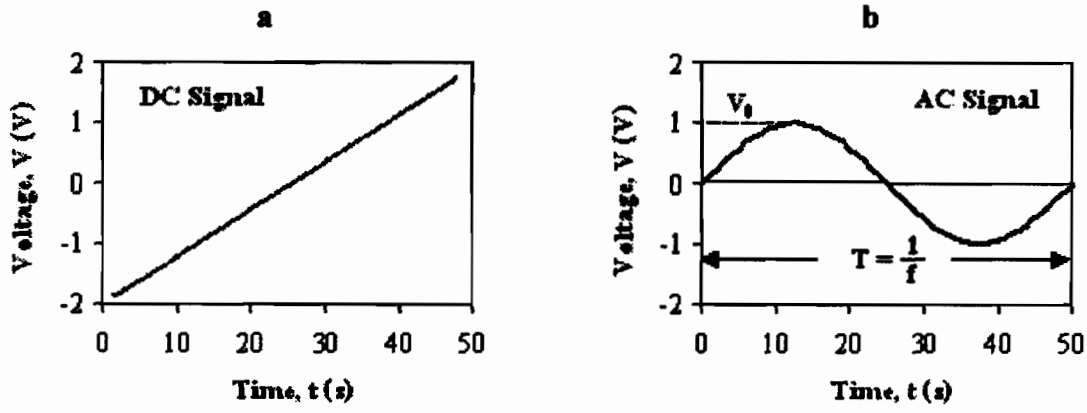

Figure 4-1 Voltage – time relationship of a dc (a) and a sinusoidal ac signal (b).

where Z is the impedance of the circuit. Unlike resistance, the impedance of a component in a circuit is not a constant but varies with the frequency, f, in hertz, of the applied signal.

A sinusoidal ac signal as shown in Fig. 4-1b can be described by

$$V(t) = V_0 \sin(\omega t) \qquad 4\text{-}3$$

where angular frequency

$$\omega = 2\pi f \qquad 4\text{-}4$$

When the above signal is applied to a circuit of resistor parallel with capacitor, as shown in Fig. 4-2a, the current flowing on it is

$$I(t) = \frac{V}{R_1} + C\frac{dV}{dt}$$

$$= \frac{V_0}{R_1}\sin(\omega t) + V_0 \omega C \cos(\omega t) \qquad 4\text{-}5$$

The two components of the current can be plotted versus time, as in Fig. 4-3. The first term is in phase with the applied voltage. The second term is 90° ($\pi/2$ rad) out of phase against the applied voltage. The magnitude of the two terms is proportional to the magnitude of the applied voltage V_0 and inversely proportional to $Z_{R1} = R_1$ and $Z_C = 1/j\omega C$ [20], which are the impedance of the resistor R_1 and the capacitance C respectively. Here operator j indicates a 90° phase shift between applied voltage and resulting current.

Assuming $V_0 / R_1 = I_0 \cos(\phi)$ and $V_0 \omega C = I_0 \sin(\phi)$, Eq. 4-5 can be written as

$$I(t) = I_0 [\sin(\omega t)\cos(\phi) + \cos(\omega t)\sin(\phi)]$$

$$= I_0 \sin(\omega t + \phi) \qquad 4\text{-}6$$

This indicates that the resulting current is a sine wave with same angular frequency (ω) as the applied voltage but shifted by an angle – phase angle (ϕ).

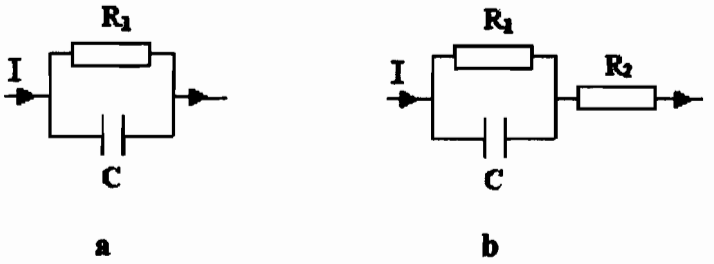

Figure 4-2 Equivalent circuits of electrode (a) and electrochemical cell (b).

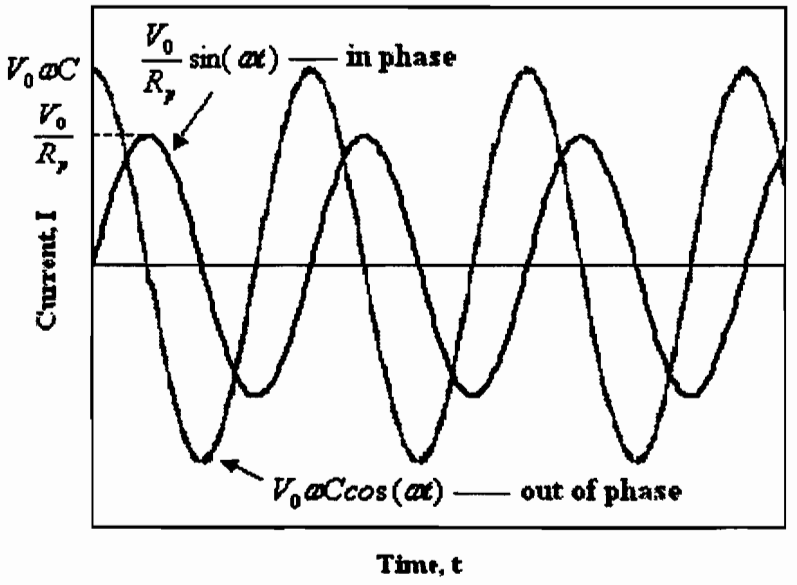

Figure 4-3 Components of current response of circuit in Fig. 4-2a.

For a RC parallel circuit as in Fig.4-2a, there is

$$\frac{1}{Z} = \frac{1}{Z_{R1}} + \frac{1}{Z_c} \qquad 4\text{-}7$$

where Z is the total impedance of the circuit. Substituting $Z_{R1} = R_1$ and $Z_C = 1/j\omega C$ into the above equation, we get

$$Z = \frac{R_1}{1 + j\omega C R_1} \qquad 4\text{-}8$$

Multiplying (1 - jωC) with the numerator and denominator of Eq. 4-8, we obtain

$$Z = \frac{R_1}{1 + \omega^2 C^2 R_1^2} - j\frac{\omega C R_1^2}{1 + \omega^2 C^2 R_1^2}$$

$$= Z' + j\,Z'' \qquad 4\text{-}9$$

where Z' and Z" are the real and imaginary part of the impedance Z respectively and where

$$Z' = \frac{R_1}{1 + \omega^2 C^2 R_1^2} \qquad 4\text{-}10$$

$$Z'' = \frac{\omega C R_1^2}{1 + \omega^2 C^2 R_1^2} \qquad 4\text{-}11$$

$$|Z|^2 = Z'^2 + Z''^2 \qquad 4\text{-}12$$

Thus the impedance modulus

$$|Z| = \frac{R_1}{\sqrt{1 + \omega^2 C_2 R_1^2}} \qquad 4\text{-}13$$

and tangent phase angle [20]

$$\tan(\phi) = \frac{Z''}{Z'} \qquad 4\text{-}14$$

Plots of Z', Z", $|Z|$, and ϕ versus frequency, i.e., *Bode Plots* of the parameters are shown in Figs. 4-4 and 4-5. Plot Z" ~ Z', *Nyquist plot*, is shown in Fig. 4-6. The plots were obtained with: R1 = 1000 Ω, C = 0.001 F.

From the Nyquist plot, we may obtain R_1 and C from [9, 19, 20]

$$R_1 = Z'_{max} \qquad 4\text{-}15$$

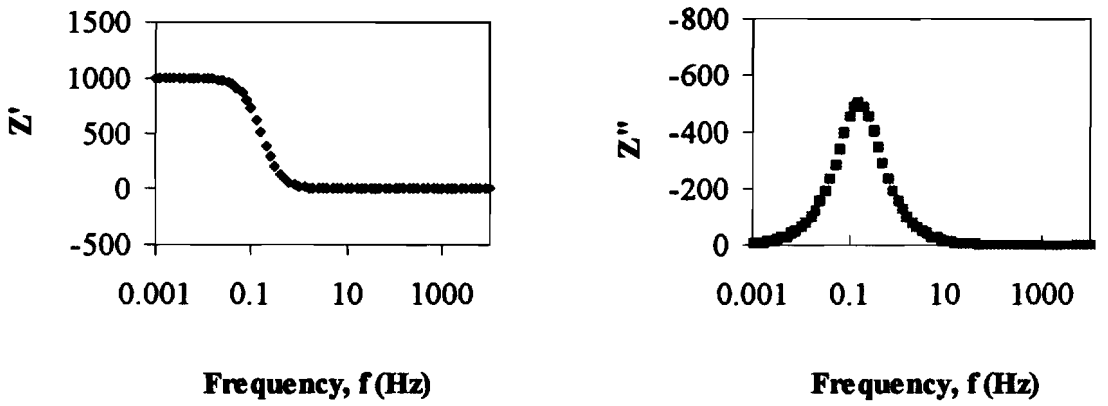

Figure 4-4 Bode plots of Z' and Z'' for the circuit in Fig. 4-2a with $R_1 = 1000\ \Omega$, C = 0.001 F.

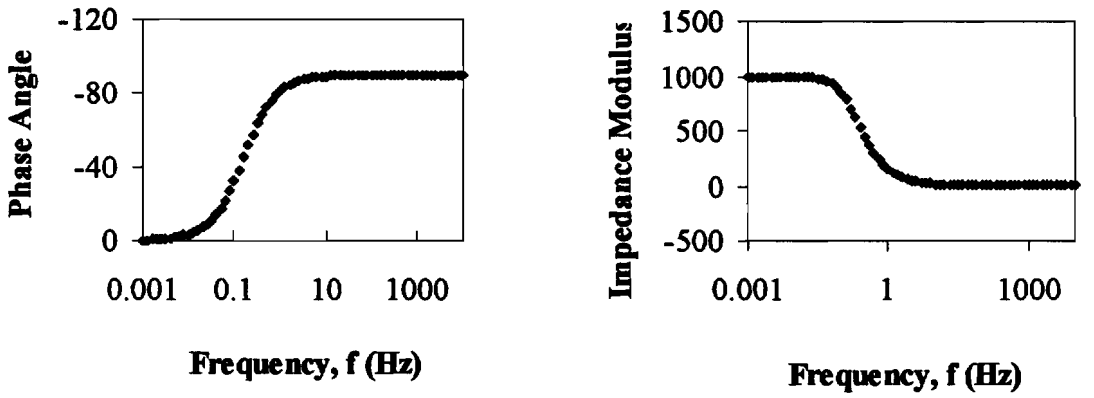

Figure 4-5 Bode plots of ϕ and $|Z|$ for the circuit in Fig. 4-2a with $R_1 = 1000\ \Omega$, C = 0.001 F.

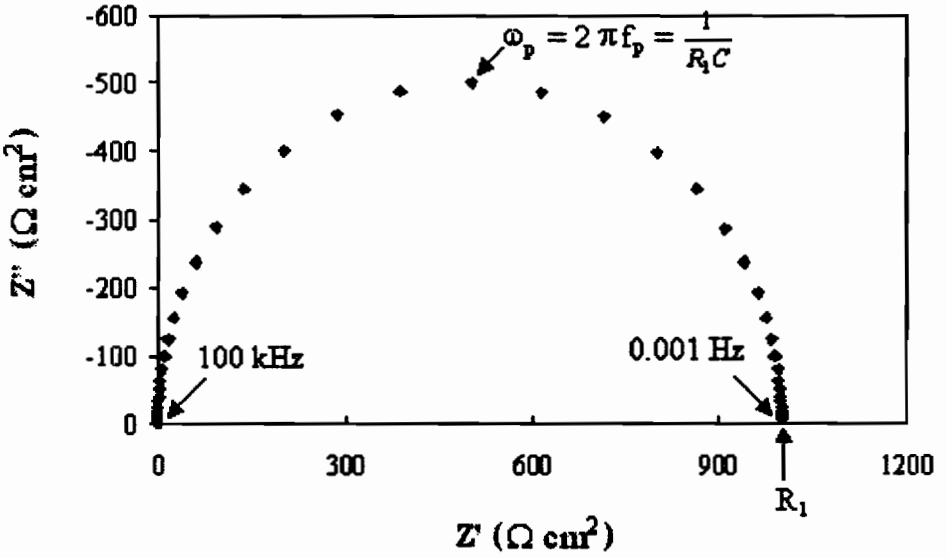

Figure 4-6 Nyquist plot for the circuit in Fig. 4-2a with R_1 = 1000 Ω, C = 0.001 F.

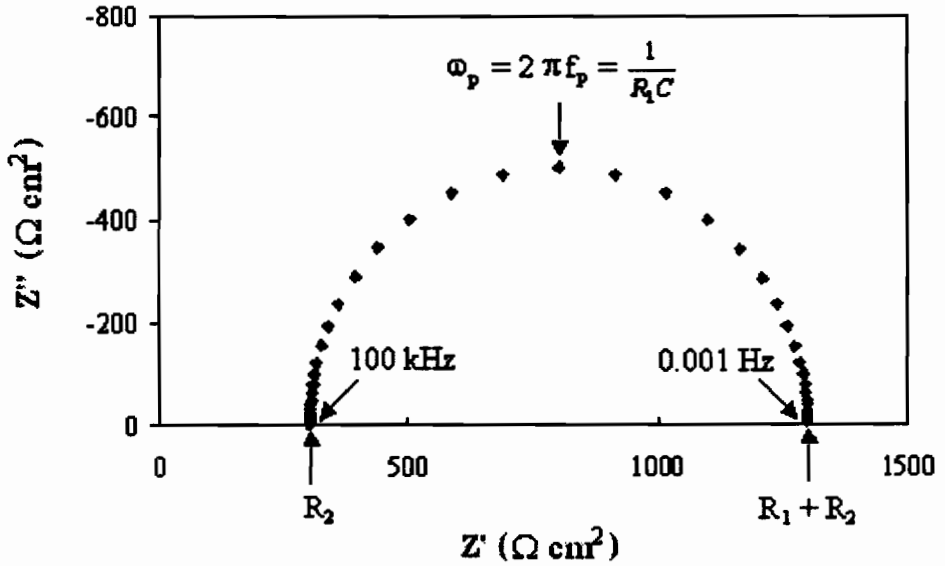

Figure 4-7 Nyquist plot for the circuit in Fig. 4-2b with R_1 = 1000 Ω, R_2 = 300 Ω, C = 0.001 F.

and

$$\omega_p = 2\pi f_p = \frac{1}{R_1 C} \qquad 4\text{-}16$$

where f_p is the frequency corresponding to Z''_{max}.

Similarly, for circuit in Fig. 4-2b, there is

$$Z = \frac{R_1}{1+\omega^2 C^2 R_1^{\,2}} + R_2 - j\frac{\omega C R_1^{\,2}}{1+\omega^2 C^2 R_1^{\,2}}$$

$$= Z' + j\,Z'' \qquad 4\text{-}17$$

where Z' and Z" are

$$Z' = \frac{R_1}{1+\omega^2 C^2 R_1^{\,2}} + R_2 \qquad 4\text{-}18$$

$$Z'' = \frac{\omega C R_1^{\,2}}{1+\omega^2 C^2 R_1^{\,2}} \qquad 4\text{-}19$$

And the Nyquist plot is shown in Figure 4-7. From the Nyquist plot, we may obtain R_1, R_2, and C from [9, 19, 20]:

$$R_2 = Z'_{min} \qquad 4\text{-}20$$

$$R_1 + R_2 = Z'_{max} \qquad 4\text{-}21$$

$$\omega_p = 2\pi f_p = \frac{1}{R_1 C} \qquad 4\text{-}22$$

4.1.3 EIS measurement

Impedance measurements use an ac generator / analyzer, e.g., a frequency response analyzer (FRA) or a lock-in amplifier, to provide an ac voltage signal and analyze current and voltage outputs from a potentiostat [21]. Commonly, the generator / analyzer and potentiostat are under computer control though they can be operated manually as well.

Fig. 4-8 shows the cell setup for EIS measurements [21]. Two or three electrodes can be used for the measurements. In the graph, WE, RE, and CE are working, reference, and counter electrodes respectively. WE is anode whose impedance is to be measured in this study. Because the electrode impedance is inversely proportional to the area of the

electrode there are sometimes benefits from using WE of larger area than is common for dc measurements.

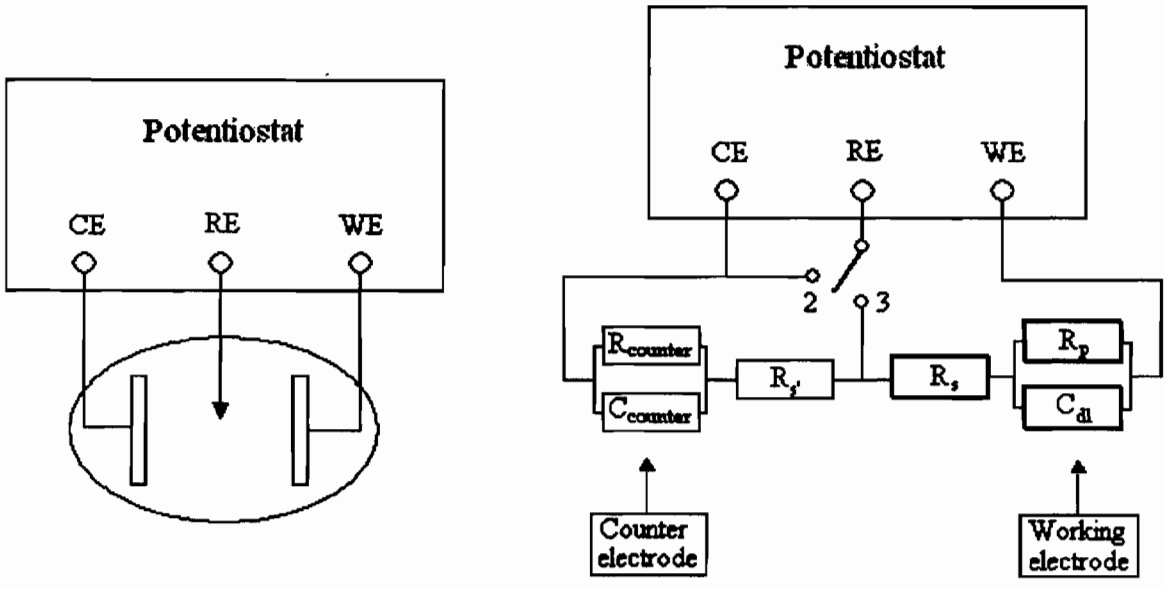

Figure 4-8 Circuit of a three-electrode cell (a) and equivalent circuits of two/three-electrode electrochemical cells (b).

RE, if used, can be one of many types, e.g., calomel, silver /silver chloride, mercury /mercurous sulfate etc. However, better data can be obtained with two-electrode setup since many high frequency distortions can be associated with high impedance and Luggin-reference electrode combination [21].

CE is usually made of stable material such as noble metals (e.g., Pt and Au) or other inert materials (e.g., graphite). The impedance of CE is unimportant in three electrode measurements, as it does not form part of the measured data. As shown in Fig. 4-8b, only right part (highlighted) of the circuit is used to control the ac signal and measure the output current. However, it is important that the shape and size of the electrode is such as to provide a uniform current distribution on WE. This is more important than for dc measurements because the impedance of the electrode is low and controlled by its capacitance at high frequency. This means that at high frequency the

current will take the shortest path between CE and WE, but will be more uniformly spread out at lower frequency [21].

To avoid noise, all the connecting wires and leads should be shielded and as short as possible. Measurements at high frequencies are often affected by distortions due to the cell and/or cell-instrument interactions, which are usually much worse when a reference electrode is used [21]. At low frequencies the practical limit is often determined by the stability of the electrode and the time allowed for the measurements.

To obtain a whole semicircle of the Nyquist plot, i.e., for Z" to approach 0 at high and low frequencies, the frequency should be in range of [21]

$$\frac{100}{2\pi RC} > f > \frac{0.01}{2\pi RC} \qquad 4\text{-}23$$

Double-layer capacitance of 50 ~ 100 μF is typical for metal surfaces. For metals with porous conducting surface film, the value can be much higher [21]. So a proper range of frequency is f = 0.8 ~ 8000 Hz for R = 20 Ω and C= 100.

In addition to frequency range, number of data points is another parameter need to be determined for the measurements. More data points may have higher accuracy of data analysis. But the total time for the data collection increases. In general, 7 ~ 10 points per decade is a good compromise between accuracy and time.

The amplitude of the ac voltage, i.e., root mean square (rms = V_{max}), is the most important experimental variable. It should be small enough to not affect the electrochemical process that is being probed. However, if it is too small, the signal to noise ratio will be small and thus impair the analysis accuracy. Generally, 5 ~ 10 mV rms is a good compromise.

Finally, electrode area is an experiment variable that can not be neglected. Notice that Z' and Z" in Nyquist plot have units of "Ω cm^2". So, for three-electrode measurements, Z' and Z" should be the measured values times the area of WE. For two-electrode system [21]:

$$Z(\Omega cm^2) = Z_{measured}\frac{A}{2} \qquad 4\text{-}24$$

if the two electrodes have equal area, or

$$Z(\Omega cm^2) = Z_{measured} \frac{A_1 A_2}{A_1 + A_2} \qquad 4\text{-}25$$

if the two electrodes have different area A_1 and A_2.

4.2 Electrode Response to dc and ac Signals

4.2.1. Electrode response to ac signal

Corrosion study indicates that ionization may occur when a metal piece, except very few noble elements such as platinum, is immersed in water or chemical solutions even without external potential applied. The ionization and electrostatic interactions between the ions and electrons result in the formation of double layer, as discussed in Chapter 2. The double layer consists of an adsorbed fixed layer on the metal surface and a diffuse mobile layer next to it (Fig. 4-9).

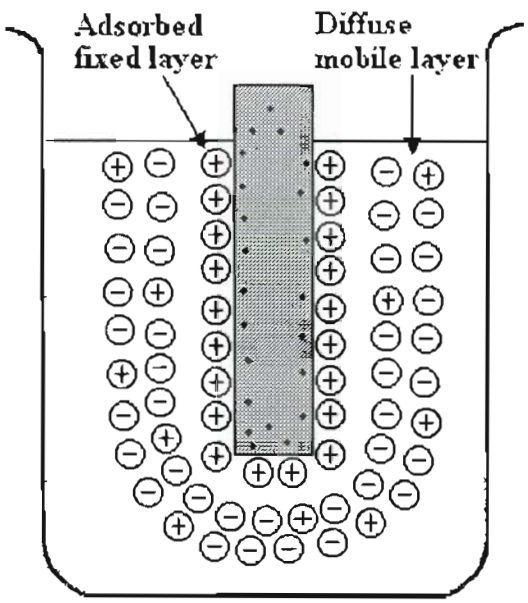

Figure 4-9 Double layer structure.

When an ac potential is applied to the metal bar (it is anode in this study), the ac power supply pushes and then pulls electrons in and out of the load, at the supply frequency. There is no net current flow.

During the positive half-cycle, conventional current flows into the electrode connected to the ac power supply. That is, the electrons are drawn out. The electrode is then less negatively charged (more positive) than before. So it attracts the diffuse mobile layer more strongly. The mobile layer moves closer, as shown in Fig. 4-10a. The conventional current that has flowed into the electrode has charged up the double layer capacitor.

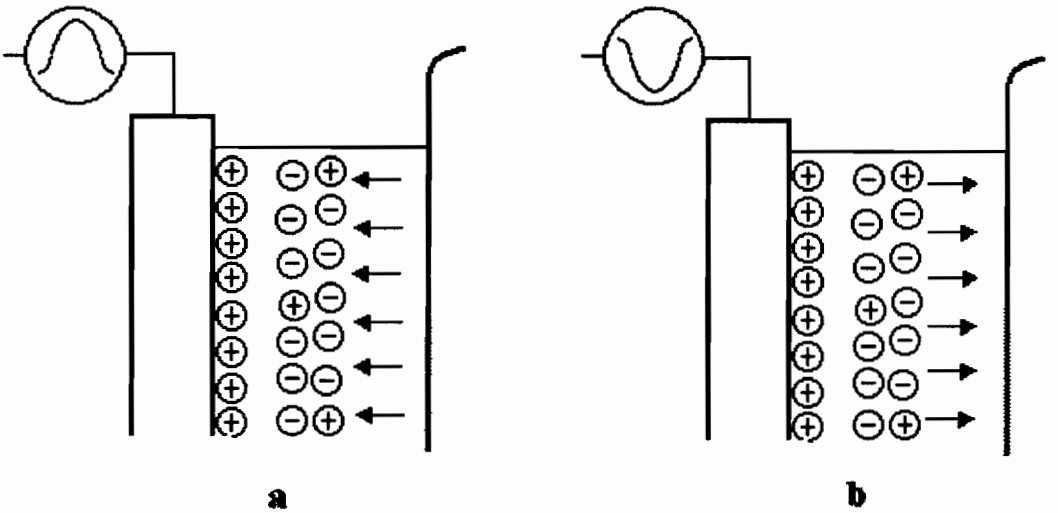

Figure 4-10 Charging (a) and discharging (b) the double layer.

During the negative half-cycle, conventional current flows back out of the electrode. That is, electrons are pushed in. The electrode is now more negatively charged than before, and so repels the mobile layer more strongly. The mobile layer moves away. This is discharging the double layer capacitor.

So an alternating potential applied to the electrode makes the diffuse mobile layer oscillate at the ac frequency. And the double layer behaves like a capacitor (C_{dl}), as illustrated in Fig. 4-11.

As commonly observed with capacitors, the current waveform leads the voltage waveform by 90°, as shown in Fig. 4-12 [22]. When the voltage is at its maximum (A),

the double layer is fully charged. The mobile layer is at its closest to the electrode, and no current flows.

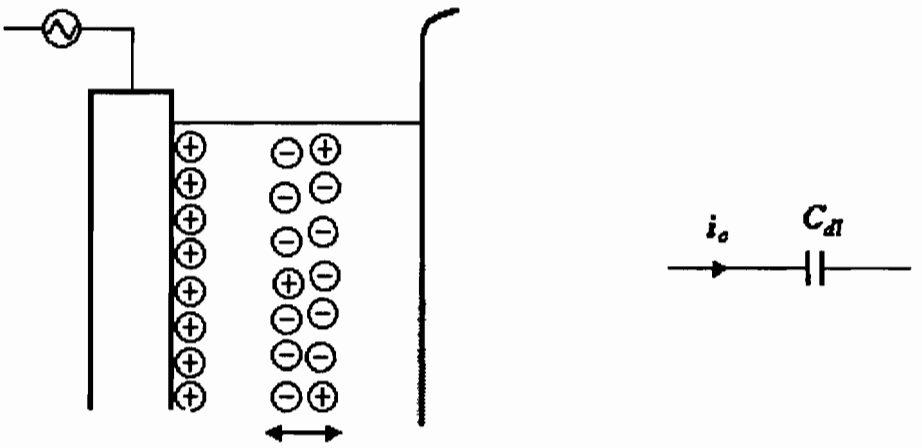

Figure 4-11 Illustration of the diffuse mobile layer oscillation (a) and the equivalent circuit (b).

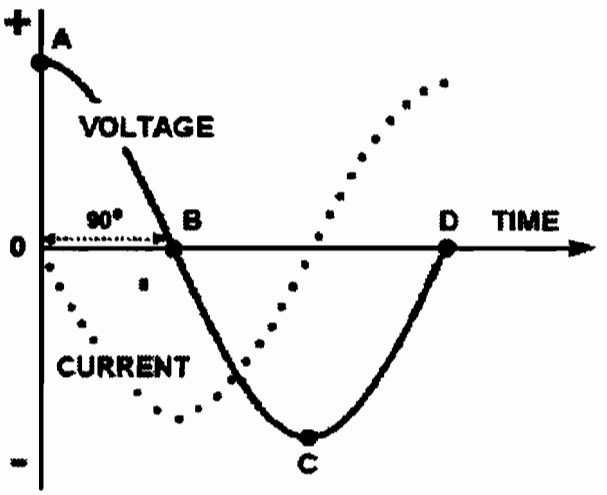

Figure 4-12 Double layer voltage & current waveforms

When the voltage is passing down through zero (**B**), the mobile layer is at its mid position, moving away at maximum speed. Here, the current flow out of the electrode is fastest.

When the voltage is at its minimum (**C**), the double layer is fully discharged. The mobile layer is at its furthest from the electrode, and again no current flows.

When the voltage is passing up through zero (**D**), the mobile layer is again at its mid position, moving in at maximum speed. Here, the current flow into the electrode is fastest.

4.2.2. Electrode response to dc signal

A direct current (dc) power supply pushes the electrons in a steady direction. Electrons flow out of the supply's negative terminal, and into its positive terminal. The conventional current flows counter to this.

A steady flow of current into the anode, that is, a steady withdrawal of electrons, is shown in Fig. 4-13. This makes the electrode positive enough to push away the adsorbed ions into the solution (adsorption). Meanwhile more surface atoms ionize to replace the desorbed ions. The electrons from this ionization flow towards the dc power supply. This is the faradic current in the metal.

The electrode loses mass (dissolves). A stream of desorbed ions passes into the diffuse mobile layer, and eventually out into the solution (See Fig. 4-13). This is the faradic current in the electrolyte.

During all this, the negative mobile layer stays at a constant distance from the electrode. This distance depends on what dc potential is being applied. The more positive the electrode, the closer is the mobile layer.

Unlike ac voltage, dc voltage makes a net current flow through the double layer, from one 'plate' to the other. The double layer capacitor 'leaks'. Therefore, with dc the double layer behaves like a resistor (R_{dl}).

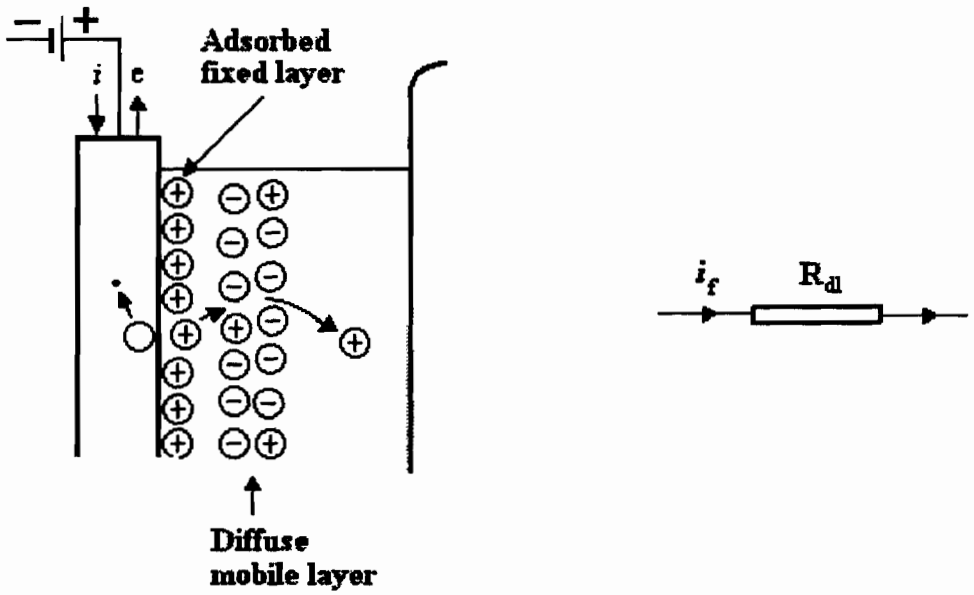

Figure 4-13 Current passing through the double layer under dc voltage.

4.2.3. Equivalent circuit of an electrochemical cell with ac + dc signal

In situ study of anodic layers formed in electrochemical polishing process, requires apply a dc potential and an ac signal (Fig. 4-14a) to the anode. In this case, the double layer is like a leaky capacitor, represented by a resistor in parallel with a capacitor (Fig. 4-14b). The ac component makes the diffuse mobile layer oscillate. The dc component (dc 'bias') causes faradic current flow and chemical reaction. It also controls the mid position of the oscillating mobile layer.

Very low frequency ac signal is the same as slowly changing dc signal. The impedance of capacitor C_{dl} is high. So most current flows through R_{dl} and R_s. And dc behavior rules.

With high frequency ac signal the impedance of C_{dl} is low. So R_{dl} is bypassed and most current flows through C_{dl} and R_s. Thus ac behavior rules.

Taking into account the resistance of electrolyte solution, R_s, the equivalent circuit is R_s in series with the parallel R_{dl} / C_{dl} circuit (Fig. 4-14c). So Fig. 4-14c is valid when the applied anode potential is lower than the potential of limiting current plateau. Here the mass transport condition, under which a diffusion layer exists, is not reached.

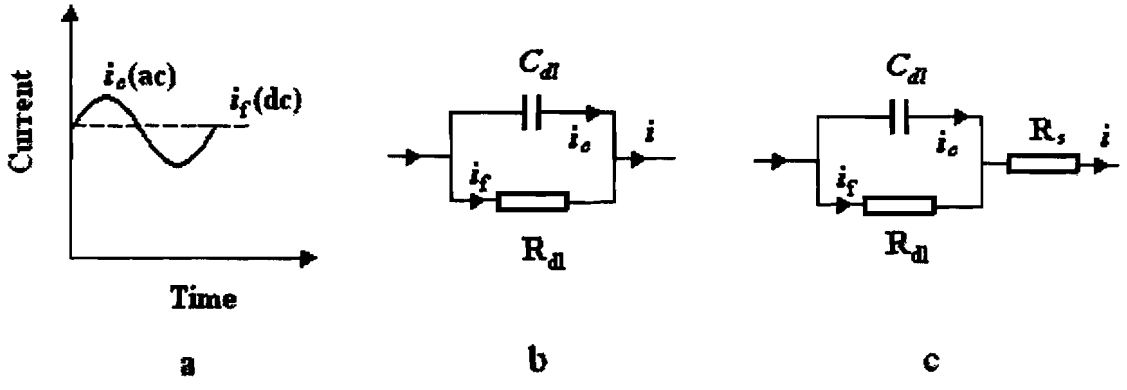

Figure 4-14 ac + dc signal and equivalent circuit of the double layer.

4.2.4. Equivalent circuit of an electrode cell under mass transport control

In an electrochemical cell with a rotating disk electrode (RDE) and/or circulated aqueous solution, the primary mechanisms for mass transport of ions between anode and cathode are ion migration, convection and diffusion processes driven by an electrical field, pressure, and concentration gradient respectively [23].

According to hydrodynamics, a boundary layer exists due to the friction between a fluid and a solid surface (See Fig.3). The thickness of this boundary layer can be determined from [24]

$$\delta = \frac{5x}{\sqrt{\mathrm{Re}_x}} \qquad 4\text{-}26$$

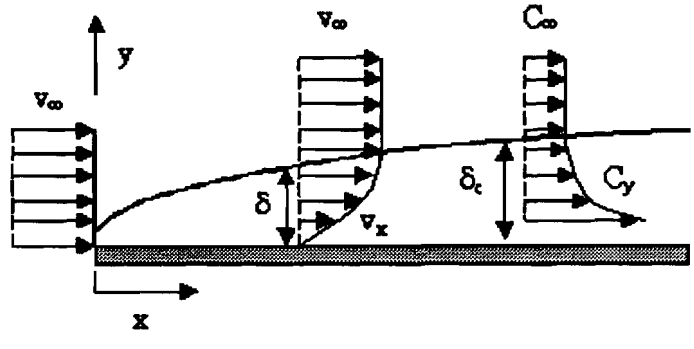

Figure 4-15 Schematic of boundary layer (δ) and diffusion layer (δ_c) on a sample surface under forced convection of solution.

where $Re_x \equiv \frac{\rho u_\infty x}{\mu}$ is the Reynolds number (in range of $10^5 \sim 3 \times 10^6$ for flow over flat plate), ρ is the density (kg/m^3) of the solution, u_∞ is the fluid velocity (m/s) in bulk solution outside the boundary layer, x is the characteristic length in the flow direction, and μ is the viscosity (kg/s-m). Under our experimental conditions, δ was estimated to be about 30 ~ 160 μm. Outside the boundary layer, mass transport is dominated by convection. Inside the boundary layer, convection is weak and mass transport is dominated by diffusion and migration (if a potential difference exists). The ratio of migration to diffusion depends on electrochemical reaction and the conductance of ions in the solution [25].

In an electrochemical system, if charge transfer and chemical reaction processes are slower than diffusion and migration, there will be zero concentration gradient in the boundary layer. However, if a potential is applied to the anode within the range of the limiting current plateau, then mass transport may become the controlling process and a concentration gradient can develop in the boundary layer (See Fig. 4-15). The thickness of the diffusion/migration layer, in case of RDE and considering diffusion only, is [26]

$$\delta_c = 1.61 D^{\frac{1}{3}} \nu^{\frac{1}{6}} \omega^{-\frac{1}{2}} \qquad 4\text{-}27$$

where D is the diffusion coefficient (cm^2/s), $\nu = \mu/\rho$ is kinematic viscosity (cm^2/s), and ω is angular frequency of rotation (s^{-1}). The concentration gradient profile produced is illustrated in Fig. 4-16a.

Further, if a salt film is formed on the anode surface, the film and a diffusion layer next to it may work together as a diffusion / migration barrier, which will limit the diffusion / migration of the dissolved metal cations (M^{n+}) from the anode surface to the bulk solution. As a result, more complicated concentration gradient profiles may develop in the layers, as shown in Fig. 4-16b. The concentration gradient profiles depend on ion migration and diffusion resistances in the layers.

In some electrochemical system, e.g., copper – phosphoric acid solution, the mass transport limiting species is so called acceptor (such as anions A^{n+} or water molecules) instead of the dissolved metal ions (cations). The anode – solution interfacial concentration profile in this case is shown in Fig. 4-16c.

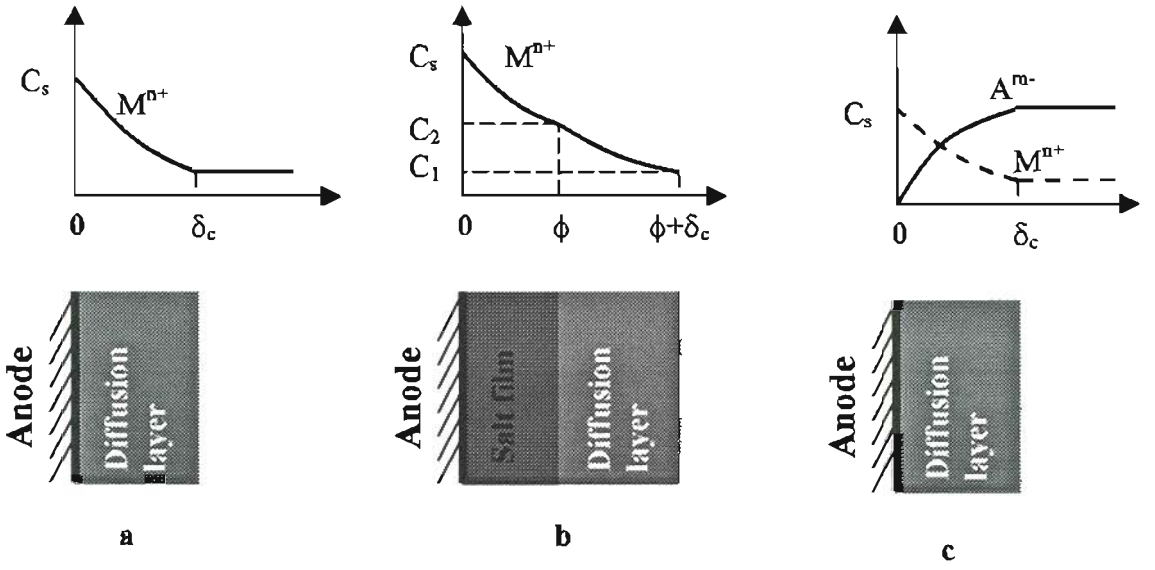

Figure 4-16 Concentration gradient profile in boundary layer (a) and in a salt film / boundary layer structure (b).

Therefore, under mass transport control, the electrode / solution double layer structure consists of the fixed layer, diffusion layer, and the diffuse mobile layer, as illustrated in Fig. 4-17. In case that M^{n+} is the mass transport control species, A M^{n+} ion in the adsorbed fixed layer has to overcome two kinds of resistances to move into bulk solution. The two resistances are: (1) the resistance from the double layer (fixed layer and diffuse mobile layer), R_{dl}, (See Fig. 4-13); (2) the resistance from the diffusion layer, R_w, which is termed Warburg impedance [20].

In case a salt film forms on the anode surface (Fig.4-18a), a desorbed ion has to overcome the resistance from the salt film, R_f, before it can pass through the double layer consists of a diffusion layer and a diffuse mobile layer. The equivalent circuit for this case is shown in Fig. 4-18b.

This is similar to the one in Fig. 4-2b. So, the ac impedance complex plot (Nyquist plot) has the form of Fig. 4-7, with

$$R_1 = R_w + R_{dl} \qquad 4\text{-}28$$

$$R_2 = R_f + R_s + R_m \qquad 4\text{-}29$$

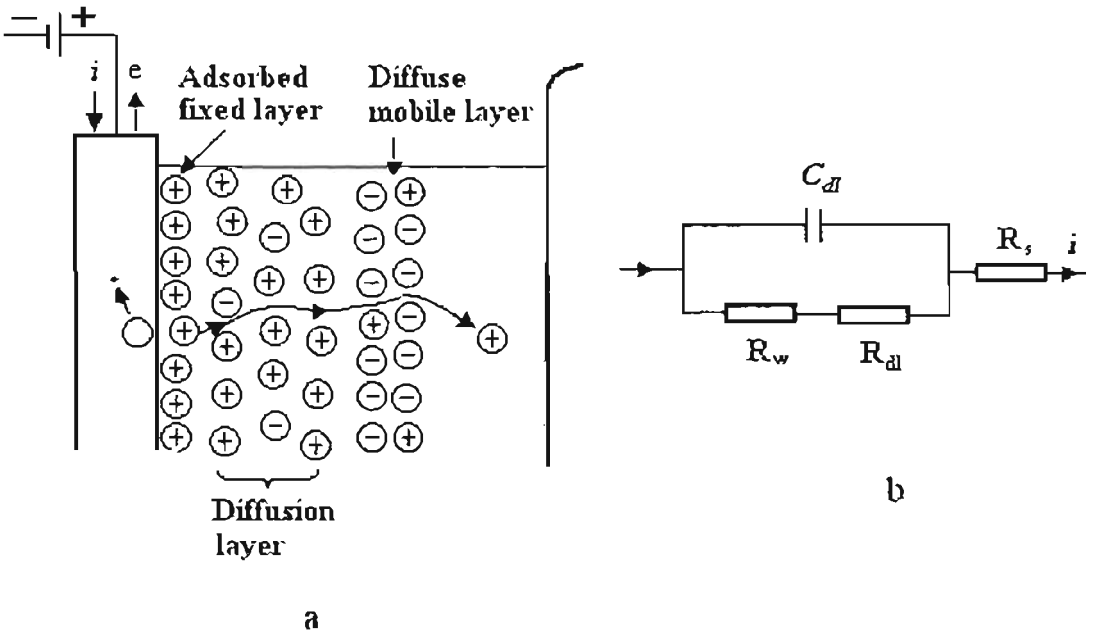

Figure 4-17 Desorbed ions passing through diffusion layer and diffuse mobile layer (a) and the equivalent circuit (b).

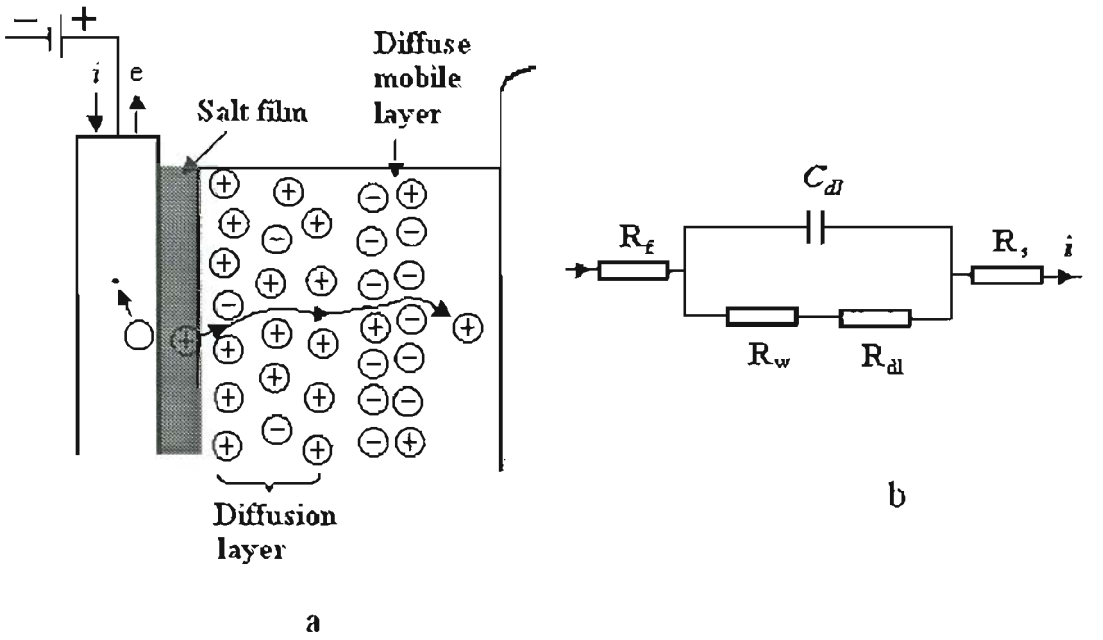

Figure 4-18 Desorbed ions pass through salt film, diffusion layer, and diffuse mobile layer (a) and the equivalent circuit (b).

where R_m is the resistance of the connections between electrodes and power / control units. Therefore, from the plot we can analyze components R_e, R_w, R_f, C_{dl} and thus the anode dissolution process.

4.3 Experimental Details

To measure ac impedance of an anodic dissolution process, an impedance analyzer (Solartron SI 1260 Impedance/Gain-Phase Analyzer) was used together with Princeton Applied Research 273A Potentiostat/Galvanostat, as illustrated in Fig. 4-19. To reduce the noise level at high frequency, reference electrode was not used. And it was internally (inside the electrometer) connected with counter electrode.

The samples used were copper disks with surface area of 1 cm^2 and 1.5 mm thickness. A copper plate 12 mm thick and 43 mm in diameter served as a cathode. As discussed earlier, the configuration of the electrochemical cell strongly affects the EIS measurements. Therefore, the cathode is chosen much larger than the anode to make sure uniform current distribution over the anode surface. In addition, the anode and cathode were set strictly parallel to each other.

The solutions studied were:

(1) Concentrated phosphoric acid,

(2) 70 v% phosphoric acid + 1.2 M copper oxide,

(3) 50 v% phosphoric acid + 50 v% ethylene glycol,

(4) 70 v% HEDP, and

(5) 70 v% phosphoric acid + 0.5 M sodium tripolyphosphate.

100 mL solution was used (in a 200 mL glass container) for each measurement. The anode rotating speed was 100 rpm during the measurements. All the measurements were carried out at room temperature.

The measurements were performed using the software Zplot (Scribner Associate, Inc.) in "controlled E sweep frequency" mode under the following conditions: controlled dc voltage at certain values, e.g., 0.25 V (lower than limiting current plateau), 1.5 V, and 1.8 V (in the range of limiting current plateau); applied 10 mV ac signal with varying frequency from 100 kHz to 0.1 Hz. Before each frequency scan, a 50-second pretreatment (i.e., applied the dc voltage while ac voltage is zero) was performed. Ten points were

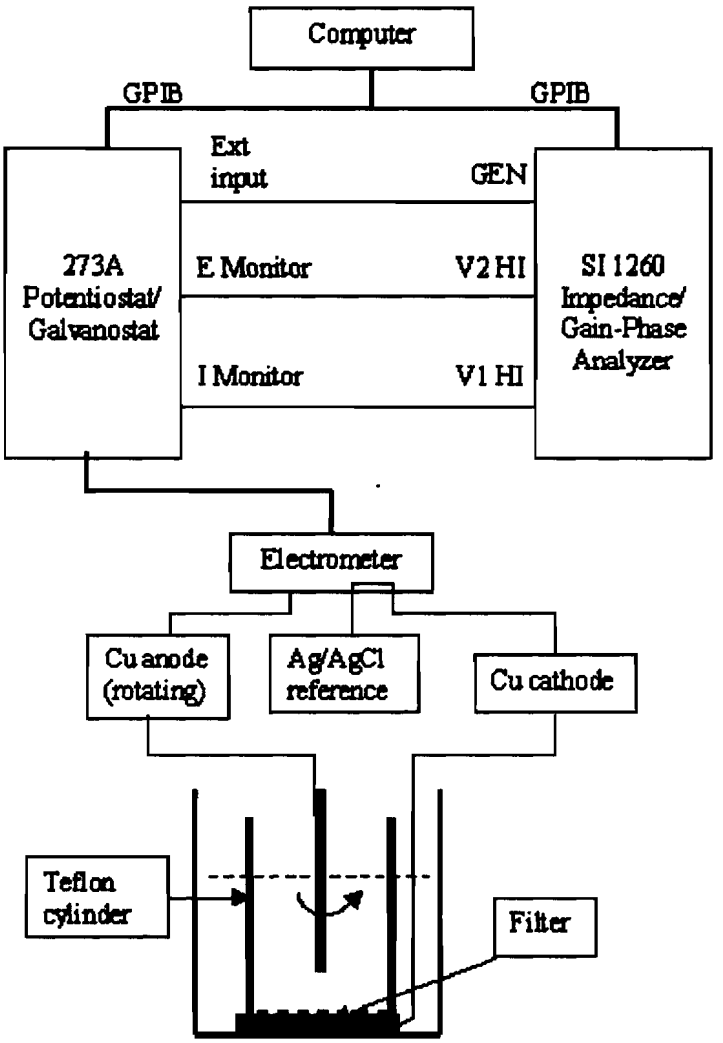

Figure 4-19 Setup for ac impedance measurements.

sampled per decade. That is, 60 points in total were obtained for each scan. The integration time for each sampling was 5 seconds. For each solution, the scan at different potentials was conducted in batch control mode.

The EIS characterized samples were examined with a scanning electron microscope (SEM). Each sample, after an ECP process in a given solution, was carefully taken out of the electrolyte with the potential on. Then it was placed in vertical position so that the solution on the surface dropped down to the lower edge. The solution was carefully wiped off. And then the anode was dried with warm air. By following this procedure, the salt film (if present) on the anode surface could be kept undamaged (in some cases) for SEM inspection.

4.4 Results and Analysis

The measured ac impedance spectra are shown in Figs. 20 ~ 24. At high frequency, a semicircle was obtained at all the dc potentials for all the solutions. At low frequency range, the EIS line shifted to left with the increase of applied dc potential for solutions 2, 3, and 5. Similar behavior was reported by Vidal and West in [9]. This phenomenon is not prominent for solution 1 and not applicable to solution 4.

R_1, R_2, and C_{dl} data were extracted from the measured impedance spectra according to their definitions in Eqs 4-20~22. These data are listed in Table 4-1.

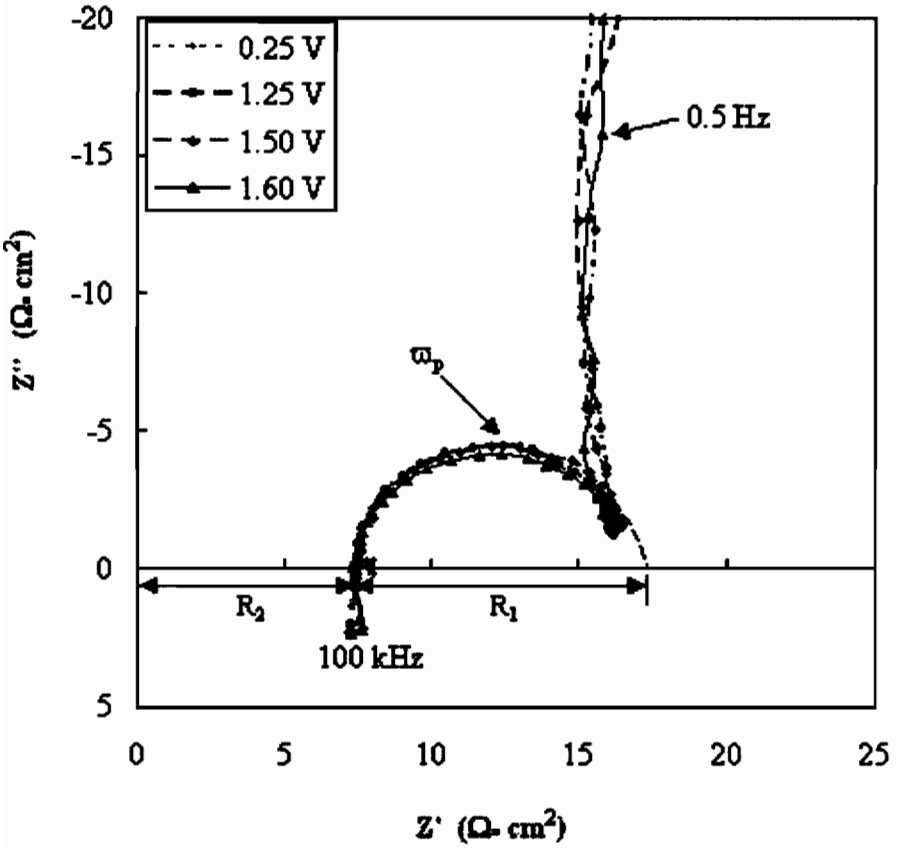

Figure 4-20 Measured ac impedance spectra obtained from concentrated phosphoric acid.

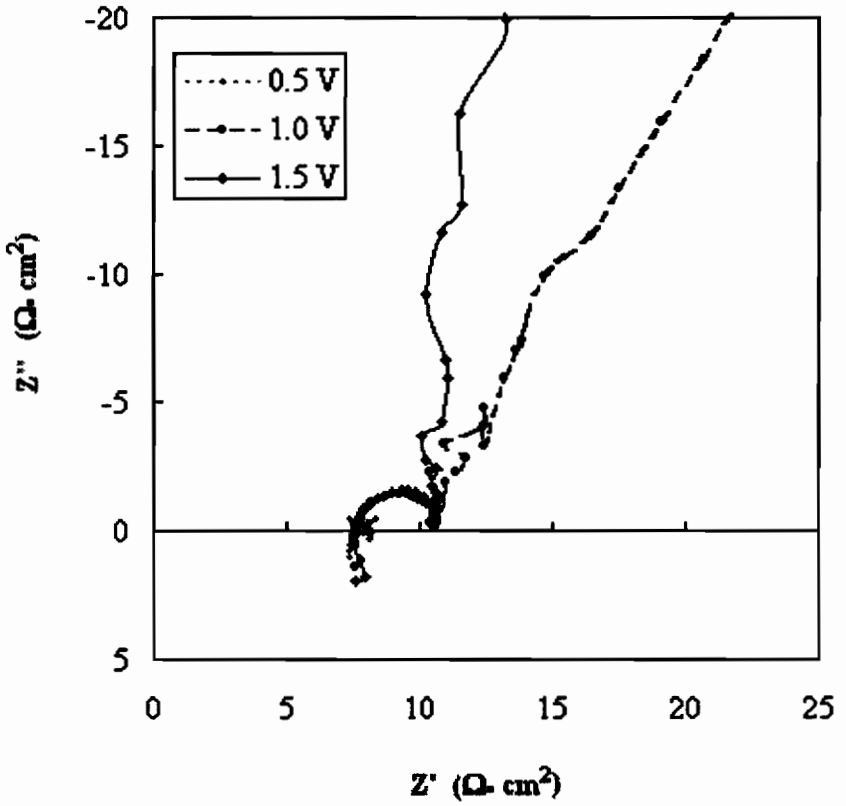

Figure 4-21 Measured ac impedance spectra obtained from 70 % phosphoric acid + 1.2 M CuO.

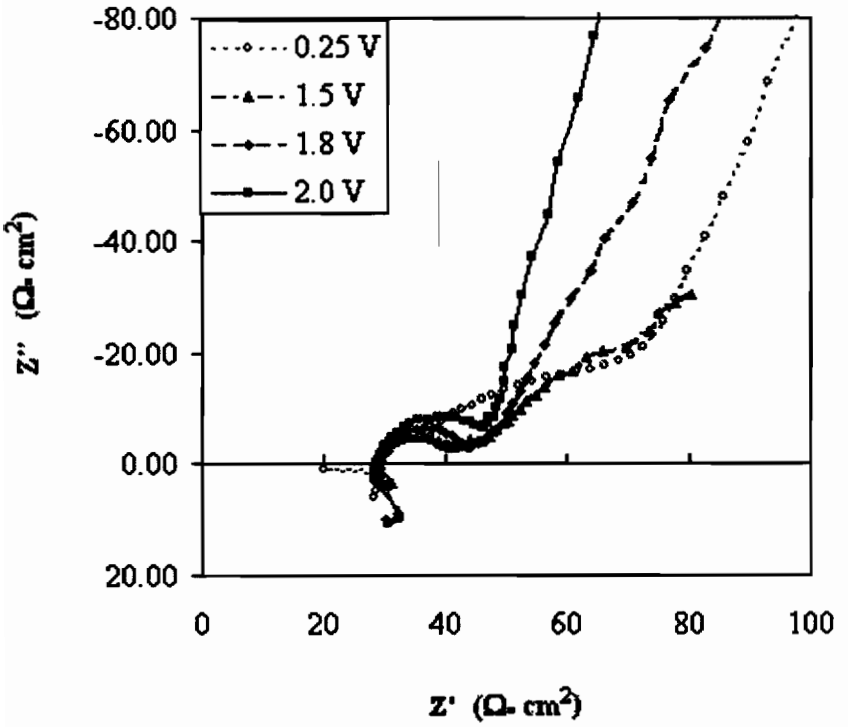

Figure 4-22 Measured ac impedance spectra obtained from 50 % phosphoric acid + 50 % ethylene glycol.

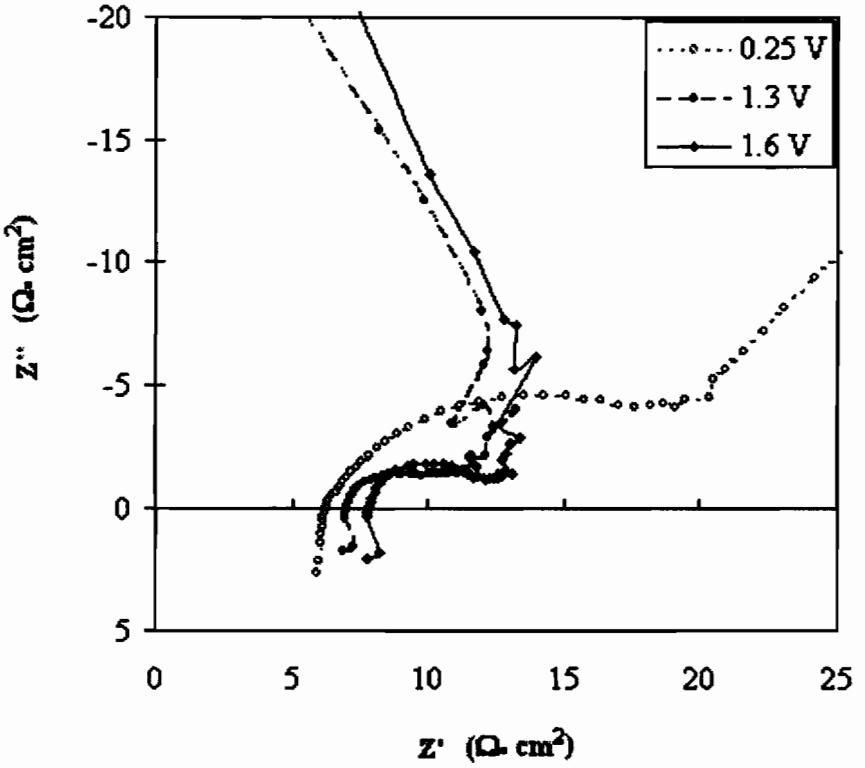

Figure 4-23 Measured ac impedance spectra obtained from 70% HEDP.

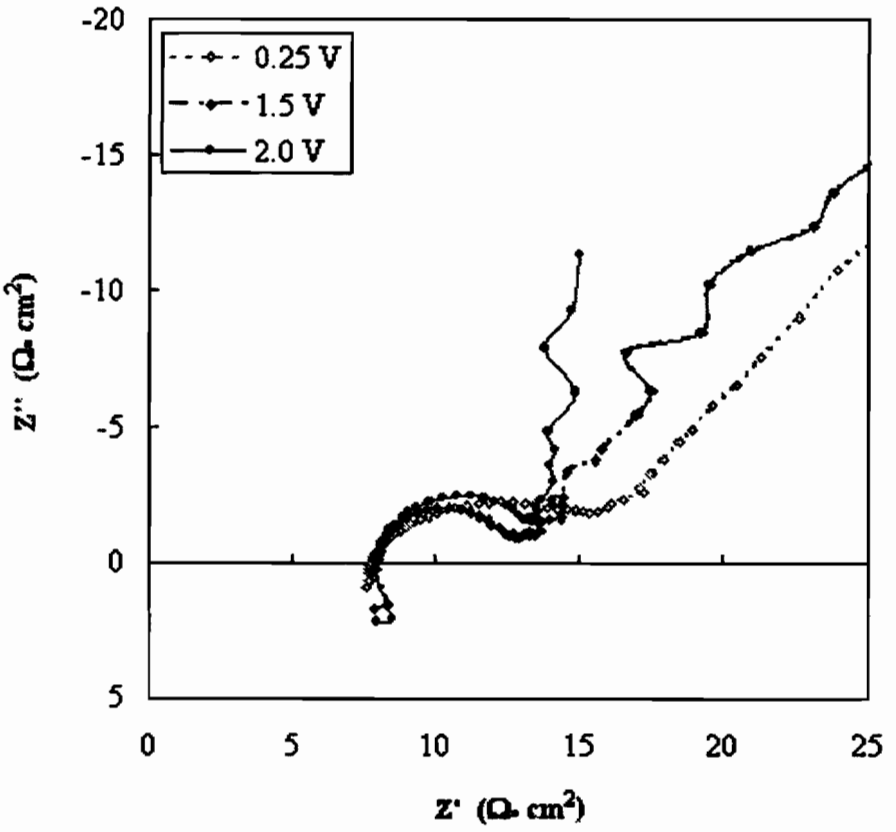

Figure 4-24 Measured ac impedance spectra obtained from 70 % phosphoric acid + 0.5 M sodium tripolyphosphate.

Table 4-1 Summary of impedance measurements.

Solution	Potential (V)	R_2 (Ω cm^2)	R_1 (Ω cm^2)	C_{dl} (μF/cm^2)
1. Concentrated cid	0.25	7.5	0.5	906
	1.25	7.5	9.0	11
	1.5	7.5	9.0	14
	1.6	7.5	9.0	18
2. 70 % phosphoric acid + 1.2 M CuO	0.25	7.6	0.4	199
	1.0	7.6	3.4	12
	1.5	7.6	3.4	74
3. 50 % phosphoric acid + 50 % ethylene glycol	0.25	29.0	-	-
	1.5	29.0	13.0	12
	1.8	29.0	15.0	11
	2.0	29.0	20.0	80
4. 70 % HEDP	0.25	6.0	14.0	180
	1.3	7.0	4.0	20
	1.6	8.0	4.5	11
5. 70 % phosphoric acid + 0.5 M sodium tripolyphosphate	0.25	8.0	9.0	88
	1.5	8.0	5.0	13
	2.0	8.0	7.0	29

4.4.1. Identification of salt film

In Table 4-1, all the dc potentials, except 0.25 V, are in the range of limiting current plateau. Since 0.25V is far below the potential range of the limiting current plateaus, no anodic film can form. Thus, according to the above discussion,

$$R_2\,(0.25V) = R_s + R_m \qquad 4\text{-}30$$

where R_m, the resistance of the connections between electrodes and power / control units, is a constant, R_s is the solution resistance between working and counter electrodes. From the data in Table 4-1, we can see that concentrated phosphoric acid and its solutions with additives: copper oxide, ethylene glycol, and sodium tripolyphosphate, all have constant value of R_2 at all the tested potentials. This indicates that no resistive salt film was formed on the anode surface at potentials in the range of limiting current plateau.

In contrast, copper-HEDP system has different values of R_2 at all the three different applied potentials. In Eqs.4-29 and 4-30, R_m does not change with solutions and applied potential. For same solution, change of R_s, due to anode material dissolved into solution, can be assumed negligible. So, from the R_2 data, we get the following values for Cu-HEDP system:

$R_e + R_m = 6\Omega$,

$R_f\,(1.3V) = 1\Omega$, and

$R_f\,(1.6V) = 2\Omega$.

This suggests the existence of an anodic salt film in Cu-HEDP system. And its thickness increases with increasing potential.

SEM observation, as shown in Fig. 4-25, further confirmed the above results. The results for HEDP solution and concentrated phosphoric acid also agree with previous studies [16, 27, 28].

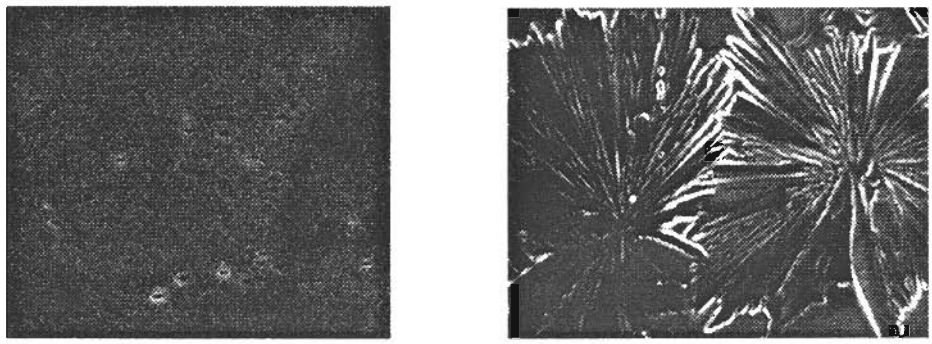

a b

Figure 4-25 SEM pictures of copper anode surface after ECP process in (a) phosphoric acid and (b) 70% HEDP solutions. ×1000.

4.4.2. Warburg impedance

At a potential lower than the limiting current plateau, the process is mainly charge transfer and / or chemical reaction controlled. So R_1 (0.25V) is mainly polarization resistance R_p. While over the range of limiting current plateau, Warburg impedance (R_w) may play a much more important role. The data of R_1 in Table 4-1 shows that in solutions 3, 4, and 5 R_1 increased with an increase of potential within the range of the limiting current plateau. This suggests that diffusion impedance (R_w) increases with the potential increase. So it is very likely that Cu^{++} is the transport limiting species. Since at higher potential, Cu atoms have more chance to be ionized to Cu^{++}. That is, more Cu^{++} ions can be produced at higher potential. However, because the process was mass transport controlled, Cu^{++} ions produced due to higher potential may not necessarily reach the cathode so to complete the charge transfer and current flow cycle. Thus the limiting current did not increase. Instead, higher concentration gradient of Cu^{++} ions in the diffusion layer was developed and therefore higher diffusion / migration resistance.

By contrast, R_1 of solutions 1 and 2 remains constant at different potentials within the range of the limiting current plateau. Previous studies by Wagner [27], Vidal and West [9] have proved that Cu^{++} is not the mass transport limiting species, instead, acceptors, such as anions or water molecules are the transport limiting species in Cu-H_3PO_4 system.

4.4.3. Double-layer capacitance

The data in Table 4-1 shows that all the solutions, except solution 4, have higher capacitance at higher potential in the range of limiting current plateau. Capacitance is defined as

$$C = \frac{dQ}{dt} \qquad 4\text{-}31$$

where Q is charge and t is time. The driving force of an electrochemical reaction is the electrical potential at the electrode surface. So higher charge transfer (e.g., $Cu - 2e \rightarrow Cu^{++}$ on anode surface) rate is expected at higher potential. That is, the adsorbed fixed layer / diffusion layer (positive ions) – diffuse mobile layer (negative ions) capacitor (See Fig. 4-17) has faster charging rate at higher potential. Again, due to the process being mass transport controlled, Cu^{++} ions produced due to higher potential may not necessarily reach cathode and complete charge transfer an thus increase the limiting current. Instead, only more Cu^{++} ions crowded in the fixed layer and diffusion layer. And correspondingly, more negative ions attracted to the diffuse mobile layer. That is, more charge to the double layer capacitor.

This may explain the above phenomena: higher capacitance at higher potential in the range of limiting current plateau.

However, for solution 4 (HEDP solution), as discussed above, a salt film was formed on the anode surface and its thickness increased with anode potential in the range of the limiting current plateau. This may inversely contribute to the capacitance, since

$$C = \frac{\varepsilon A}{d} \qquad 4\text{-}32$$

where A is the area, ε and d are the electrical permittivity and thickness of the media between the capacitor plates, respectively. From Eq. 4-32 we can see that C decreases with an increase of d. Therefore, when a thicker salt film was formed at higher potential, the capacitance dropped. This explains why solution 4 has a lower capacitance at 1.6V than at 1.3V.

All the solutions in table I have a much higher capacitance at 0.25V than that at potentials in the range of limiting current plateau. At such a low potential, the double layer is only a couple of atomic layer thick (See Fig. 4-9). So the thickness (d) of the

double layer capacitor, in this case, is thousands of times thinner than that with diffusion layer (Refer to Chapter 2) under mass transport condition. According to Eq. 4-32, the capacitance should be thousands of times higher. Nevertheless, the charge transfer ($Cu - 2e \rightarrow Cu^{++}$) rate (dQ / dt) is low at low potential. Thus the capacitance should be small according to Eq. 4-31. Therefore the capacitance at 0.25V depends on solutions and is very different than it at limiting current plateau.

4.5 Summary

The structures of electrode double layer at kinetic condition and steady state were discussed, as well as the double layer responses to dc and ac signals and the principle of EIS.

EIS was successfully used to identify copper anodic salt film and mass transport limiting species in solutions of H_3PO_4, H_3PO_4 + CuO, H_3PO_4 + $C_2H_6O_2$, H_3PO_4 + $H_5Na_5O_{10}P_3$, and HEDP.

Cu – H_3PO_4 and Cu – (H_3PO_4 + CuO) systems have identical ac impedance spectra at all the tested potentials. Cu – (H_3PO_4+$C_2H_6O_2$) and Cu – (H_3PO_4+$H_5Na_5O_{10}P_3$) systems have ac impedance spectra with the same original points but different diameters of Nyquist semicircles at varying potentials. Cu – HEDP system has very different ac impedance spectra at different potentials.

Analysis of these spectra suggested that a resistive salt film was formed on the copper anode surface in HEDP solution while no salt film formed in the other solutions. The analysis also suggested that Cu^{++} was the mass transport controlling species in solutions of HEDP and phosphoric acid with additives ethylene glycol and sodium tripolyphosphate. Water molecules are the mass transport controlling species in solutions of phosphoric acid and phosphoric acid with copper oxide.

References

1. R. D. Grimm, A. C. West, and D. Landolt, AC Impedance Study of Anodically Formed Salt films on Iron in Chloride Solution, *J. Electrochem. Soc.*, **139,** 6 (1992), 1622-1629.
2. N. Sridhar, D.S. Dunn, In situ study of salt film stability in simulated pits of nickel by Raman and electrochemical impedance spectroscopies, *J. Electrochem. Soc.*, **144**, 12 (1997), 4243-4253.
3. F.K. Crundwell, Model for the ac-impedance of an electrode coated by a precipitated salt film, *Electrochimica Acta*, **36**, 7(1991), 1183.
4. D. Landolt, Review Article Fundamental Aspects of Electropolishing, *Electrochim. Acta*, **32**, 1 (1987), 1-11.
5. K. Kojima and C. W. Tobias, Solution-Side Transport Processes in the Electropolishing of Copper in Phosphoric Acid, *J. Electrochem. Soc.*, **120** (1973), 1026-1033.
6. J. Edwards, The Mechanism of Electropolishing of Copper in Phosphoric Acid Solutions, *J. Electrochem. Soc.*, **100,** 8(1953), 223C-230C.
7. S. H. Glarum and J. H. Marshall, The Anodic Dissolution of Copper into Phosphoric Acid, I. Voltammetric and Oscillatory Behavior, *J. Electrochem. Soc.*, **132**(1985), 2872-2878.
8. S. H. Glarum and J. H. Marshall, The Anodic Dissolution of Copper into Phosphoric Acid, II. Impedance Behavior, *J. Electrochem. Soc.*, **132**(1985), 2878-2885.
9. R. Vidal and A. C. West, Copper Electropolishing in Concentrated Phosphoric Acid, I. Experimental Findings, II. Theoretical Interpretation, *J. Electrochem. Soc.*, **142**(1995), 2682-2694.
10. J. Huo, R. Solanki, and J. McAndrew, Electrochemical Planarization of Patterned Copper Films for Microelectronic Applications, *Proceedings of the 22nd Heat Treating Society Conference and the 2nd International Surface Engineering Congress*, 15-17 September 2003, Indianapolis, Indiana, USA, 389-397.
11. E.P. Simonen, R.H. Jones, M.J. Danielson, Predicted salt film formation effects on stage I stress corrosion cracking of anodically polarized nickel *Corrosion Science*, **34**, 6 (1993), 899-914.
12. P. Neufeld and T. Zervas, The Relationship Between Polarization Characteristics and the Electropolishing Behavior of Copper, *Surf. Tech.*, **8**, (1979), 129-135.
13. I. A. S. Mansour and T. H. El Sherify, Electropolishing of Horizontal Copper Ring Disks in H_3PO_4 Solutions, *Surf. Tech.*, **19** (1983), 355-361.
14. M. Novak, A. K. N. Reddy, and H. Wroblowa, An Ellipsometric Study of Surface Films on Copper Electrodes Undergoing Electropolishing, *J. Electrochem. Soc.*, **117**, 6 (1970), 733-737.

15. R. J. Schaefer and J. A. Blodgett, Holographic Study of Electropolishing, *J. Electrochem. Soc.*, **123**, 11 (1976), 1701-1705.

16. J. L. Fang and N. J. Wu, Determination of the Composition of Viscous Liquid Film on Electropolishing Copper Surface by XPS and AES, *J. Electrochem. Soc.*, **136**, 12 (1989), 3800-3803.

17. S. Magaino, M. Matlosz, and D. Landolt, An Impedance Study of Stainless Steel Electropolishing, *J. Electrochem. Soc.*, **140**(1993), 1365-1373.

18. M. Matlosz, S. Magaino, and D. Landolt, Impedance Analysis of a Model Mechanism for Acceptor-Limited Electropolishing, *J. Electrochem. Soc.*, **141**(1994), 410-418.

19. R. Cottis, S. Turgoose, and B. C. Syrett, **Corrosion Test Made Easy Electrochemical Impedance and Noise**, NACE International, USA, 1999, 1.

20. J. Koryta, J. Dvořák, and L. Kavan, **Principles of Electrochemistry**, 2nd ed. John Wiley & Sons, Inc., New York, 1993, 301-303.

21. R. Cottis, S. Turgoose, and B. C. Syrett, **Corrosion Test Made Easy Electrochemical Impedance and Noise**, NACE International, USA, 1999, 19-33.

22. A. M. Kaufman, **Understanding Electrochemical Cells**, Solartron Instruments, Hampshire, UK, 1997, 21.

23. A. J. Bard and L. R. Faulkner: **Electrochemical Methods Fundamentals and Application**, 2nd edn, Jone Willey & Sons, Inc., New York, 2001, 137.

24. F. P. Incropera, D. P. DeWitt: **Fundamentals of Heat and Mass Transfer**, 4th edn, Jone Willey & Sons, Inc., New York, 1996, 294-351.

25. A. J. Bard and L. R. Faulkner: **Electrochemical Methods Fundamentals and Application**, 2nd edn, Jone Willey & Sons, Inc., New York, 2001, 141.

26. A. J. Bard and L. R. Faulkner: **Electrochemical Methods Fundamentals and Application**, 2nd edn, Jone Willey & Sons, Inc., New York, 2001, 611.

27. C. Wagner, Contributions to the Theory of Electropolishing, *J. Electrochem. Soc.*, **101**(1954), 225-228.

28. J. Huo, R. Solanki and J. McAndrew, Electrochemical Polishing of Copper for Microelectronic Applications, *Surf. Eng.*, **19** (2003), 11-16.

29. S. C. Chang, J. M. Shieh, C. C. Huang, and et al, Microleveling mechanisms and applications of electropolishing on planarization of copper metallization, *J. Vac. Sci. Technol.* **B20** (2002), 2149 - 2153.

Chapter 5

Electrochemical Planarization of Copper Disks and Electroplated Thin Films on Silicon Wafers

As stated earlier, electrochemical polishing (ECP) occurred in the limiting current condition where the process is mass transport controlled. There are two types of ECP mechanisms: (1) brightening (or microsmoothing), which refers to the elimination of surface roughness of scale comparable to the wavelength of visible light; and (2) leveling (or macrosmoothing), which refers to the elimination of larger surface roughness. Leveling results from the fact that protruding parts of a rough surface dissolve faster than recessed parts [1, 2]. This can be achieved under ohmic or mass transport control [3]. Brightening can be achieved only under mass transport control, which suppresses crystallographic etching [1, 3-5]. Hence, mass transport process is a critical condition for ECP. It is known that anodic films formed during electropolishing and worked as barriers to the mass transport limiting species: cation of dissolving metal (M^{n+}), electrolyte anion (A^{m-}), and water molecules [3].

However, the knowledge about ECP mechanisms is so far based on the study of copper bulk material in limited electrolytes, mostly phosphoric acid. It has been shown that copper bulk material and copper films electroplated on trenched wafers have different surface profiles [6]. It was also found that ECP efficiency was influenced by the pattern of surface profile [7].

Therefore, a thorough study of ECP mechanisms and their effects on different surface profiles is very important for optimizing process parameters such as electrolyte composition and operating voltage/current in order to obtain satisfactory ECP for microelectronic fabrication. This chapter presents ECP data of copper bulk and films electroplated on trenched silicon wafers in various electrolyte solutions. A detailed description of ECP mechanisms, the correlation between ECP efficiency and surface

profile, and the optimal conditions for the ECP of copper films electroplated on patterned silicon wafers are given as well.

5.1 Experimental Details

ECP of copper disks and copper films on deep trenched silicon wafer coupons was performed with computer-controlled chronoamperometry (CA), i.e., potential control. A typical chronoamperometry curve is shown in Fig. 5-1. The control system, as shown in Fig. 5-2, consisted of 273A Potentiostat/Galvanostat (Princeton Applied Research), a computer, and customized cells. For ECP of copper disks, the cell (Fig. 5-2a) used was a 200 ml glass beaker. A 12 mm thick and 43 mm in diameter copper plate served as a cathode. A Teflon cylinder with a filter on the bottom was placed on the cathode to block hydrogen bubbles, produced during ECP, from reaching the anode copper disk to be polished.

For ECP of copper film on silicon wafer coupons, a customized sample holder was made to hold 5 cm × 5 cm wafer coupons. A larger cylindrical container (about 3 liter volume) and copper cathode were used (Fig. 5-2b). A conical filter was also used to block hydrogen bubbles from reaching the anode surface. The inter electrode distance was about 15 mm.

The copper disks used for ECP were 1.5 mm thick, 11.28 mm in diameter (i.e., surface area = 1 cm^2), with a purity of 99.99% Cu. As discussed in Chapter 2, ECP effect is very sensitive to the anode surface state. Therefore all samples for ECP were carefully prepared. Before the ECP process, the copper disks were hand polished with sand papers of 1μm grit (9μm, 5μm, and 3 μm grit papers were also used if needed), followed with methanol rinse and pressured nitrogen dry. The wafer coupons for ECP were cut from 200 mm diameter deep trenched wafers with electroplated copper film. The copper plating on 200 mm wafers was performed with OGI's in house wafer plating system.

The controlled potentials for ECP were the middle points of the limiting current plateau (E_L) on the polarization curves, which were presented in Chapter 3. The duration time of ECP for each sample was determined such that the original rough surface layer could be removed. For copper disks, generally a 10 μm thick layer was removed by the

ECP process. The electrolyte solutions used for ECP are listed in Table 5-1. 100 ml solution was used for ECP of each copper disk. For wafer coupons, various ECP time were used to observe the surface planarization effects. 1300 ml solution was used for ECP of each wafer coupon. All the experiments were performed at room temperature.

Surface profiles of the samples before and after ECP were examined with an atomic force microscope (AFM), optical and electron microscopes, as well as a surface profilometer. For each sample, three AFM images were taken at different locations and the average (R_a) of the three measured mean roughness were determined.

Polishing (or removal) rate R_d was calculated from the weight of the copper disks measured before and after electropolishing. The data were compared with the calculated values determined from the polishing current. This verified the number of charge transferred in an anodic reaction.

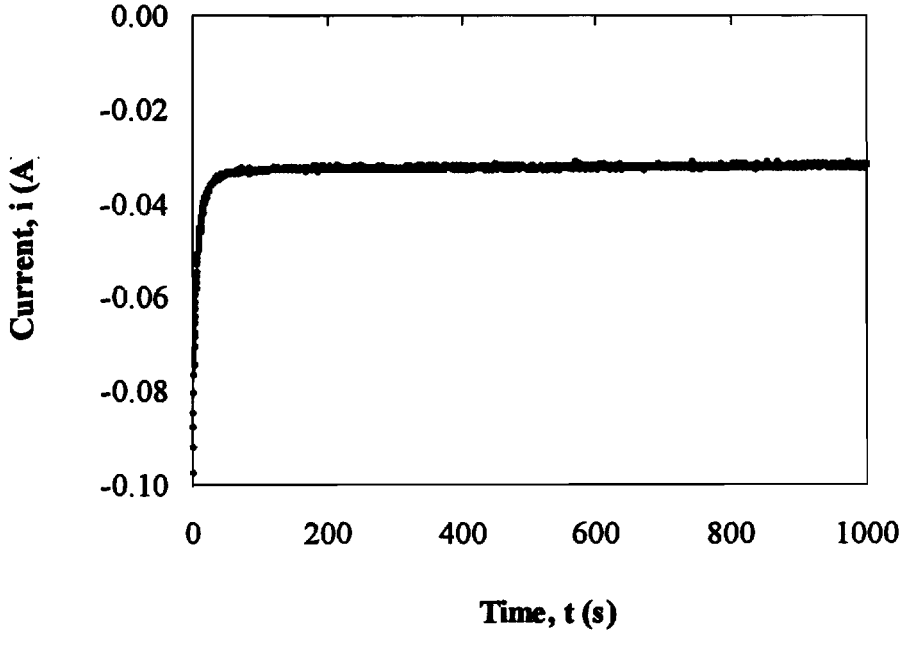

Figure 5-1 The chronoamperometry curve obtained from Cu (anode) – 70% HEDP system with controlled potential at 1.0 V.

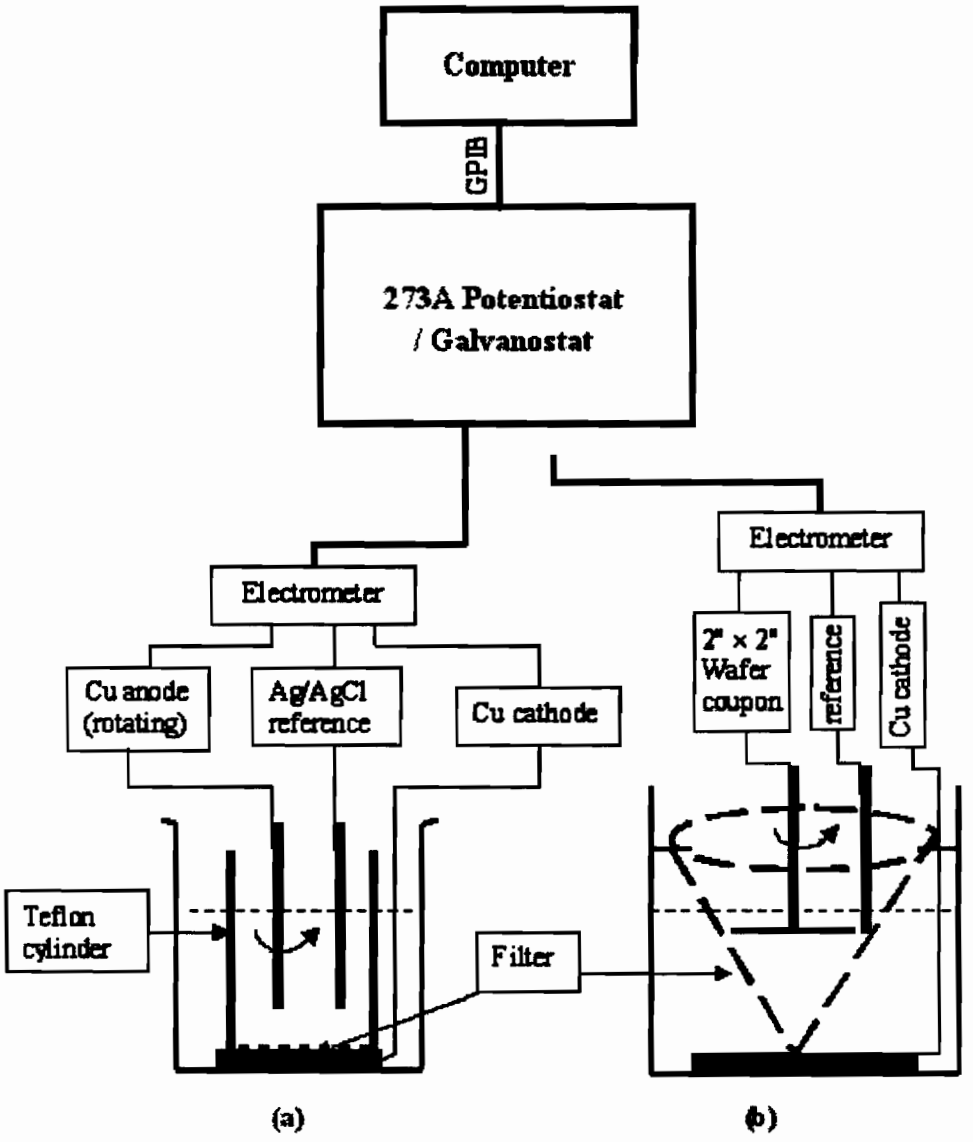

Figure 5-2 Schematic of ECP system for copper disks (a) and wafer coupons (b).

Table 5-1 Electrolytes Used for ECP of copper disks

Solution No.	Chemical 1	Concentration (% Volume)	Chemical 2	Concentration (Mole / L)
1	Phosphoric acid (85% H_3PO_4)	30, 40, 70, 100. 70.	Copper oxide (CuO)	0. 0.5, 1.2, 2.0.
2	Phosphoric acid (85% H_3PO_4)	70	Ethylene glycol ($C_2H_6O_2$)	5, 15, 25 (% vol)
3	Phosphoric acid (85% H_3PO_4)	70	Sodium tripolyphosphate ($Na_5P_3O_{10}$)	0.1, 0.25, 0.5
4	Hydroxyethyliden ediphosphonic acid (HEDP)	20 ~ 80	Phosphoric acid (85% H_3PO_4)	10 ~ 30 (% vol)
5	Ethylene glycol ($C_2H_6O_2$)	20 ~ 100	Sodium chloride (NaCl)	0 ~ 2
6	Sulphuric acid (H_2SO_4)	20	Sodium / Potassium Nitrate ($NaNO_3$ / KNO_3)	1.0, 2.0.

5.2 Experimental Results

5.2.1 ECP of copper disks

An AFM topography image of copper disk surface before ECP is shown in Fig. 5-3. The surface profile exhibits sharp undulation. A typical average mean-roughness, R_a, before ECP is about 280 nm. The ECP efficiency of an ECP process can evaluated by [8]

$$P_B = \frac{R_a^o - R_a}{R_a^o} \qquad 5\text{-}1$$

where R_a^o and R_a are the average mean-roughness before and after electropolishing, respectively. The maximum brightening effect is characterized by $P_B = 1$, and no brightening effect at all when $P_B = 0$. ECP effects include ECP efficiency, removal rate

(R_d), surface appearance, and other qualities. In this work, R_a is reported since all copper disks had about the same R_a values before ECP.

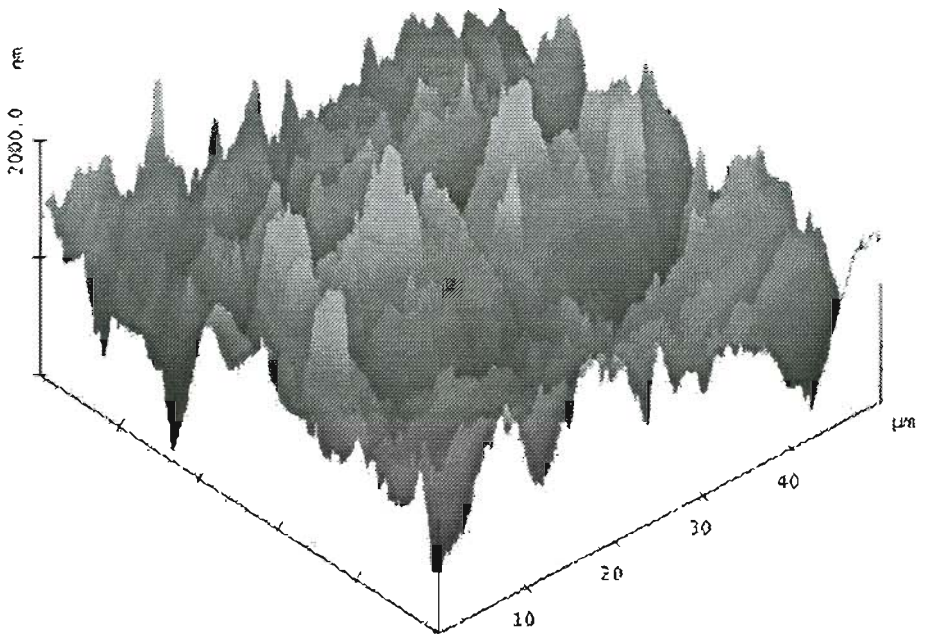

Figure 5-3 AFM image of surface profile of copper bulk material, R_a = 280 nm.

5.2.1.1 ECP of copper disks in H_3PO_4 – CuO solutions

Copper disk ECP was performed in solutions of phosphoric acid and phosphoric acid - copper oxide listed in Table 5-2. The controlled potential and measured current during the ECP processes are listed in the table as well. Typical AFM images of copper disk surface after ECP are shown in Fig. 5-4. The average mean-roughness measured with AFM and removal rate (R_d) calculated from the weight loss are listed in Table 5-2.

The data shows very good ECP effect (R_a < 10 nm) obtained from phosphoric acid solutions with or without CuO when phosphoric acid concentration was 70% or higher. At lower concentration of phosphoric acid, copper ECP effect decreases with decreasing phosphoric acid concentration. Adding CuO, more or less, did not affect the ECP efficiency of 70% phosphoric acid solution. However, higher phosphoric acid concentration or more CuO resulted in lower limiting current and thus lower removal rate,

which is important to ECP of copper films electroplated on silicon wafer (See section 5.2.2).

Table 5-2 Summary of ECP data with solutions of H_3PO_4 and H_3PO_4 – CuO

Solution (% vol.)	**Potential** (V)	**Current** (mA)	**Roughness** (nm)	**Removal Rate** (μm/min)
30 phosphoric acid	1.75	200	29	4.4
40 phosphoric acid	1.7	180	18	4.0
70 phosphoric acid	1.4	50	8	1.1
100 phosphoric acid	1.2	12	5	0.26
70 phosphoric acid + 0.5M CuO	1.2	45	5	1.0
70 phosphoric acid + 1.2M CuO	1.1	30	6	0.7
70 phosphoric acid + 2.0M CuO	1.1	20	6	0.44

5.2.1.2 ECP of copper disks in H_3PO_4 – EG solutions

The effect of ethylene glycol (EG) on copper ECP in phosphoric acid solutions was tested. Table 5-3 lists the compositions of the solutions used. Typical AFM image of copper disk surface after ECP in H_3PO_4 – EG solutions is shown in Fig. 5-5. The ECP data (controlled potential for ECP, measured current during ECP, roughness after ECP, and removal rate) are listed in Table 5-3. The data indicate that adding ethylene glycol in a mount of 5% ~ 25% does not affect the ECP efficiency of 70% phosphoric acid solution. However, adding ethylene glycol into phosphoric acid solution changed the limiting current, and thus changed the removal rate. The more EG was added, the more decrease of the limiting current and removal rate.

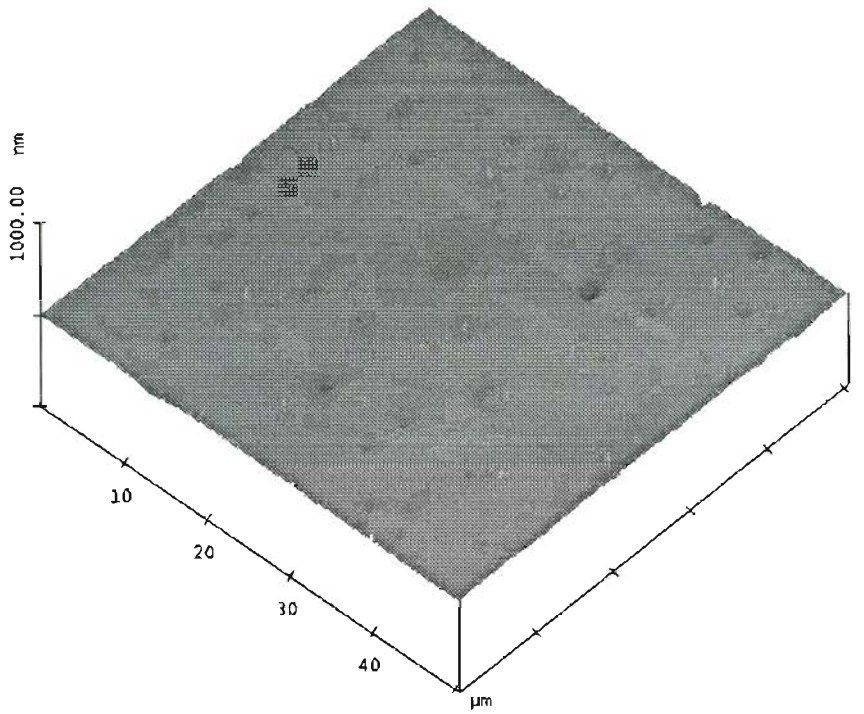

Figure 5-4 AFM image of copper disk surface after ECP in 100% phosphoric acid solution. R_a = 5 nm.

Table 5-3 Summary of ECP data with solutions of H_3PO_4 – EG

Solution (% vol.)	**Potential** (V)	**Current** (mA)	**Roughness** (nm)	**Removal Rate** (µm/min)
70 phosphoric acid	1.4	50	8	1.1
70 phosphoric acid + 5 EG	1.2	46	5	1.0
70 phosphoric acid + 15 EG	1.2	25	6	0.55
70 phosphoric acid + 20 EG	1.2	14	8	0.3

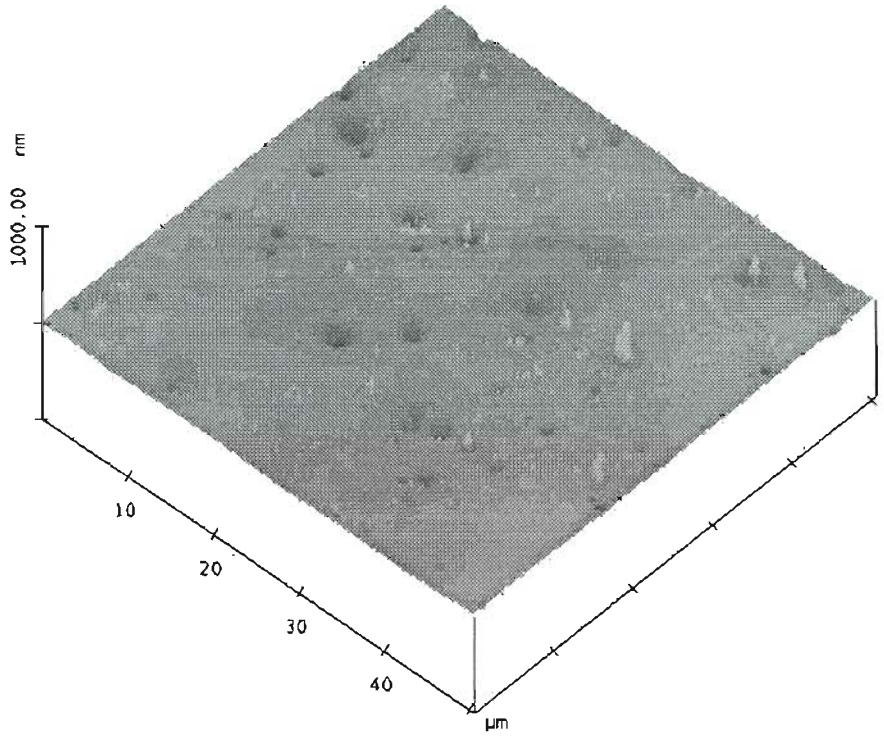

Figure 5-5 AFM image of copper disk surface after ECP in 70% phosphoric acid + 15% EG solution. R_a = 6 nm.

In Fig. 5-5 we can see some pits on the surface. They were caused by hydrogen bubbles. To verify this, an experiment with a different setup (illustrated in Fig. 5-6) was performed. In this experiment, two 2" × 2" copper plates were used as anode and cathode. They were placed vertically against the walls at the ends of a rectangular tank. In this way, the hydrogen bubbles produced on cathode mostly got out of the solution surface rather than reaching the anode surface when the inter-electrode distance is long. With this setup, a very shiny (R_a = 5 nm) surface was produced by ECP in 70% phosphoric acid + 5 EG solution, as shown in Fig. 5-7. From the AFM image we can see that the surface is smooth and there are no pits. Therefore, we conclude that the pits were caused by hydrogen bubbles, which could be seen during an ECP process, formed on the cathode. Some of the hydrogen bubbles passed through the filter on top of cathode, and reached the anode surface in a system shown in Fig. 5-2. A detailed discussion about how gas bubbles cause pits was presented in Chapter 3.

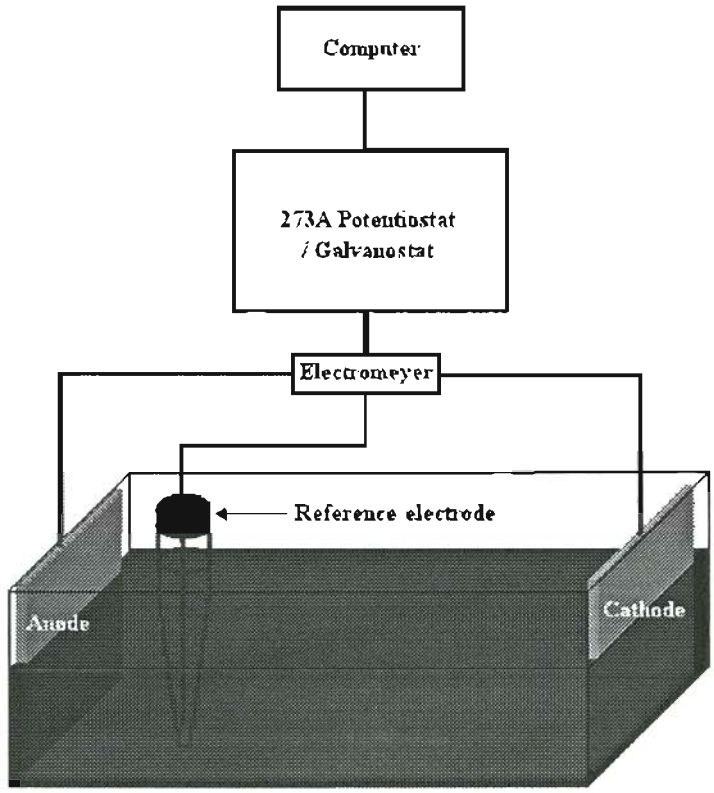

Figure 5-6 ECP system for reducing the influence of hydrogen bubbles on the anode surface.

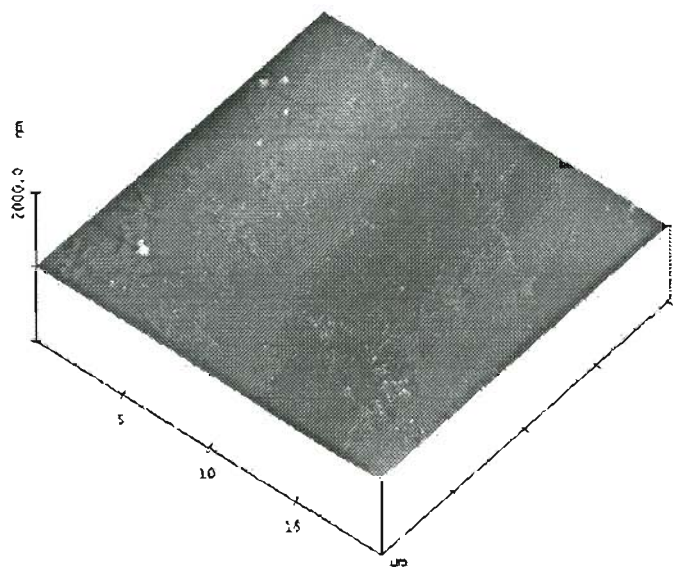

Figure 5-7 AFM image of copper plate surface after ECP with a system shown in Fig. 5-5 in 70% phosphoric acid + 5% EG solution. R_a = 5 nm.

5.2.1.3 ECP of copper disks in $H_3PO_4 - Na_5P_3O_{10}$ solutions

The influence of sodium tripolyphosphate ($Na_5P_3O_{10}$) on ECP of copper disks in phosphoric acid solutions was studied. Chemical composition of the electrolyte solutions and ECP data are listed in Table 5-4. A typical AFM image of the surface profile after ECP in H_3PO_4 – $Na_5P_3O_{10}$ solutions is shown in Fig. 5-8. It was shown that a small amount of sodium tripolyphosphate did not affect the ECP efficiency. When more sodium tripolyphosphate (e.g., > 0.25M) was added into phosphoric acid solution, ECP efficiency slightly decreased (i.e., roughness increases) and the removal rate also decreased.

Table 5-4 Summary of ECP data with solutions of $H_3PO_4 - Na_5P_3O_{10}$

Solution (% vol.)	**Potential** (V)	**Current** (mA)	**Roughness** (nm)	**Removal Rate** (μm/min)
70 phosphoric acid	1.4	50	8	1.1
70 phosphoric acid + 0.1M $Na_5P_3O_{10}$	1.45	45	7	1.0
70 phosphoric acid + 0.25M $Na_5P_3O_{10}$	1.2	40	17	0.9
70 phosphoric acid + 0.5M $Na_5P_3O_{10}$	1.1	32	16	0.7

5.2.1.4 ECP of copper disks in HEDP – H_3PO_4 solutions

The ECP effects of copper disks in HEDP and HEDP – H_3PO_4 solutions were investigated and listed in Table 5-5. A typical AFM image of copper disk surface after ECP in HEDP solution is shown in Fig. 5-9.

The experimental data indicate that certain ECP efficiency was achieved with HEDP solutions. Increasing HEDP concentration (larger than 40%) did not improve ECP efficiency. However, removal rate decreases with increasing HEDP in all concentration range.

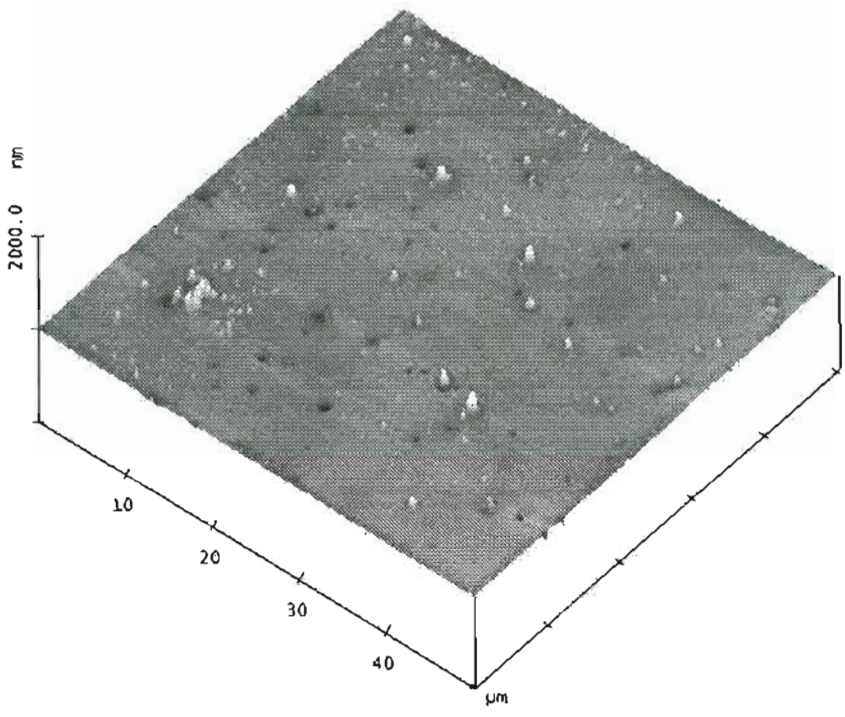

Figure 5-8 AFM image of copper disk surface after ECP in 70% phosphoric acid + 0.1M $Na_5P_3O_{10}$ solution. R_a = 7 nm.

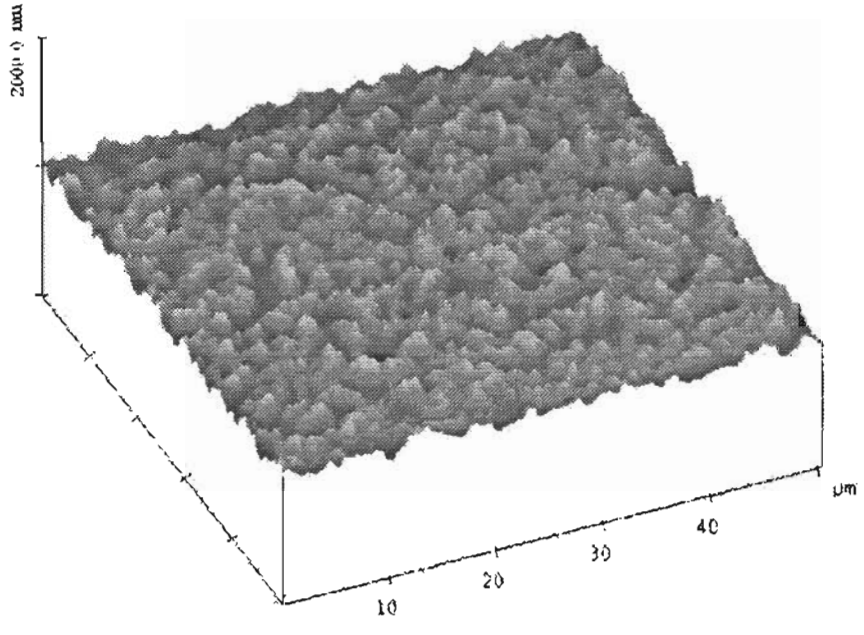

Figure 5-9 AFM image of copper disk surface after ECP in 30% HEDP + 30% H_3PO_4 solution. R_a = 57 nm

Table 5-5 Summary of ECP data with solutions of HEDP and HEDP – H_3PO_4

Solution (% vol.)	Potential (V)	Current (mA)	Roughness (nm)	Removal Rate (μm/min)
20 HEDP	1.45	86	243	2.1
40 HEDP	1.10	60	186	1.5
80 HEDP	0.90	14	190	0.3
70 HEDP + 10 H_3PO_4	0.90	14.5	162	0.3
30 HEDP + 10 H_3PO_4	1.20	120	132	3.0
30 HEDP + 20 H_3PO_4	1.20	115	76	2.5
30 HEDP + 30 H_3PO_4	1.10	82	57	1.8
20 HEDP + 20 H_3PO_4	1.40	167	134	3.7
10 HEDP + 30 H_3PO_4	1.40	150	67	3.5
0 HEDP + 30 H_3PO_4	1.75	180	29	4.6

Adding phosphoric acid into 30% HEDP solution improved ECP efficiency and decreased removal rate. The effects increased with increasing phosphoric acid concentration. Adding 10% HEDP into 30% phosphoric acid solution decreased the ECP efficiency and removal rate of the phosphoric acid solution.

All these suggest that the ECP efficiency of HEDP solutions was not as good as phosphoric acid solutions. And adding HEDP had a negative effect to the ECP efficiency in HEDP - phosphoric acid solutions.

However, further study showed that the salt film formed on the anode surface (refer to Chapter 4) was rough (See Fig. 4-24b) and not easy to be cleaned off. If the salt film or part of it was not thoroughly cleaned off, the surface would appear reddish. In this case, the measured roughness would be much higher than that of the copper surface under the film. Fig. 5-10 is an AFM image of copper surface after ECP in 70% HEDP solution followed by a surface clean procedure. The surface roughness is only 6 nm.

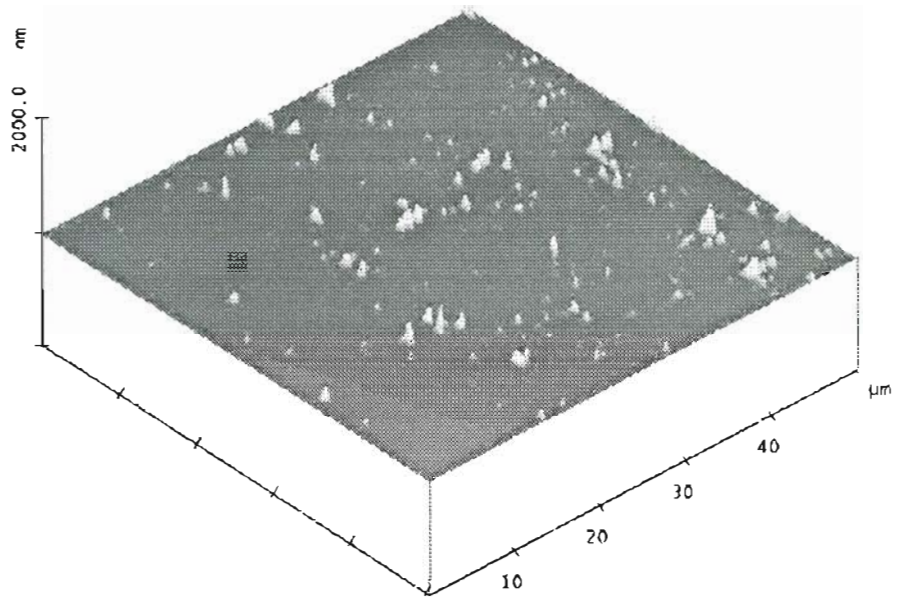

Figure 5-10 AFM image of copper disk surface after ECP in 70% HEDP solution and cleaned the surface layer. R_a = 6 nm.

5.2.1.5 ECP of copper disks in ethylene glycol – sodium chloride solutions

The ECP effects of copper disks in ethylene glycol (EG, $C_2H_6O_2$) – sodium chloride (NaCl) solutions were investigated and listed in Table 5-6. A typical AFM image of copper disk surface after ECP is shown in Fig. 5-11.

Table 5-6 ECP data of copper disk in solutions of EG – NaCl

Solution (% vol.)	**Potential** (V)	**Current** (mA)	**Roughness** (nm)	**Removal Rate** (μm/min)
50 EG + 1 M NaCl	3.25	20	91	0.44
20 EG + 1 M NaCl	3.25	27	83	0.6
20 EG + 2 M NaCl	3.25	50	63	1.1
30 EG + 2 M NaCl	3.75	50	79	1.1

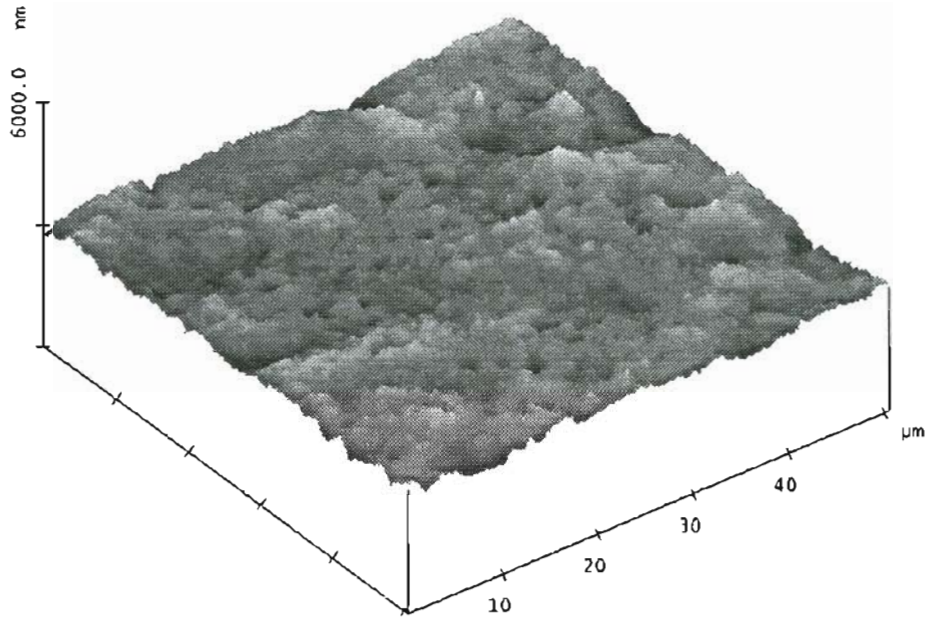

Figure 5-11 AFM image of copper disk surface after ECP in 50% EG + 1 M NaCl. R_a = 91 nm.

The data indicate that copper ECP efficiency was not significantly affected by changing the concentrations of EG and NaCl. Though copper removal rate was decreased by increasing EG concentration or decreasing NaCl concentration.

5.2.1.6 ECP of copper disks in H_2SO_4 – KNO_3 / $NaNO_3$ solutions

The ECP effects of copper disks in sulphuric acid (H_2SO_4) – potassium nitrate (KNO_3) and sulphuric acid (H_2SO_4) – sodium nitrate ($NaNO_3$) solutions were tested and listed in Table 5-7. A typical AFM image of copper disk surface after ECP is shown in Fig. 5-12.

The data in Table 5-7 indicate that ECP effect can be achieved with H_2SO_4 solution. But adding KNO_3 or $NaNO_3$ did not improve ECP efficiency. Instead, adding KNO_3 or $NaNO_3$ into H_2SO_4 solution largely reduced the ECP efficiency. This is probably because both SO_4^{++} and NO_3^- are strong chemical etchants of copper. Therefore, the chemical etching effect overwhelmed ECP effect and resulted in rough surfaces.

Table 5-7 ECP data of copper disk in solutions of HEDP and HEDP – H_3PO_4

Solution (% vol.)	**Potential** (V)	**Current** (mA)	**Roughness** (nm)	**Removal Rate** (μm/min)
20 H_2SO_4	2.5	70	72	1.54
20 H_2SO_4 + 1 M KNO_3	3.25	90	265	2
10 H_2SO_4 + 1 M KNO_3	2.0	230	283	5.1
20 H_2SO_4 + 1 M $NaNO_3$	3.0	80	279	1.75
20 H_2SO_4 + 2 M $NaNO_3$	3.5	70	276	1.53

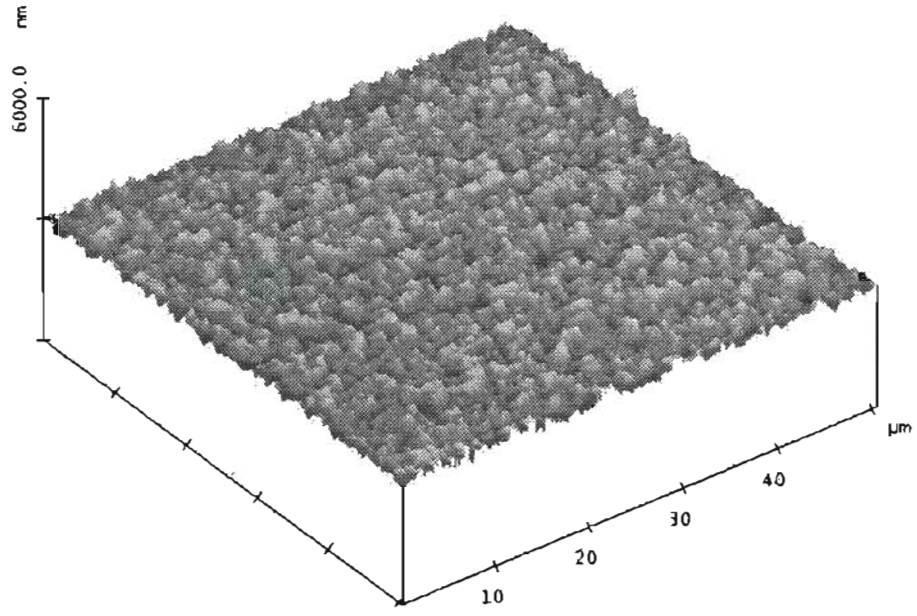

Figure 5-12 AFM image of copper disk surface after ECP in 20% H_2SO_4 solution. R_a = 72 nm.

5.2.1.7 Summary of copper disks ECP in various solutions

In summary, very good ECP efficiency of copper disks was achieved in solutions of phosphoric acid, HEDP, and phosphoric acid with additives copper oxide, ethylene glycol, and sodium tripolyphosphate. However, copper disk ECP efficiency in ethylene glycol - sodium chloride, sulfuric acid, sulfuric acid - sodium nitrate, and sulfuric acid - potassium nitrate solutions was not so good. The data of best ECP efficiency obtained from each electrolyte system are listed in Table 5-8.

Table 5-8 Summary of copper disk ECP data in various solutions.

Solution	Limiting Current i_L (mA)	Removal Rate R_d (μm /min)	Roughness Ra (nm)
1. 70~100 % phosphoric acid	12~50	0.26~1.10	4~9
2. 70 % phosphoric acid + 0.5 M CuO	45	0.99	5
3. 70 % phosphoric acid + 5 % ethylene glycol	46	1.01	5
4. 70 % HEDP	30	0.66	6
5. 70 % phosphoric acid + 0.1 M sodium tripolyphosphate	40	0.88	7
6. 30 % ethylene glycol + 2 M sodium chloride	50	1.10	63
7. 20 % sulfuric acid	70	1.54	72

Note: phosphoric acid = 85 % H_3PO_4.

5.2.2 ECP of copper film

The surface profile of copper film electroplated on deep trenched wafers is characterized as flat and shiny surface with bumps and pads (200 ~ 500 nm high), as shown in Fig. 5-13a. The bumps and pads are corresponding to trenches and vias in the silicon substrate, as shown in Fig. 5-13b. Compared to the surface profile of copper bulk materials (Fig. 5-3), the geometric change from flat area to the peaks of the bumps and pads is much gentler and smoother (Fig. 5-13c).

Among the electrolyte systems that can produce good ECP effect, phosphoric acid and HEDP solutions were chosen to study the ECP effect of copper film electroplated on deep trenched wafers. The choice was based on the knowledge from previous study:

(1) Good ECP effect of copper can be achieved in phosphoric acid (with or without additives) and HEDP solutions;

(2) Anodic layers formed during ECP process play a critical role to ECP effects; and

(3) The electrolyte solutions that can produce good ECP effects fall in two different groups:

a. HEDP solutions, which form salt film on copper anode surface during ECP;
b. Solutions of phosphoric acid and phosphoric acid with additives, which do not form films on copper anode surface during ECP.

Fig. 5-14 shows SEM (Scanning electron microscope) images of copper film – silicon cross-section after ECP in phosphoric acid and HEDP solutions respectively. A planar surface is obtained from ECP in HEDP solution, as shown in Fig. 5-14a. Nevertheless, the ECP result of wafer coupons with phosphoric acid was not as good. Bumps over dense structures were left behind after ECP. As shown in Fig 5-14b, the area over trenches still had 0.6 μm thick of Cu film left while the Cu film over the area without trenches or vias had been totally removed.

Why did the two solutions have different planarization effects on copper films electroplated on trenched silicon wafers while good ECP results for copper disks were obtained from both of the solutions? To explain this phenomenon, we need to have a thorough understanding of the ECP mechanisms.

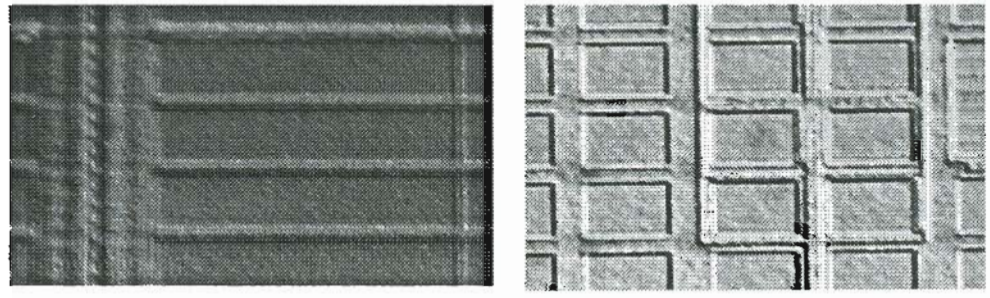

a

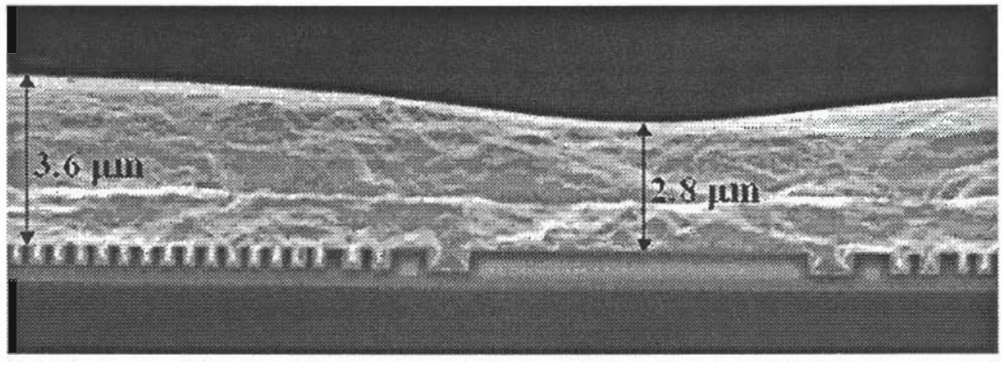

b

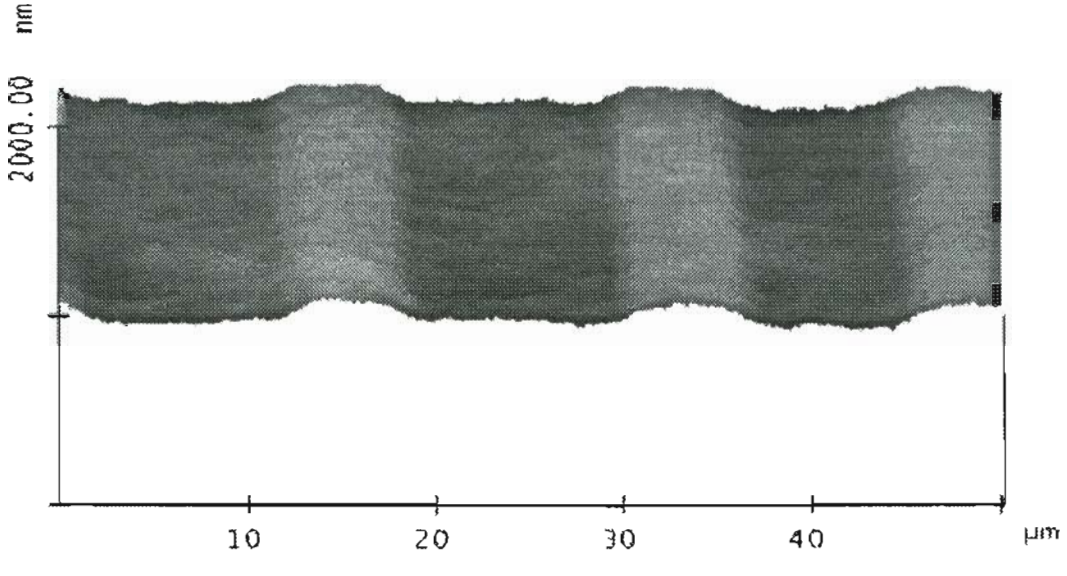

c

Figure 5-13 Surface profile of copper film plated on deep trenched Si wafer: (a) optical image ×50; (b) AFM image; and (c) SEM image of the cross section.

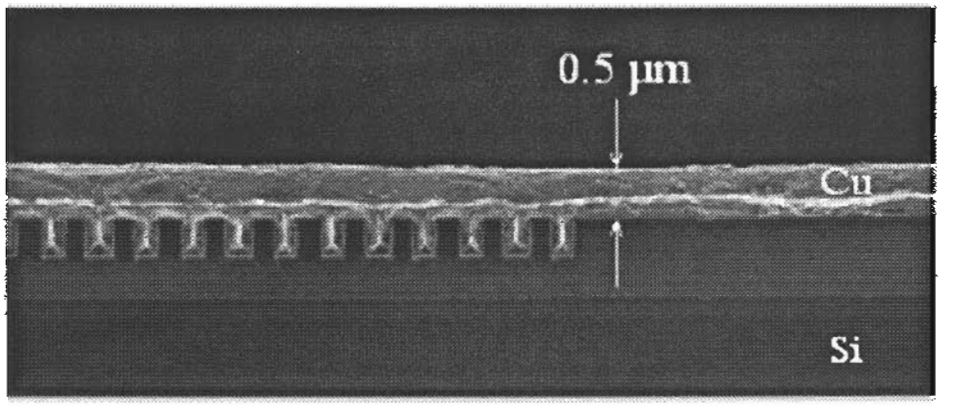

a

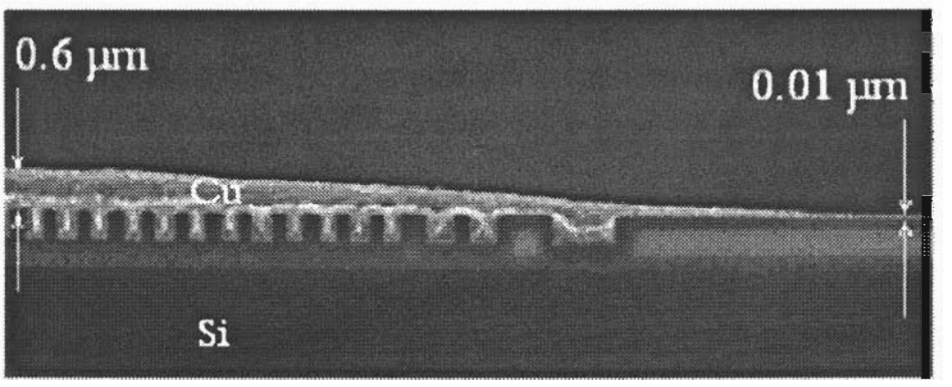

b

Figure 5-14 SEM images of copper film – silicon cross-section after ECP in HEDP (a) and phosphoric acid solutions (b).

5.3 Mechanisms of Electrochemical Polishing

5.3.1 Ohmic Leveling

As mentioned previously, leveling can be achieved under ohmic control or mass transport control. Under ohmic control, current density is determined by the electrolyte resistance (R_e) between the electrodes:

$$J = \frac{V}{R_e A} \qquad 5\text{-}2$$

where V (= V_1 - V_0) is the potential difference between anode and cathode. Since

$$R_e = \rho_e \frac{l}{A} \qquad 5\text{-}3$$

Eq. 5-2 may be rewritten as

$$J = \frac{V}{\rho_e l} \qquad 5\text{-}4$$

where ρ_e is the resistivity of the medium between the cathode and anode, and l is the distance between the electrodes. From Eq. 5-4 we can easily see that the current density (J_P) at protruding point P is higher than the current density (J_Q) at recessed point Q due to the difference ($2b = l_P - l_Q$) of inter electrode distance, as shown in Fig.5-15.

Surface removal rate (or dissolution rate, R_d, cm/s), from Eq. 2-28, may be expressed as

$$R_d = \frac{JM}{nFd} \qquad 5\text{-}5$$

where M is the atomic weight (63.5 g for Cu) and d is the density of the anode material (8.96 g/cm^3 for Cu), n (2 for Cu – 2e → Cu^{++} reaction) is the number of electrons transferred in the oxidation reaction of an anode atom, while F (= 96485 C) is Faraday constant. Substituting Eq. 5-4 into Eq. 5-5, results in

$$R_d = \frac{MV}{nFd\rho_e l} \qquad 5\text{-}6$$

For given electrode potential, anode material, and anodic dissolution reaction, $\frac{MV}{nFd} = f$ is a constant. Therefore, ohmic leveling efficiency, which is the difference of the removal rate between protruding point (P) and recessed point (Q), can be expressed as

$$\Delta R_d = R_d(P) - R_d(Q) = f\frac{2b}{\rho_e(l^2 - b^2)} \qquad 5\text{-}7$$

Equation 5-7 indicates that ohmic leveling efficiency depends on the surface profile and inter electrode distance. Larger surface roughness and closer electrodes (i.e., smaller l) may produce better leveling effect. In addition, smaller resistivity (ρ_e) of the electrolyte solution and higher voltage (V) between the electrodes also facilitate ohmic leveling.

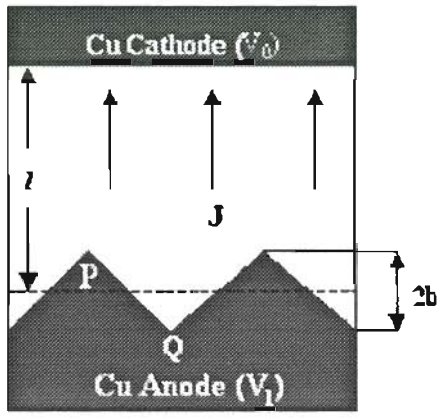

Figure 5-15 On a rough anode surface with uniform potential (V_1), peaks have higher current density due to different inter electrode distance: $l_P > l_Q$.

Assuming ρ_c = 10 Ω-cm [9], 2b = 0.5 μm, l = 20 cm, and V = 2V, we calculated $\Delta R_d = 9.18 \times 10^{-9}$ μm/s, which is negligible compared to the average removal rate $R_d = 4.4 \times 10^{-3}$ μm/s at limiting current i_L = 12 mA for concentrated phosphoric acid (i.e., 85% H_3PO_4) solution. This indicates that the ohmic leveling effect could be negligible under normal wafer ECP conditions.

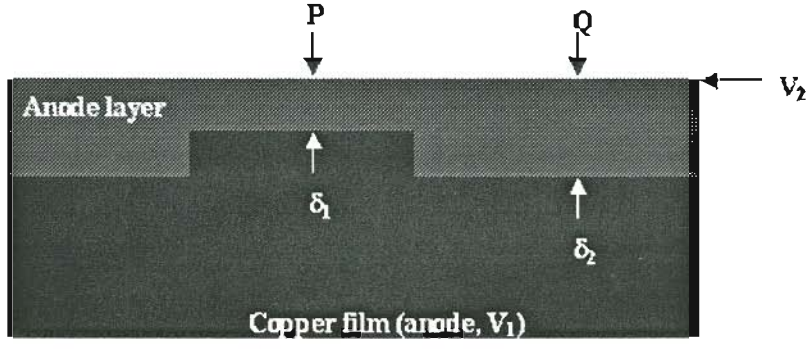

Figure 5-16 Salt film formed on anode surface facilitates surface smoothing due to ion migration and / or ohmic smoothing effect.

Nevertheless, the ohmic leveling effect can be noticeable under certain hydrodynamic conditions, if an electrically resistive and non-conformal anode layer forms on the anode surface (See Fig. 5-16). A non-conformal (also called "macro profile")

anode layer means that the anodic layer-solution interface is flat instead of taking the anode surface profile). In this case, the current density is determined by the anodic layer, since the process is mass transport controlled. Thus, from Eqs. 5-6 and 5-7 we obtain

$$\Delta R_d = R_d(P) - R_d(Q) = f\frac{\delta_2 - \delta_1}{\rho_f \delta_1 \delta_2} \qquad 5\text{-}8$$

where ρ_f is the electrical resistivity of the anode layer, δ_1 and δ_2 are the thickness of the anode layer at point P and Q, respectively (See Fig. 5-16). Assuming $\delta_2 = 0.5$ μm, $\delta_1 = 0.25$ μm, $\rho_f = 2 \times 10^4$ Ω-cm (estimated from the EIS measurement, in the case of 70% HEDP solution), and $V = V_2 - V_1 = 0.2$V (voltage across the anode layer), we calculated $\Delta R_d \approx 0.07$ μm/s, according to Eq. (16). In comparison, the average removal rate $R_d \approx 0.01$ μm/s at limiting current $i_L = 30$ mA for 70% HEDP solution. In other words, the removal rate at protruding point (P) is about seven times higher than the average removal rate on the flat area due to ohmic leveling effect.

From Eq. 5-18 we can see that ohmic leveling effect can be enhanced by increasing the overall thickness of the anode layer and lowering its resistivity. Better ohmic leveling effect can also be obtained at higher anode potential in the range of limiting current plateau, due to higher f value in Eq. 5-8.

5.3.2 Migration Smoothing

Another geometrical-dependent leveling mechanism results from migration, which is due to the electric field distribution on a rough surface. It is known that an arbitrary two-dimensional surface profile can be described by a Fourier sine series where the individual Fourier coefficients behave independently [3]. We therefore calculated the electric field distribution along a sinusoidal surface. A sine waveform is located at the center of the anode surface in a 2D electrochemical cell, which has parameters close to an actual 300 mm wafer polishing system (See Fig. 5-17). This simulation was performed using a boundary element simulation software. The simulation data (See Fig. 5-18a) indicates that the amplitude of normal electric field (**En**) varies along the sinusoidal surface, similar to the shape of the surface profile except at the origin and end points of the sine waveform where a sharp geometrical change occurs. For certain amplitude (b) of the sine wave, the difference of the normal electric field E_n(P) at the peak point P and

$E_n(Q)$ at the recessed point Q increases as the wavelength (T) decreases (i.e., the frequency f increases), as indicated in Fig. 5-18b. The orientation of the normal electric field depends on the location too. At peaks and valleys, (points P and Q), $\mathbf{E}_n$ points perpendicular to the cathode, and deviates from this direction at other locations.

Once a copper atom is oxidized to Cu^{++} on the anode surface, a force

$$\mathbf{F}_E = q\,\mathbf{E} \qquad 5\text{-}9$$

acts on the Cu^{++} resulting from the electric field $\mathbf{E}_n$. As a result, Cu^{++} ions tend to move away from the anode surface towards cathode under force

$$\mathbf{F} = \mathbf{F}_E - \mathbf{F}_r = q\,\mathbf{E} - \mathbf{F}_r \qquad 5\text{-}10$$

where q is the charge of Cu^{++} and $\mathbf{F}_r$ is the resistive force as Cu^{++} ions move through the anode film and the solution. According to Newton's second law of motion, the Cu^{++} ions accelerate at $\mathbf{a} = \mathbf{F} / m$, and therefore migrate a distance

$$s = \frac{1}{2}at^2 \qquad 5\text{-}11$$

in time t. From the above three equations, one can estimate the velocity of Cu^{++} migration

$$v = \frac{s}{t} = \frac{1}{2m}(qE_n - F_r)t \qquad 5\text{-}12$$

where m is the mass of Cu^{++}.

In bulk solution F_E is negligible compared to the convection force (F_c) when a forced convection is applied. Nevertheless, inside anodic layers, it may play an important role. The anodic layers may be a solid film and / or a boundary layer with concentration gradient of cations or acceptors, as discussed in the previous chapters.

The magnitude and orientation distribution of the electric field $\mathbf{E}_n$ along the surface favors the diffusion of Cu^{++} at the peak areas where E_n has the highest value $E_n(P)$ and points towards the cathode. Therefore, Cu^{++} at peak area has the highest migration speed according to Eq.5-12. In contrast, Cu^{++} in the valley has the slowest migration speed. Consequently, a leveling effect can be achieved.

Since surface removal rate R_d is proportional to v, i.e., $R_d = \alpha\, v$ (where α is a constant), the difference of the removal rate between protruding point (P) and recessed point (Q) can be expressed as

$$\Delta R_d = R_d(P) - R_d(Q) = \alpha(v_P - v_Q) \qquad 5\text{-}13$$

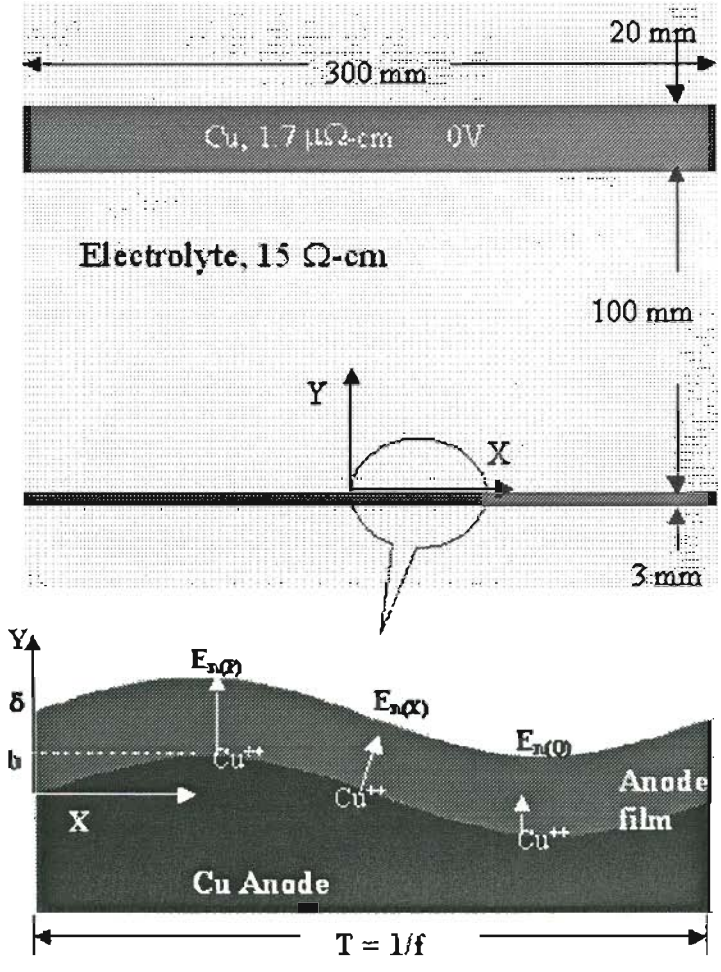

Figure 5-17 Schematic of an electropolishing cell and the local surface profile of the anode. The electric field (E) varies in amplitude and orientation along the sinusoidal surface.

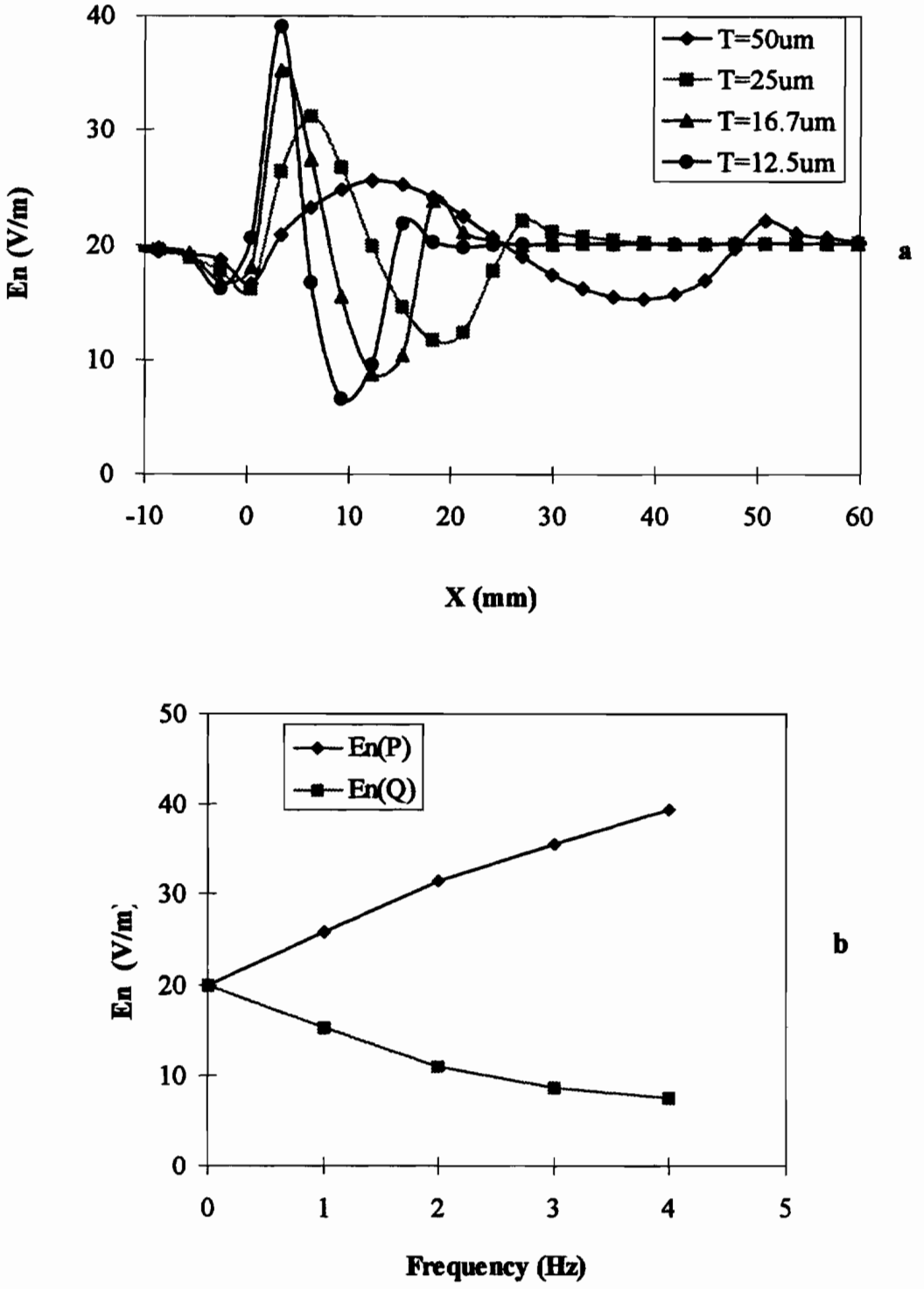

Figure 5-18 The amplitude of normal electric field along the sinusoidal anode surface, obtained by simulation (a); Amplitude of normal electric field at the peak and valley of the sinusoidal surface, versus the frequency of the sine wave (b).

Hence, the migration smoothing effect may be obtained from Eqs.5-12 and 5-13:

$$\Delta R_d = \frac{\alpha q}{2m}[E_n(P) - E_n(Q)]t \qquad 5\text{-}14$$

From Eq.5-14 and Fig. 5-18b we may conclude that ECP, due to ion migration mechanism, removes shorter waves faster than longer waves.

5.3.3 Diffusion Smoothing

Diffusion smoothing is the ECP effect due to diffusion, driven by the concentration gradient. Wagner [10] calculated the dissolution speed of copper according to diffusion law (Fick's second law), under mass transport control and acceptor mechanism condition. In this case, the concentration distribution of the acceptor has a profile as shown in Fig. 5-19. In the figure, C_b is the bulk concentration of the acceptor. δ_c is the thickness of the diffusion layer.

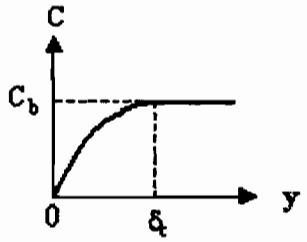

Figure 5-19 Acceptor concentration as a function of distance from the electrode.

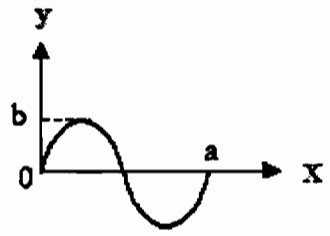

Figure 5-20 Anode surface profile.

Assume the anode surface (in 2D) has a sinusoidal profile, as shown in Fig. 5-20. The surface profile can be expressed as

$$y = b\sin(\frac{2\pi}{a}x) \qquad 5\text{-}15$$

where y is the distance from the average surface plane, a and b are respectively the wavelength and amplitude of the sine wave. In condition of a and b are much smaller than δ_c, Fick's second law applies to the anode surface and adjacent area. At steady-state conditions, there is

$$\frac{\partial c}{\partial t} = D(\frac{\partial^2 C}{\partial x^2} + \frac{\partial^2 C}{\partial y^2}) = 0 \qquad 5\text{-}16$$

with boundary conditions in Figs. 5-19 and 5-20 and assumption b << a, a<< δ_c, an approximated solution of Eq. 5-16 can be obtained [10]

$$(\frac{\partial C}{\partial y})_{y=b\sin(\frac{2\pi}{a}x)} = B[1 + 2\pi\frac{b}{a}\sin(\frac{2\pi}{a}x)] \qquad 5\text{-}17$$

where B = $(\frac{\partial C}{\partial y})_{avg}$ is the average value of concentration gradient at the anode surface.

Since the dissolution rate (R_d) due to diffusion is proportional to the concentration gradient of the acceptor, it can be deduced from Eq. 5-17 that [10]

$$R_d = C(2\pi\frac{b}{a})\sin(\frac{2\pi}{a}x) \qquad 5\text{-}18$$

Comparing Eqs.5-15 and 5-18, we can see that the dissolution rate versus location x has the same shape as the geometric profile of the anode surface. That is, R_d at the peak is greater than that at the valley of the anode surface. Eq. 5-18 also suggests that R_d increases with decreasing wavelength a. In other words, "microroughness" will disappear more rapidly than "macroroughness". Therefore, ECP due to diffusion dissolution mechanism approaches a sine wave profile involving the greatest wavelength of the original pattern. This effect is same as that of migration smoothing. The situation can be improved if the diffusion layer has a macro profile. In this case, the diffusion distance (of the mass transport limiting species) at peak points is shorter than that at the valley points (See Fig. 5-16).

Although the above deduction assumed b << a, a<< δ_c, the conditions are applicable to the situation of copper film electroplated on trenched silicon wafer where surface undulation is gentle (b<<a). The feature dimensions are also smaller compared to the thickness of the diffusion layer (refer to Chapter 4).

5.4 Interpretation of the Experimental Results

From the above discussion, it can be seen that sharper geometrical profiles have better ECP efficiency due to migration and migration smoothing mechanisms. This explains why very good ECP efficiency was obtained from several solutions with copper disks, which have sharp surface profiles (See Fig.5-3). Yet ECP efficiency is largely reduced in case of gentle surface profiles, such as the surface features of EP copper films on a patterned silicon wafer, as shown in Fig. 5-13. On the surface of EP copper films, large pads and wide stripes were about 0.2 ~ 0.5 μm higher than the flat areas and had gentle geometrical changes, especially after a period of ECP process. Therefore, due to gentle surface undulation, and/or due to lack of ion migration mechanism (e.g., water molecules instead of Cu ions as the mass transport control species), the dissolution rates at protruding and at recess areas were not very different in phosphoric acid. Therefore, the original surface profile was changed little, as shown in Fig. 5-14b.

However, the situation improved when an electrically resistive salt film with macro profile formed on the anode surface, as shown in Fig. 5-16. In this case, a good ECP efficiency can be achieved by ohmic leveling mechanism, as discussed above. In addition, due to the existence of a potential difference across the film, migration smoothing mechanism works as well. Because the thickness of the anodic layer varies with location, the migration distance of Cu^{++} at point P, where anode layer is thinner (δ_1), is shorter than that at the point Q, where anode layer is thicker (δ_2), although the ion migration velocity at peak (P) and valley (Q) points are not much different due to the gentle geometric change. Therefore, the removal rate at protruding areas is higher than recessed parts due to ion migration mechanism and ohmic leveling effect in the salt film layer, even though the surface has a gentle geometric profile. This explains why good planarization effect was obtained on copper films plated on trenched wafers in HEDP solution, as shown in Fig. 5-14a.

5.5 Optimal Conditions for ECP of Copper Film Electroplated on Trenched Silicon Wafer

5.5.1. Limiting current

Chronoamperometric curve (Fig. 5-1), i ~ t curve under potential control, indicates that a transition time exists at the beginning of an ECP process. The transition time is about 50 ~ 100 seconds. At the beginning of an ECP process, anode surface is clean. So the anodic dissolution can process at a very high speed, which is demonstrated by high current. From Fig. 5-1, we can see that the initial current measured is several times higher than the limiting current. As an anodic layer gradually forms, the process gradually reaches to mass transport control and thus the measured current continually decreases until reaches the stable value – limiting current (steady-state).

Apparently, a layer of copper dissolved during the transition time. Yet ECP can be achieved only in condition of mass transport control, i.e., after the transition time. For ECP of copper bulk material, to remove a micron thick layer or more is usually not a problem. But for ECP of copper films electroplated on silicon wafers, the thickness of copper film is limited and usually the extra layer to be removed is about 1 μm thick or so. In this case, suppose the transition time is 50s, the average current during transition time is twice the limiting current, and a layer of copper at least 0.5 μm thick (since the height of bumps and pads is about 0.2 ~ 0.5 μm) should be left for steady-state (after transition time) ECP. According to Eq.2-28, we can calculate that the limiting current should be no more that 13.5 mA. Of course, the productivity would be too low if the current is too low. For ECP of copper films electroplated on silicon wafers, a feasible current is therefore about 10 mA. To ensure ECP effect, thicker copper films and thus longer time in steady-state will be helpful.

5.5.2. Mass transport control and ECP potential

In order to achieve ECP effect, the potential has to be controlled such that the process is mass transport controlled. The presence of a current plateau with an anodic film on the surface is not a sufficient criterion for microsmoothing [3]. For example, transpassive nickel dissolution in sulfuric acid yields well-defined current plateaus but only in a certain concentration and temperature range are they mass transport controlled

[3, 11]. Levich plot can be used to verify the process is transport controlled, as discussed in Chapter 3.

In conditions of mass transport control, higher potential may produce better ECP effect. This is due to better ohmic leveling effect at higher anode potential, according to Eq.5-8.

5.5.3. Electrolyte solution

Electrolytes and their concentrations in an ECP solution determine the values of limiting current and potential range of the limiting current plateau, mass transport limiting species, anodic layers, and other physical and chemical properties of the solution such as viscosity, diffusion coefficient. All these have a direct influence on ECP effects. An ideal electrolyte solution should have:

(1) A flat and level limiting current plateau with wide potential range and current value feasible for the application (e.g., around 10 mA for EP copper films on silicon wafers);

(2) An electrically resistive salt film forms on anode surface under ECP conditions; the diffusion layer and/or the salt film has a macro profile; and

(3) Ionic mass transport limiting species, which can have migration smoothing effect.

5.5.4. Solution circulation

Solution circulation is usually performed with a pump and / or the anode disk rotating. A good circulation should produce:

(1) Uniform ECP effects over a large area of anode surface; and

(2) A macro profile of the diffusion layer and the salt film on anode surface during ECP.

Factors to be controlled include the speed, paths, and directions of the circulation.

5.5.5. Inter-electrode distance

From Eq. 5-7 we can see that ohmic leveling effect can be increased by decreasing inter electrode distance (l). For example, deceasing l from 20cm to 0.1 cm, the

ohmic leveling effect increases more than 40,000 times (from 9.18×10^{-9} μm/s to 3.67×10^{-4} μm/s). However, it is hard to control and the solution circulation will be poor if the inter electrode distance is too small. Also gas bubbles would reach anode surface easily if the inter electrode distance is too small. However, it could be beneficial to perform ECP with extreme close inter electrodes at the beginning to even out the bumps and pads.

5.5.6. Preventing gas bubbles reaching anode surface

As pointed previously, if the hydrogen bubbles reach the anode surface, they may produce pits or particles on the surface. It is challenging to prevent gas bubbles from reaching the anode surface. A filter between anode and cathode may resist gas bubbles from reaching the anode surface. The finer porosity of the filter, the better filtering effect. But it also resists solution circulation. An electrochemical cell with vertical electrodes and filter close to anode, as shown in Fig.5-21, favors resisting hydrogen bubbles from reaching the anode surface. Placing filter close to anode has two benefits. First, larger surface area of solution allows hydrogen bubbles to get out of the solution. Secondly, hydrogen bubbles become larger when they reach the filter. So filter with larger hole size can be used, which allows better solution circulation.

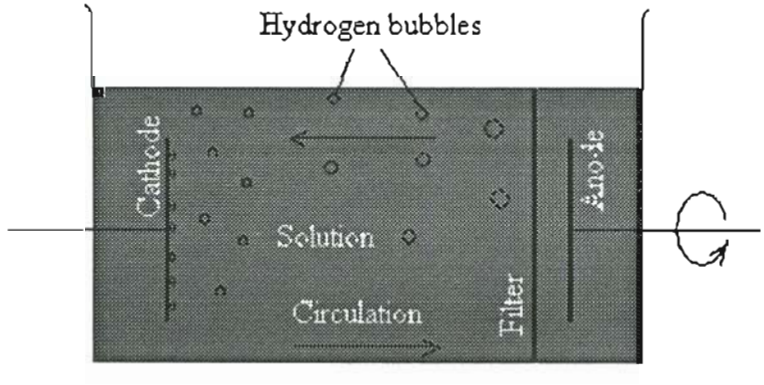

Figure5-21 A design of electrochemical cell preventing hydrogen bubbles from reaching anode surface.

5.5.7. Temperature

Temperature is not involved in this work. Processing at higher or lower than room temperature means increasing facility cost. However, temperature can affect many factors of ECP process. These factors include charge transfer, diffusion coefficient, and viscosities of solution and anode layer. Therefore, one should be aware that temperature is an experimental variable and can possibly be used to manipulate factors such as limiting current plateau, and anode layer structure when needed.

5.6 Summary and Conclusions

Very good electropolishing results (surface mean roughness $R_a < 10$ nm) of bulk copper were obtained in solutions of phosphoric acid, HEDP and phosphoric acid with additives copper oxide, ethylene glycol, and sodium tripolyphosphate. But electropolishing of electroplated copper films on patterned silicon wafers showed different results. Gently protruding areas were not planarized by an ECP process with phosphoric acid while a good planarization was obtained in HEDP solutions, where salt films formed on the anode surface. A salt film with macro profile on the anode may benefit from ohmic leveling, migration smoothing, and migration smoothing effects.

If the surface layer has a micro profile, the ECP effect depends on the sharpness of the surface undulation. Therefore, the surface profile of the anode layer is crucial to ECP of copper films electroplated on patterned silicon wafers. The surface profile of anode layer depends on the viscosity of the layer and the convection strength of the electrolyte solution.

Ideal conditions for ECP of copper films electroplated on patterned silicon wafers are:

(1) Relatively low limiting current (e.g., 10 mA);

(2) Wide potential range of limiting current plateau;

(3) An electrically resistive salt film forms on anode surface during ECP, the surface profile of the film or diffusion layer is non-conformal to the surface profile of the copper film to be planarized;

(4) Good circulation of the electrolyte solution to ensure uniform ECP over large area of anode surface;

(5) Certain design of the ECP cell to prevent hydrogen bubbles from reaching anode surface;

(6) Extremely close inter electrode distance facilitates ohmic leveling effect. However, this also makes hydrogen bubbles reach anode surface easier.

These conditions depend on electrolytes and their concentration, as well as temperature. Further research is expected to explore more ideal electrolytes and corresponding optimal ECP conditions.

References

1. R. Soutebin and D. Landolt, Anodic Leveling under Secondary and Tertiary Current Distribution Conditions, *J. Electrochem. Soc.*, **129**(1982), 946-953.
2. R. Soutebin H. Froidevaux, and D. Landolt, Theoretical and Experimental Modeling of Surface Leveling in ECM under Primary Current Distribution Conditions, *J. Electrochem. Soc.*, **127**(1982), 1096-1100.
3. D. Landolt, Review Article Fundamental aspects of Electropolishing, *Electrochim. Acta*, **32**(1987), 1 – 11.
4. H. Abrams and C. L. Mantell, Electrolytic Polishing of Copper and Nickel Silver, *Electrochem. Tech.*, **5**(1967), 287-292.
5. M. Matlosz, S. Magaino, and D. Landolt, Impedance Analysis of a Model Mechanism for Acceptor-Limited Electropolishing, *J. Electrochem. Soc.*, **141**(1994), 410-418.
6. J. Huo, R. Solanki, J. McAndrew, Study of anodic layers and their effects on electropolishing of bulk and electroplated films of copper, *J. Appl. Electrochem.*, to be published.
7. S.-C. Chang, J.-M. Shieh, C.-C. Huang, B.-T. Dai and M.-S. Feng, Pattern Effects on Planarization Efficiency of Cu Electropolishing, *Jpn. J. Appl. Phys.*, **41** (2002), 7332–7337.
8. J. Huo, R. Solanki and J. McAndrew, Electrochemical Polishing of Copper for Microelectronic Applications, *Surf. Eng.*, **19** (2003), 11-16.
9. K. Dianatkhah, 'Passivation Behavior of Copper Thin Films for Electrochemical Planarization Application', MS thesis, (Oregon Graduate Institute of Science and Technology, Beaverton, Oregon, 1999).
10. C. Wagner, Contribution to the Theory of Electropolishing, *J. Electrochem. Soc.*, **101**(1954), 225-228.
11. I.L. Alanis and D.J. Schiffrin, The Influence of Mass Transfer on the Mechanism of Electropolishing of Nickel in Aqueous Sulphuric Acid, *Electrochim. Acta*, **27**, (1982), 837-845.

Chapter 6

Conclusions and Future Directions

6.1 Summary and Conclusions

This investigation has shown that electrochemical polishing (ECP) can be achieved under mass transport controlled conditions. Factors determining and affecting mass transport processes and ECP effects include: electrolytes and their concentrations, anode surface profiles, anode rotating speed, solution circulation, interelectrode distance, temperature, applied potential (and thus current density), as well as the configuration of the ECP system.

Mass transport control is characterized as a limiting current plateau on an anodic polarization curve and can be further confirmed by steady-state data (Levich plot). Copper anodic polarization curves were measured with nine electrolyte systems. Limiting current plateaus were demonstrated in these solutions with limiting current (i_L) and potential range (E_L) of the plateaus, listed in Table 6-1.

Table 6-1 Summary of copper anodic polarization data

No.	Electrolyte System	i_L (mA)	E_L (V)
1	11~85 % H_3PO_4	31 ~ 284	0.7~1.7
2	20~85 % H_3PO_4 + 0.5~2 M CuO	9 ~ 206	0.8~1.7
3	11~64 % H_3PO_4 + 13~75 % $C_2H_6O_2$	10 ~ 77	1.1~1.8
4	8.5~76.5 % H_3PO_4 + 0.1~0.5 M $Na_5P_3O_{10}$	16 ~ 90	0.6~1.6
5	1.5~60 % $C_2H_8O_7P_2$	6 ~ 81	0.5~1.4
6	0~54 % $C_2H_8O_7P_2$ + 8.5~25.5 % H_3PO_4	8 ~ 217	0.5~1.4
7	10~50 % $C_2H_6O_2$ + 1~4 M NaCl	20 ~ 131	2.0~4.0
8	1~20 % H_2SO_4 + 0.5~2.5 M $NaNO_3$	63 ~ 175	2.0~4.0
9	1~20 % H_2SO_4 + 0.5~2.5 M KNO_3	69 ~ 422	1.6~3.0

Electrochemical impedance spectroscopy (EIS) was successfully used to identify copper anodic salt film and mass transport limiting species in solutions of H_3PO_4, H_3PO_4 + CuO, $H_3PO_4 + C_2H_6O_2$, $H_3PO_4 + H_5Na_5O_{10}P_3$, and HEDP. The measured EIS spectra and SEM observation indicated that a resistive salt film formed on the copper anode surface in HEDP solution whereas no salt film was detected in the other solutions. Analysis of the EIS data suggested that Cu^{++} was the mass transport controlling species in solutions of HEDP and phosphoric acid with additives ethylene glycol and sodium tripolyphosphate. Non-ionic species such as water molecules are suggested to be the mass transport controlling species in solutions of phosphoric acid and phosphoric acid with copper oxide.

Very good electropolishing results (surface mean roughness $R_a < 10$ nm) of bulk copper were obtained in solutions of phosphoric acid, HEDP and phosphoric acid with additives copper oxide, ethylene glycol, and sodium tripolyphosphate. But electrochemical planarization of copper films electroplated on patterned silicon wafers is more difficult. An ECP process with phosphoric acid did not planarize gently protruding areas on silicon wafer. A good planarization effect on electroplated copper films on patterned silicon wafer coupons was obtained in HEDP solutions.

Three types of ECP mechanisms were distinguished:

(1) **Ohmic leveling** describes the ECP effect that depends on the current density distribution on a rough anode surface. Ohmic leveling can be enhanced by an electrically resistive anode layer with a surface of macro profile and short interelectrode distance.

(2) **Migration smoothing** describes the ECP effect resulting from a non-uniform distribution of normal electric field along a rough surface.

(3) **Diffusion smoothing** effect results from a non-uniform concentration gradient distribution of mass transport limiting species along a rough surface.

Migration smoothing and diffusion smoothing effects strongly depend on anode surface profile. A surface profile that involves shorter wavelength has better migration smoothing and diffusion smoothing effects. And therefore is easier to be planarized than a surface profile that involves longer wavelength.

The surface of copper films electroplated on trenched silicon wafers consists of gentle bumps and pads on flat areas. The surface profiles involve much longer wavelength, compared to mechanically polished bulk copper surface, and therefore are more difficult to be planarized. To obtain the best ECP effects for copper films electroplated on patterned silicon wafers, one needs to use:

(1) Electrolyte solution that has:
   (i) Relatively low limiting current (e.g., 10 mA),
   (ii) Wide potential range of limiting current plateau,
   (iii) An electrically resistive salt film forms on anode surface during ECP. The surface profile of the film or diffusion layer is non-conformal to the surface profile of the copper film to be planarized.

(2) Higher applied potential in the range of limiting current plateau.

(3) Optimal anode rotating speed and solution circulation to ensure uniform ECP over large area of anode surface;

(4) Optimal ECP system design to prevent hydrogen bubbles from reaching anode surface;

(5) Extremely close inter electrode distance facilitates ohmic planarization effect.

(6) Other parameters such as temperature may be taken into account as well.

6.2 Recommendations for Future Work

Based on the experimental results and knowledge obtained through this study, following research is recommended for future work.

(1) Study of the correlation between the surface profile of anodic layer / film and the hydrodynamic conditions in an ECP system. This may lead to identification of the optimal conditions for the formation of a macro surface profile of anodic layer / film, which is very important to the ECP of copper films electroplated on patterned silicon wafers.

(2) Investigation of new electrolyte solutions that can form easy-cleaning and electrically resistive copper complexes, which facilitate ohmic leveling and migration smoothing effects.

(3) Investigation of the factors that affect the uniformity of ECP over a large surface area, for example, a 300mm wafer. These factors include solution viscosity, anode rotating speed, solution flow rate, the design of ECP cell, and others.

(4) End point, the moment that ECP process should be stopped, is another challenging issue need to be found out.

(5) Between copper film and ILD layers are tantalum and tantalum nitride barrier layers. These thin layers (about 20nm thick) need to be cleaned too. It is necessary to find out the anodic behavior of these materials under copper ECP conditions. Electrolytes and ECP conditions that can remove these layers are needed. Further, how such electrolytes and ECP conditions affect the copper surface smoothness is important to know.

BIOGRAPHICAL SKETCH

Mr. Jinshan Huo was born in Sichuan, P. R. China in March 1962. He studied in the Department of Metallurgy and Materials Engineering at Chongqing University, Chongqing, China during 1979~1983 and 1985~1988, from which he received Bachelor and Master degrees respectively.

Mr. Huo worked at Shanxi Heavy Vehicle Plant, Shanxi, P. R. China during 1983~1985. Performed materials / failure analysis and wrote technical reports.

He then worked as an instructor (1988~1995) and associate professor (1995~1997) at Sichuan Institute of Technology (now Xihua University), Chengdu, P. R. China. He taught courses such as X-ray Crystallography, Electron Microscopy, Physical Properties of Metal Materials, and Microcontroller System Design. His research work involved materials structure-property relation, metal heat treatment and control. He co-invented Non-Contact Thermal Uniformity Detector. He was honored as Sichuan Province Outstanding Young Teacher by Sichuan Province Education Committee in 1995. He received several awards from the school, government agencies and academic association.

Mr. Huo came to the United States and enrolled in the PhD program of Materials Science and Engineering at Oregon Graduate Institute of Science and Technology in the fall of 1997. He received Master's degree and transferred to the Department of Electrical and Computer engineering in 1999 while the Department of Materials Science and Engineering was being shut down. Since 1997, Mr. Huo has done researches including failure analysis and mechanical tests of metal materials, characterization of biomaterials and biosensor, characterization of thin films and nanowires of electronic materials, copper thin film electrodeposition and electropolishing for microelectronic applications.

Mr. Huo worked as an Intel-University Project Contractor at Intel during 2001~2002. He did thin film characterization and electrochemical deposition of copper alloys onto silicon substrate. In recent two years he has filed two patents and published several papers on copper interconnect technology.

Selected Publications and Patent

- J. Huo, R. Solanki, and J. McAndrew, A Novel Design of Electrochemical Planarization System, USPTO, submitted.

• J. Huo, R. Solanki, and J. McAndrew, Methods of Planarizing Copper Electroplated Silicon Wafers, USPTO, submitted.

• J. Huo, R. Solanki, and J. McAndrew, Electrochemical Polishing of Patterned Copper Films, 2004 IEEE International Interconnect Technology Conference, June 7 - 9, 2004, San Francisco, California, USA.

• J. Huo, R. Solanki, and J. McAndrew, Study of anodic layers and their effects on electropolishing of bulk and electroplated films of copper, Journal of Applied Electrochemistry, to be published.

• J. Huo, R. Solanki, and J. McAndrew, Electrochemical Planarization of Patterned Copper Films for Microelectronic Applications, 2nd Surface Engineering Congress & Exposition, 15-17 September 2003, Indianapolis, Indiana, USA.

• J. Huo, R. Solanki, and J. McAndrew, Electrochemical Polishing of Copper for Microelectronic Applications, Surface Engineering, vol.19, no.1, 11-16, 2003.

• R. Solanki, J. Huo, J.L. Freeouf and B. Miner, Atomic Layer Deposition of ZnSe/CdSe Superlattice Nanowires, Applied Physics Letters, vol. 81, no. 20, 3864-3866, 2002.

• J. Huo, G. M. Kloster, R. Solanki, and S. Hearne, Electrochemical Deposition of Cu-Ni-W Alloys from Aqueous Solutions, Confidential of Intel Corporation.

• J. Huo, R. Solanki, and J. McAndrew, Characteristics of Copper films Produced via Atomic Layer Deposition, J. Mater. Research, vol.17, no.9, 2394-2398, 2002.

• X. Wang, J. Huo, Control of Heating Process and Detecting of Temperature Equalization Time, Journal of Sichuan Institute of Technology, vol.16, No.1, 1-8 1997.

• J. Huo, Zero-Phase-Triggering On-Off Controller, Radio Magazine, No.6, 54-55, 1995.

• G. Sheng, J. Huo, S. Gong, The Influences of Microalloying on Fatigue Properties of HSLA Steels, Journal of Chongqing University, vol.16, no.2, 88-92, 1993.

• J. Huo, X. Wang, Determination of Optimal Heating Time with Computer Aid, Congress Book of the 8th International Congress on Heat Treatment of Materials, pp.601-604, Kyoto, Japan, Nov.1992.